Copy No. 71
NCHRP 10-48

ASSESSING PAVEMENT LAYER CONDITION USING DEFLECTION DATA

FINAL REPORT

Prepared for
National Cooperative Highway Research Program
Transportation Research Board
National Research Council

Y. R. Kim, S. R. Ranjithan, J. D. Troxler, B. Xu
North Carolina State University

November 2000

ACKNOWLEDGMENT OF SPONSORSHIP

This work was sponsored by the American Association of State Highway and Transportation Officials, in cooperation with the Federal Highway Administration, and was conducted in the National Cooperative Highway Research Program, which is administered by the Transportation Research Board of the National Research Council.

TABLE OF CONTENTS

LIST OF FIGURES

LIST OF TABLES

LIST OF SYMBOLS

H_{ac} = thickness of AC layer in inch,

H_{abc} = thickness of base layer in inch,

H_{pcc} = thickness of PCC layer in inch,

H_{ctb} = thickness of cement treated base layer in inch,

D_i = deflections where i is the distance in inches from the load center;

E_i = surface modulus where i is the distance in inches from the load center;

p = load pressure;

a = radius of load plate;

μ = Poisson's Ratio;

R_i = the adjusted radial distance at the i^{th} sensor;

E_{ac} = the AC modulus;

T = the AC mid-depth temperature;

ε_{ac} = the tensile strain at bottom of AC layer in microstrain;

E_{Ri} = the subgrade modulus in ksi at 6 psi deviator stress;

α_1 = temperature correction factor for ε_{ac} for full-depth pavements;

ε_{ac,T_m} = AC tensile strain in microstrain at measured temperature T_m;

ε_{ac,T_r} = AC tensile strain in microstrain at reference temperature T_r of 25°C;

E_{ac,T_m} = AC modulus in ksi at measured temperature T_m;

E_{ac,T_r} = AC modulus in ksi at reference temperature T_r of 25°C;

T_m = measured temperature in °C;

T_r = reference temperature of 25°C;

N_f = a number of load repetitions to failure;

ε_{sg} = the compressive strain on top of subgrade in microstrain;

σ_d = the deviator stress of subgrade;

q_u = unconfined compressive strength of cohesive soil;

c = cohesion for cohesive soil;

D_{sg} = the thickness of subgrade in feet;

E_{smin} = the smallest value of surface moduli;

F_{ac} = the effect of AC layer on the surface modulus;

α_2 = temperature correction factor for ε_{sg} for full-depth pavements;

ε_{sg,T_m} = subgrade compressive strain in microstrain at measured temperature T_m;

ε_{sg,T_r} = compressive strain in microstrain at reference temperature T_r of 25°C;

N_d = a number of strain repetitions to limit the rutting of subgrade;

α_3 = temperature correction factor for ε_{ac} for aggregate base pavements;

ε_{ac,T_m} = AC tensile strain in microstrain at measured temperature;

ε_{ac,T_r} = AC tensile strain in microstrain at reference temperature of 25°C;

ε_{abc} = compressive strain at the top of the aggregate base layer, in microstrain;

α_4 = temperature correction factor for ε_{abc} for aggregate base pavements;

ε_{abc,T_m} = compressive strain on top of base layer in microstrain at measured temperature T_m;

ε_{abc,T_r} = compressive strain on top of base layer in microstrain at reference temperature of 25°C;

α_5 = the temperature correction factor for ε_{sg} of aggregate base pavements;

ε_{sg,T_m} = the subgrade compressive strain in microstrain at measured temperature T_m;

ε_{sg,T_r} = compressive strain in microstrain at reference temperature of 25°C;

l = the radius of relative stiffness;

Δ_j = the non-dimensional representation of deflections at each loading condition;

δ_l = the deflection of the loaded side (D_0) in AC/PCC void detection;

δ_u = the deflection of the unloaded side at the same distance from the joint (D_{48}) in AC/PCC void detection;

OD = the offset distance from slab edge to the edge of the loading plate in inches;

D_{i0} = the deflection at the i^{th} sensor with zero offset (OD=0);

D_{iOD} = the deflection at the i^{th} sensor with some offset (OD<1.5l);

$AREA_{OD}$ = the corner deflection AREA measure at some offset (OD<1.5l);

$AREA_0$ = the corner deflection AREA measured at zero offset (OD=0);

α = temperature adjustment factor;

T_d = AC temperature at depth d, °C;

IR = infrared surface temperature, °C;

d = depth at which temperature is to be predicted, mm;

1-day = average air temperature the day before testing;

sin = sin function in 18 hour clock system, with 2π radians equal to one 18-hour cycle,

hr_{18} = time of day, in 24-hour system, but calculated using an 18 hour AC temperature rise and fall time cycle, as indicated below:

When using the $\sin(hr_{18}-15.5)$ function, only use times from 11:00 to 05:00 hrs. If the actual time is not within this time range, consider 11:00 hrs as the actual time. If the actual time is between 0:00 and 5:00 hrs, add 24 to the actual time. The calculate as follows: If the time is 13:15, then in decimal form, 13.25-15.50=-2.25; -2.25/18=-0.125; -0.125 x 2π=-0.785 radians; sin(-0.785)=0.707.

When using the $\sin(hr_{18}-13.5)$ function, only use times from 09:00 to 03:00hrs If the actual time is not within this time range, consider 09:00 hrs as the actual time. If the actual time is between 0:00 and 3:00 hrs, add 24 to the actual time.

ACKNOWLEDGMENTS

The research reported herein was performed under NCHRP Project 10-48 by the Department of Civil Engineering, North Carolina State University, and the Texas Transportation Institute. North Carolina State University was the contractor for this study. The work undertaken at the Texas Transportation Institute was under a subcontract with North Carolina State University.

Y. Richard Kim, Professor of Civil Engineering, North Carolina State University was the principal investigator. The other authors of this report are S. Ranji Ranjithan, Associate Professor of Civil Engineering, North Carolina State University; Jeremy D. Troxler, Research Assistant, North Carolina State University; and Bing Xu, Research Assistant, North Carolina State University.

The work was done under the general supervision of Professor Kim. The work at Texas Transportation Institute was done under the supervision of Tom Scullion with the assistance of Mr. Seung-Wook Yang.

ABSTRACT

This report documents and presents the results of the study of condition assessment of pavement layers using deflection data. Finite element forward models were used to simulate field behavior of pavements under Falling Weight Deflectometer loads for the range of pavement layer thicknesses found in the LTPP DataPave database. Deflection history, stress, and strain information was recorded for a full permutation of full depth, aggregate base, cement treated base, and asphalt overlain portland cement concrete pavement thicknesses and moduli. Nonlinearity in unbound layers was considered in cases deemed appropriate by material behavior study results. DBPs, artificial neural networks, and surface modulus methods utilized the synthetic database in the determination of pavement layer condition. Field data retrieved from state departments of transportation and DataPave 2.0 was used in the testing and verification of condition assessment procedures. The study resulted in condition evaluation methods for asphalt-surfaced pavements based on a combination of DBPs, artificial neural networks, regression equations, and surface modulus.

SUMMARY

Many of the pavements in the nation's highway network are nearing the end of their design life. Therefore, the main concern of state highway agencies has shifted, in part, from building new interstates and high-volume roadways to maintaining the existing pavement network. Consequently, condition assessment of pavements has become an important issue for developing effective rehabilitation and maintenance strategies. Visual observation of the pavement surface usually does not render sufficiently reliable information on pavement condition. Therefore, nondestructive deflection testing has become an integral part of the condition assessment process for state highway agencies in recent years. According to the survey conducted at the beginning of this project, the Falling Weight Deflectometer (FWD) is the prevailing deflection testing device used by these agencies.

The main concept behind current deflection analysis procedures is that each pavement layer is intact and is characterized by its elastic modulus and Poisson's ratio. These procedures assume that the effect of distresses in a layer is accounted for by the reduction of the elastic modulus for that layer. Therefore, research efforts have mainly centered around the backcalculation of layer moduli for the condition assessment of pavement layers. This project seeks to improve the ability of assessing pavement layer conditions from deflections by identifying condition indicators other than layer moduli and developing algorithms to estimate these indicators from surface deflections. This project examined different pavement types surfaced with asphaltic materials. Due to a large number of variables affecting surface deflections and their interactions, synthetic data generated from dynamic finite element analysis were used in developing the layer condition assessment procedures. For each layer, several

condition indicators were identified as promising. These indicators are categorized into the following groups: (1) deflection basin parameters; (2) stresses and strains; and (3) layer moduli. Artificial Neural Networks and regression equations were developed to estimate these indicators from the surface deflections. These procedures were calibrated using field data obtained from various state DOTs. The calibrated procedures were implemented into a Visual Basic computer program that has a user-friendly graphical interface.

The major strengths of the developed procedures are: (1) that the dynamic effect of FWD loading and nonlinear behavior of unbound materials were accounted for; (2) that the time to obtain results from the program is insignificant because these dynamic and nonlinear effects were included in the Artificial Neural Networks and regression equations; (3) that the relationships used in estimating the condition of different layers in the procedures are independent of each other, unlike current deflection analysis procedures; and (4) that some of the relationships constituting these procedures do not require all seven deflections, thus allowing the analysis of irregular deflection basins that occur frequently in distressed pavements for the layer condition assessment.

CHAPTER 1

INTRODUCTION

RESEARCH PROBLEM STATEMENT

The use of nondestructive deflection testing has become an integral part of the structural evaluation and rehabilitation process of pavements in recent years. Various types of equipment, such as the Falling Weight Deflectometer, Road Rater, and the Dynaflect, are used by state highway agencies to apply patterns of loading and record deflection data along the pavement. When pavements experience some form of distress, variations in pavement deflections and shape of deflection basins along a project can be caused by differences in the condition of pavement layers. For example, the presence of rutting, stripping, cracking or debonding in the layers of flexible pavements will contribute to changes in deflection data. However, current deflection analysis procedures do not identify pavement layer distress. It appears that procedures that take into account the effects of loading schemes, deflection measurement locations, deflection basin parameters, and other related factors can be used to analyze deflection data and identify the presence, location, and extent of distress within the pavement structure.

Thus research is needed to identify and evaluate methods for assessing pavement layer condition based on deflection measurements and to develop better procedures to relate deflection data to layer condition and distress. This research will provide a cost-effective means for assessing pavement layer condition, while reducing the need for destructive testing. Such information will help engineers select appropriate rehabilitation strategies.

RESEARCH OBJECTIVE

The objective of the research is to develop procedures to assess the condition of pavement layers based on deflection measurements. This research is related to all layers of rigid and flexible pavements that include an asphalt concrete surface layer.

SCOPE

The scope of this study encompasses the condition assessment of all layers of flexible and rigid pavements that include an asphalt concrete surface layer. These pavements can be categorized into the following five types:

1. Asphalt pavement with aggregate base course (Aggregate base pavement)
2. Asphalt pavement with bituminous-treated base course (Full-depth pavement)
3. Asphalt pavement with cement-treated base course (CTB)
4. Asphalt overlay over PCC pavement (AC/PCC)
5. Asphalt overlay over cracked and seated or rubblized PCC pavement (AC/Fractured PCC)

Little field data were available for AC/Fractured PCC pavements that can be used in developing a layer condition assessment procedure. Since these pavements have similar characteristics to that of aggregate base pavements in forward modeling, no separate analysis was performed on this type of pavements. Recommendations made in this research for aggregate base pavements should be applicable to AC/Fractured PCC pavements.

Table 1 summarizes layer condition parameters for different pavements investigated in

this study. All the modeling and data collection efforts were aimed to develop deflection interpretation procedures that can predict the layer condition parameters in Table 1.

RESEARCH APPROACH

Development of a reliable procedure for pavement layer condition assessment is a challenging task owing to the large number of factors to be considered, their interactions, and randomness of the distresses in terms of location, severity, and extent. One approach of developing this procedure is to conduct deflection tests on a number of pavements with varying distress characteristics in different environmental conditions and to relate the observed deflection behavior to the input variables, so-called an empirical approach. Knowing the large number of combinations of these factors, this approach will be time consuming and costly, if not impossible due to the large data requirements. The other approach, so-called a mechanistic approach, is to employ mechanics of materials equations that relate an input such as an FWD loading history to an output or pavement responses such as deflections. Depending upon the type of layer materials used, appropriate material models can be employed with varying complexities. The effects of environmental conditions are usually reflected through these material models. The main question becomes then how accurate and realistic the analytical model is in predicting pavement responses under varying conditions.

The research approach taken in this study describes a mechanistic-empirical method of developing a simple, practical deflection interpretation procedure for condition assessment of distressed pavement layers. This approach optimizes the application of the two approaches described above to develop a reliable, simple procedure for state highway agencies.

ABAQUS finite element program was used in this research to develop synthetic

Table 1. Layer condition parameters investigated in this study

Pavement Type	Layer Type	Layer Condition
Aggregate Base Pavement	Asphalt layer	Cracking potential
		Strength (Stripping)
		Debonding
	Aggregate base	Strength
	Subgrade	Strength
	Stiff layer	Depth
Full-Depth Pavement	Asphalt layer	Cracking potential
		Strength (Stripping)
		Debonding
	Subgrade	Strength
	Stiff layer	Depth
CTB	Asphalt layer	Debonding
	Cement-treated base	Cracks
	Subgrade	Strength
	Stiff layer	Depth
AC/PCC	Asphalt layer	Debonding
	PCC slab	Voids beneath PCC slab
	Subgrade	Strength
	Stiff layer	Depth
AC/ Fractured PCC	Asphalt layer	Cracking potential
		Strength (Stripping)
		Debonding
	Fractured PCC layer	Strength
	Subgrade	Strength
	Stiff layer	Depth

databases that cover all the pavement structures presented in DataPave 2.0. Axisymmetric, dynamic finite element analysis was performed on various pavement structures modeled by both linear elastic and nonlinear elastic material models. A 9,000-lb FWD load time history was used in the finite element modeling to compute deflections, stresses, and strains at various locations in the pavement system that are critical for the condition and performance evaluation. The resulting synthetic databases are composed of pavement structural and material characteristics (such as layer thicknesses and material coefficients) as well as pavement responses (such as stresses, strains, and deflections). Details on the finite element modeling can be found in Appendix A.

In addition to the synthetic databases, a field database was constructed using information supplied by state highway agencies and DataPave 2.0. Since the field data can be complex and sometimes misleading, the nature of the information provided by the agencies and DataPave was carefully examined for its appropriateness. For model development, selected high quality data from the agencies were used. DataPave data were mostly used for the verification of the models. Detailed descriptions of the field database are presented in Appendix B.

Both the field deflection data and the calculated synthetic deflections were used in identifying a set of "damage indicators," including deflection basin parameters (DBPs), effective moduli, and stress/strain parameters. The relationships among these damage indicators and known distress characteristics were studied systematically along with structural characteristics using regression analysis and artificial neural networks (ANNs). Various DBPs were studied as condition indicators for different layers. All the DBPs investigated in this research are summarized in Table 2, and a detailed study of these DBPs is presented in Appendix C.

Table 2. Available deflection basin parameters

Deflection Parameter	Formula	Measuring Device	Reference
Area	$AREA = \frac{6(D_0 + 2D_{12} + 2D_{24} + D_{36})}{D_0}$	FWD	Hoffman 1981
Add. Areas	$AREA_2 = \frac{6(D_{12} + 2D_{18} + D_{24})}{D_0}$ $AREA_3 = \frac{6(D_{24} + 2D_{36} + D_{48})}{D_0}$	FWD	
Area Indexes	$AI_1 = \frac{D_0 + D_{12}}{2D_0}$ $AI_2 = \frac{D_{12} + D_{24}}{2D_0}$ $AI_3 = \frac{D_{24} + D_{36}}{2D_0}$ $AI_4 = \frac{D_{36} + D_{48}}{D_0}$	FWD	
Area Under Pavement Profile	$AUPP = \frac{5D_0 - 2D_{12} - 2D_{24} - D_{36}}{2}$	FWD	Hill & Thompson
Base Curvature Index	$BCI = D_{60} - D_{48}$ or $BCI = D_{24} - D_{36}$	Dynaflect FWD	Peterson 1972
Base Damage Index	$BDI = D_{12} - D_{24}$	RR & FWD	
Bending Index	$BI = D_0 / a$	BB	Hveem 1954
Deflection Ratio	$DR = D_r / D_0$	FWD	Classen 1976
Load Spreadability Index	$LSI = (D_{48} / D_{24})xF$	FWD	Wimsatt 1995
Maximum Deflection	D_0	BB Dynaflect	Shrivner 1968
Radius of Curvature	$R = \frac{r^2 *}{(2D_0(D_0 / D_r - 1))}$	CM & BB	Dehlen 1962
Radius of Influence	$RI = x / D_0$	BB	Ford 1962
Shape Factors	$F_1 = (D_0 - D_{24}) / D_{12}$ $F_2 = (D_{12} - D_{36}) / D_{24}$	FWD	Hoffman 1981
Add. Shape Factor	$F_3 = (D_{24} - D_{48}) / D_{36}$	FWD	
Slope of Deflection	$SD = \tan^{-1}[(D_0 - D_r) / r]$	BB	Kung 1967
Spreadability	$S = \frac{25(D_0 + D_{12} + D_{24} + D_{36})}{D_0}$	Dynaflect RR FWD	Vaswani 1971
Structural Strength Index	$SSI = A_x / (X_{min} xE_{min})$	FWD	Jung 1992
Structural Integrity Index	$SII = A_x / (X_x xE_m)$	FWD	Jung 1992
Surface Curvature Index	$SCI = D_0 - D_{12}$	BB RR Dynaflect FWD	Shrivner 1968
Tangent Slope	$TS = (D_0 - d_x) / x$	FWD	Stock 1984

Table 2. (Cont'd)

D_r	Surface deflection	BB	Benkelman Beam
r	Distance from the load center (inch)	RR	Road Rater
a	¼ of deflection basin length	FWD	Falling Weight Deflectometer
x	Distance from point of maximum deflection to tangent point	CM	Curvaturemeter
		*	r=127 mm
d	Deflection at the tangent point		
F	Minimum of D_{12}/D_0, D_{24}/D_{12}, …, or D_{72}/D_{60}		
A_s	Area under the surface modulus profile to X_s or to the minimum value (E_{min}) at $X = X_{min}$		
E_m	Estimated subgrade modulus		
X_s	Radial distance from the test load		

In developing the condition assessment procedures in our investigation, several predictive models were needed. Where no existing model was available, an empirical modeling approach was adopted for such predictive purposes. In cases where the nature of the relationship between a set of input parameters and an output parameter was sufficiently understood, the functional form of the relationship was first selected accordingly and then a statistical regression approach was used. Standard statistical routines available within Matlab® were utilized to carry out the regression. In cases where the functional form was not well understood, an artificial neural network (ANN) based approach (using the feed forward type networks) was utilized. The primary advantage of this approach over statistical regression is that the functional form of the relationship is not needed a priori. Again, the ANN libraries available within Matlab® were utilized for training the ANNs. Details of this ANN based approach are given in Appendix D.

Major findings from this study are detailed in Chapter 2. Based on these findings, pavement layer condition evaluation procedures for different pavements were developed. These procedures are described in Chapter 3. Conclusions advanced from this research and suggested areas for future research are presented in Chapter 4.

CHAPTER 2

FINDINGS

The following is a discussion of the conclusions found from the study performed to determine the condition of pavement layers using deflection data. Indicators of layer condition were developed during the investigation of deflection basin parameters (DBPs), artificial neural networks (ANNs), and surface modulus methods.

Field deflection information was received from state DOTs and was retrieved from DataPave 2.0. Very little high quality data were present, but layer thickness and condition were used when available. All available state DOT field data were used in either the development or the validation of condition assessment procedures. DataPave data were used as a check of general expected trends.

Synthetic data were generated for the full range of pavement thicknesses found in the DataPave 2.0 field database. Linear elastic models for all pavement types, and nonlinear elastic models for all flexible pavements were produced. A parametric study of DBPs for the synthetic database was completed and the DBPs most effective in identifying changes in layer properties were found.

ANN structures were generated for all pavement types for the prediction of layer moduli or thicknesses. Synthetic data were used to train the networks. The networks were then used to directly predict pavement layer condition.

Details of the findings from the investigation of layer condition indicators for full-depth, aggregate base, cement treated base, and asphalt overlain portland cement concrete pavements are presented below.

SYNTHETIC AND FIELD DATABASES

Synthetic deflections were calculated using the ABAQUS finite element commercial software package for various pavement structures. This database formed a discrete set of structures for each pavement type. In order to cover as many existing pavements as possible, pavement thicknesses in DataPave 2.0 were surveyed. Table 3 summarizes the thickness range and actual modulus and thickness values used for each pavement type.

In full-depth and aggregate base pavements where nonlinearity was included in unbound layers, additional material properties had to be included. The model constants of unbound granular materials were selected from the report of Garg and Thompson (1). Thirteen sets of model constants representing six classes of granular materials were developed from that study. Santha (2) developed 87 sets of model constants for various types of subgrade soils. All 87 sets of constants are used in this research. This new set of synthetic data was created using a randomized approach (see Appendix A for details). In this approach, a range of thicknesses and moduli was defined for each pavement layer. FEM models were then created with values randomly selected from the given thickness and modulus ranges. Table 4 illustrates the modulus and thickness ranges used in creating the additional nonlinear synthetic database. This effort resulted in a total of 34,000 cases for the linear elastic database and 10,000 cases for the nonlinear elastic database.

Availability of large amounts of high quality field data was deemed a critical factor in the success of developing reliable procedures for condition assessment of pavement layers. Field data were gathered from state DOTs and from the DataPave field database created as part of the LTPP study. DataPave 2.0 is an extensive database of pavement testing information. Pavement

Table 3. Synthetic database structures for linear elastic analysis

Pavement Type	Pavement Layer	Thickness (in.)	Modulus (ksi)
Aggregate Base Pavement	AC	4, 9, 13, 18, 26 (2-24)*	100, 200, 400, 800, 1600
	Aggregate Base	6, 12, 18, 24 (6-54)*	25, 50, 75, 100, 200
	SG	30, 39, 79, 157, ∞	5, 10, 15, 20, 25
Full Depth Pavement	AC (Surf. & Base)	4, 9, 13, 18, 26 (2-28)*	50, 100, 200, 400, 800, 1600, 2400
	SG	30, 39, 79, 157, ∞	5, 10, 15, 20, 25
CTB Pavement	AC	2, 4, 6, 8, 12 (2 - 18)*	100, 200, 400, 800, 1600
	CTB	6, 8, 10, 12, 24 (5 – 26.5)*	500, 1000, 1500, 2000, 2500
	SG	30, 39, 79, 157, 197, 315, ∞	5, 10, 15, 20, 25, 50, 100
AC/PCC Pavement	AC	2, 4, 6, 8 (1.5 – 6.5)*	100, 200, 400, 800, 1600
	PCC	6, 8, 9, 10, 12 (7 – 10.8)*	3000, 3500, 4000, 4500, 5000
	SG	30, 39, 79, 157, 197, 315, ∞	5, 10, 15, 20, 25, 50, 100

Note: * ranges from DataPave field database.

Table 4. Material properties and thickness ranges used in nonlinear FEM runs

		AC Layer	Base Layer	Subgrade
Modulus (ksi) or Model Constants	Aggregate Base Pavement	50 ~ 2500	13 sets from Garg and Thompson (1)	87 sets from Santha (2)
	Full-depth Pavement	50 ~ 2500	---- ---- ----	87 sets from Santha (2)
Thickness	Aggregate Base Pavement	1 ~ 24 (in)	3 ~57 (in)	1 ~ 20 (ft)
	Full-depth Pavement	6 ~26 (in)	---- ----	1 ~ 20 (ft)

layer condition information is not provided in DataPave, however. Stiff layer depth information is scattered, and when it is available, coring was done outside the test section. For these reasons, information obtained from DataPave was considered and utilized for procedure verification only. The high quality data were to come from the state DOTs. The state DOT field database was much smaller than anticipated. The data received were used in the development of condition assessment procedures. Table 5 shows the states from which FWD deflection information was used in the development and verification of condition assessment procedures.

PARAMETRIC SENSITIVITY STUDY

To investigate the effectiveness of DBPs in representing the condition of pavement layers, it was desirable to identify a smaller set of DBPs that were promising so that an in-depth study could be done more effectively. The synthetic database was studied to determine the most effective DBPs in describing the condition of each of the pavement layers set forth in the research plan. Included in the study were the DBPs in Table 2 and the seven measured deflections. In the FEM analysis, thickness and modulus for each layer were changed to represent the range of permutations encountered in the field. The synthetic database was used to isolate a specific pavement characteristic for comparison. Pavement characteristics in question were fixed to minimum and maximum values. All other conditions were allowed to change, and DBPs were calculated. The results were analyzed and a percent Root Mean Square Error (RMSE) was calculated for each DBP. The DBPs with the highest RMSEs were most sensitive to changes of the parameter in question. Therefore, the DBPs with the largest RMSEs were considered the best indicator for that particular pavement characteristic.

Table 5. Summary of states contributing to field database

Pavement Type	State Database	DataPave 2.0
Full-Depth	North Carolina, Ohio	Arizona, Kentucky, Tennessee, South Dakota
Aggregate Base	North Carolina, Texas, Ohio, Montana, Washington, Minnesota	Arizona, Delaware, Nevada, Virginia
CTB	Florida, North Carolina, Nevada, Ohio, Texas	Arizona, California, Florida, Maryland, Mississippi, North Dakota, Oklahoma, Texas, Virginia, Wyoming
AC/PCC	Ohio, Montana, Washington	Colorado, Georgia, Nebraska, South Dakota, Ontario

Tables 6 through 9 show the results of the parametric study for the full-depth pavement, the aggregate base pavement, the cement treated base (CTB) pavement, and the asphalt overlain portland cement concrete (AC/PCC) pavement. The results are quite similar as expected. Many of the DBPs are the same, only in differing order. The research team created several new DBPs that were included in this study, such as $AREA_2$, $AREA_3$, F_3, AI_1, AI_2, AI_3, and AI_4. These parameters, as defined in Table 2, were designed to reflect various layer properties of pavements. Take $AREA_2$, $AREA_3$, and F_3 for examples. $AREA_2$ was derived from the more familiar AREA parameter that describes overall pavement strength. $AREA_2$ is defined as:

$$AREA_2 = \frac{6(D_{12} + 2D_{18} + D_{24})}{D_0} \quad (1)$$

It was believed that if the middle deflections were considered instead of the entire deflection basin, the base layer condition could be isolated. Similarly, $AREA_3$ was created in an attempt to isolate lower layer condition. $AREA_3$ is defined as:

$$AREA_3 = \frac{6(D_{24} + 2D_{36} + D_{48})}{D_0} \quad (2)$$

F_3 is a shape factor describing the tail of the deflection basin curve. It is an extension of the F_1 and F_2 shape factors and is defined as:

$$F_3 = \frac{D_{24} - D_{48}}{D_{36}}. \quad (3)$$

F_3 was expected to describe lower layer condition or depth to a stiff layer since the sensors farthest from the load center are most likely to represent lower layer properties. Similarly, based on their definitions, AI_1 was created to reflect the condition of upper layer, while AI_4 was created to reflect the condition of subgrade. AI_2 and AI_3 were expected to be more related to the conditions of the middle layers.

Table 6. Parametric study results for full-depth pavements

RMSE (%) (H_{ac})		*RMSE (%)* (H_{sg})		*RMSE (%)* (E_{ac})		*RMSE (%)* (E_{sg})	
BDI	1069	F_3	1452	*SCI*	3385	AI_4	1811
F_3	953	F_2	214	*AUPP*	2375	*BCI*	327
AUPP	756	F_1	113	*BDI*	1216	*BDI*	154
SCI	654	AI_4	78	D_0	717	AI_3	150
BCI	580	AI_3	60	*BCI*	576	D_0	30

Table 7. Parametric study results for aggregate base pavements

RMSE (%) (H_{ac})		*RMSE (%)* (H_{abc})		*RMSE (%)* (H_{sg})		*RMSE (%)* (E_{ac})		*RMSE (%)* (E_{abc})		*RMSE (%)* (E_{sg})	
BDI	296	*BCI*	174	F_3	255	*SCI*	859	*BDI*	243	AI_4	206
AUPP	256	*BDI*	145	F_2	124	*AUPP*	598	*BCI*	191	*BCI*	104
SCI	252	F_3	107	F_1	77	F_1	271	*AUPP*	129	AI_3	67
BCI	177	D_0	59	AI_4	64	*BDI*	248	*SCI*	108	D_0	67
D_0	122	*AUPP*	54	AI_3	45	D_0	209	D_0	107	F_1	50

Note: Definitions of all parameters are described in Table 2

Table 8. Parametric study results for CTB pavements

RMSE (%) (H_{ac})		RMSE (%) (H_{ctb})		RMSE (%) (H_{sg})		RMSE (%) (E_{ac})		RMSE (%) (E_{ctb})		RMSE (%) (E_{sg})	
BDI	25	*BDI*	66	F_3	244	*SCI*	975	*BDI*	131	D_{48}	1267
BCI	23	*BCI*	59	F_2	173	*AUPP*	671	*BCI*	96	*LSI*	203
AUPP	19	F_3	32	F_1	154	F_1	493	*AUPP*	60	D_{18}	166
SCI	18	F_2	31	D_{48}	80	D_0	225	F_2	54	$AREA_3$	128
D_{48}	14	D_{18}	27	$AREA_3$	56	*BDI*	175	*SCI*	53	*BCI*	76

Table 9. Parametric study results for AC/PCC pavements

RMSE (%) (H_{ac})		RMSE (%) (H_{pcc})		RMSE (%) (H_{sg})		RMSE (%) (E_{ac})		RMSE (%) (E_{pcc})		RMSE (%) (E_{sg})	
BDI	19	*BDI*	86	F_3	227	*SCI*	1189	*BDI*	31	D_{48}	1267
BCI	18	*BCI*	72	F_2	187	*AUPP*	830	*BCI*	25	D_{18}	203
F_1	13	F_3	40	F_1	186	F_1	635	F_2	14	$AREA_3$	166
AUPP	12	F_2	36	D_{48}	77	D_0	264	F_3	13	*LSI*	128
D_{18}	11	D_{18}	32	D_{18}	60	*BDI*	155	D_{18}	13	$AREA_2$	76

Note: Definitions of all parameters are described in Table 2

FULL-DEPTH PAVEMENTS

The following sections describe the efforts made in determining the condition of full-depth pavements as listed in the research plan. For distressed pavements, cracking, stripping, and debonding in the AC layer, subgrade strength, and depth to a stiff layer were investigated. Fatigue cracking and rutting potentials were also studied for intact pavements. The DBPs selected from the sensitivity study were investigated along with optimized ANN structures. A set of regression equations that correlates the DBPs to layer condition indicators also resulted from the synthetic data. The final results of these investigations are presented below.

AC Layer Condition

Cracking and Stripping

Both cracking and stripping reduce the stiffness of the AC layer as well as cause discontinuities in pavements. When severe discontinuities exist, the FWD deflection basins may show unusual shapes. The following two criteria are proposed to identify such unusual cases:

$$\text{Criterion 1:} \quad d_i < d_{i+1}, \qquad i = 1,2,...,6 \tag{4}$$

$$\text{Criterion 2:} \quad E_i > E_{i+1} \quad and \quad E_i > E_{i-1}, \qquad i = 2,3,...,6 \tag{5}$$

where d_i is the deflection at the i^{th} sensor, and E_i is the surface modulus at the i^{th} sensor, which is calculated from the following equations:

$$E_i = \frac{2(1-\mu^2)p}{ad_i} \qquad when \quad i = 1 \tag{6}$$

$$E_i = \frac{(1-\mu^2)pa}{R_i d_i} \qquad when \quad i = 2,3,...,7 \tag{7}$$

where p is the load pressure, a is the radius of load area, R_i is the adjusted radial distance at the i^{th} sensor. The adjusted radial distances were suggested by Johnson and Baus (3) as 7.095,11.414,

17.52, 23.41, 36, and 48 inches for sensors 2 to 7, respectively. These radial distance adjustments are made to correct for the error induced by the point-load approximation of FWD loading.

Criterion 1 is used to check if an outer sensor deflection is greater than an inner sensor deflection, which happens when severe discontinuities exist in upper layers. Criterion 2 is used to avoid the appearance of peak surface modulus value between the center and the outermost sensor. In intact pavements, peak surface modulus occurs at either the center sensor due to the high stiffness of the AC layer, or the outermost sensor due to the high stiffness of the stiff layer (see Appendix C for details). When either of the above criteria is met, the pavement at the test location is considered to be severely cracked or stripped. Figure 1 shows the plot of four measured deflection basins from NC 421 test sections. The calculated surface modulus profiles of these four deflection bowls are presented in Figure 2. These deflection bowls meet the two criteria, suggesting severe cracking and/or stripping at the test locations. These indications were confirmed by visual observation of the cores obtained from the test locations.

Besides the above two criteria, the SLIC method, developed by Stubstad et al. (4), can also be used to detect unusual deflection basins. In the SLIC method, S_i, radial distance of the i^{th} sensor, is first plotted against d_1/d_i, deflection ratio of the center deflection to the deflection at the i^{th} sensor, in a log-double log scale. A 2nd order polynomial function is then applied to fit the relationship between S_i and d_1/d_i, which is expressed as follows:

$$\ln(S_i) = a + b * \ln(\ln(\frac{d_1}{d_i})) + c * [\ln(\ln(\frac{d_1}{d_i}))]^2, \qquad i = 2,3,...,7 \tag{8}$$

where a, b, and c are regression constants. A high R-squared value will be obtained if the deflection basin is normal. A poor curve fitting usually indicates severe discontinuities in the AC layer, unless the sensor spacing is wrongly recorded.

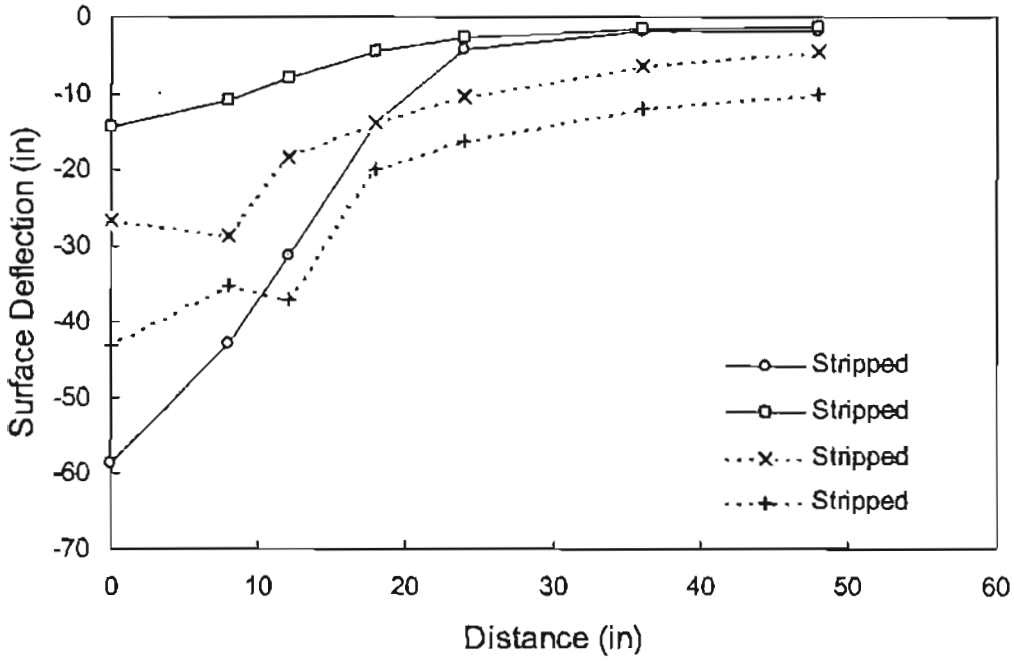

Figure 1. Deflection basins from NC 421 pavements

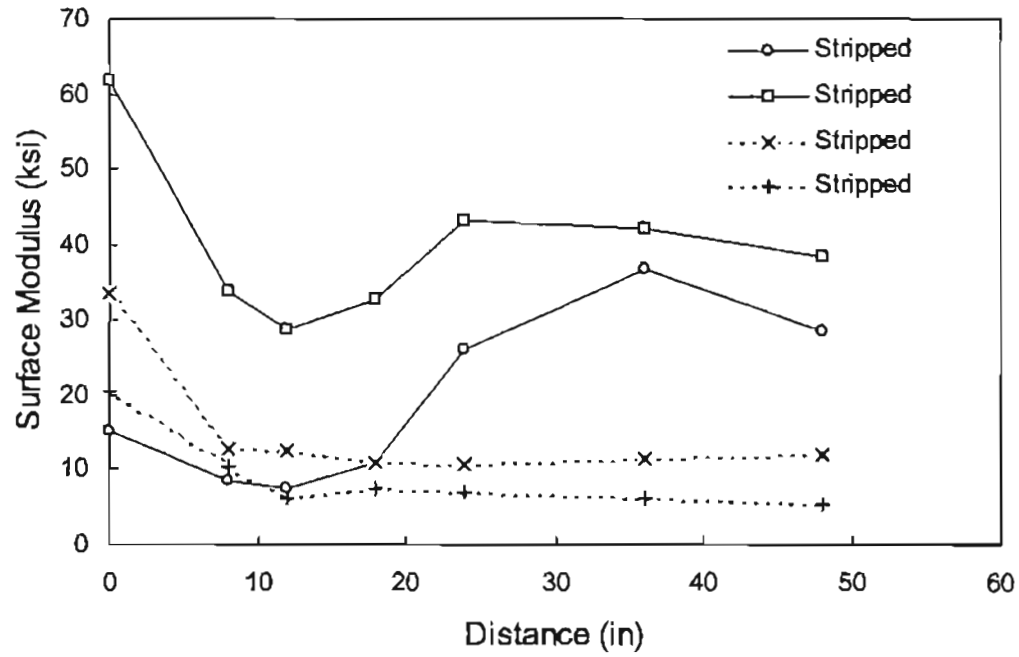

Figure 2. Surface modulus profiles from NC 421 pavements

Another method to detect cracking or stripping in the AC layer is to use the predicted value of AC modulus as an indicator. Assuming that the AC modulus can be predicted based on the FWD measurements, one can compare the predicted AC modulus against the AC modulus value corresponding to intact pavements at a measured temperature, which can be obtained from the AC modulus vs. temperature relationship. The AC layer is considered distressed depending on the deviation of AC modulus value from that represented in the modulus vs. temperature relationship. This relationship for intact pavements can be expressed in a general form as:

$$\log(E_{ac}) = a - b * T \tag{9}$$

where a and b are the constants related to the physical properties of asphalt concrete. The values of a and b are estimated by the regression of the predicted E_{ac} values and mid-depth temperature values for intact pavements.

Two approaches were used in this research to predict E_{ac} values from FWD measurements. Both approaches use the synthetic database generated from the dynamic, nonlinear analysis to develop a relationship between E_{ac} and the parameters that are based on FWD measurements and layer thicknesses. The first approach uses an ANN to relate E_{ac} values with the deflection values at the first three sensors at 0, 8, and 12 inch offsets, the deflection basin parameter *SCI* value, and the AC layer thickness. *SCI* is defined as:

$$SCI = D_0 - D_{12} \tag{10}$$

It was found that using only the first three deflections as ANN inputs gave improved predictions of field measurements over using all seven deflections. This observation is meaningful since the deflections close to the load center are affected more by the upper layer conditions, and therefore better represent the AC layer condition.

The second approach uses statistical regression to predict E_{ac} as a function of SCI and H_{ac} values. The following relationship best fits the synthetic data:

$$\log(E_{ac}) = -1.0831 * \log(SCI) - 2.6210 * \log(H_{ac}) + 0.0482 * H_{ac} + 5.2961 \qquad (11)$$

$$R^2 = 0.994 \qquad SEE = 0.028$$

The performance of these two approaches in predicting field measurements was found to be similar (see Appendix D for details.)

The data from the Arizona full-depth pavement 04-1015 in DataPave 2.0 were used to validate the above procedure in detecting cracking and stripping in the AC layer. FWD tests were performed in both March 1989 and December 1994. Measured air and pavement surface temperatures were also available from DataPave 2.0. Figure 3 shows the plots of predicted E_{ac} values versus pavement surface temperatures in both 1989 and 1994. It can be seen that, in general, the predicted E_{ac} values in 1994 fell below the AC modulus-temperature curve developed in 1989, indicating possible distress development in the AC layer after 1989. Unfortunately, AC mid-depth temperatures were not available in these cases, prohibiting a more meaningful comparison. Since, however, FWD tests were all performed about the same time in the early morning, the trend between 1989 and 1994 data should remain about the same.

Debonding

As debonding causes a significant loss of stiffness of the entire pavement, larger deflections would result at both inner sensors and outer sensors. One could attribute the large inner sensor deflections to a distressed AC layer. One could also mistakenly attribute the large outer sensor deflections to a weak subgrade condition. A single load FWD measurement, therefore, is not sufficient to distinguish between a debonded pavement and an intact pavement

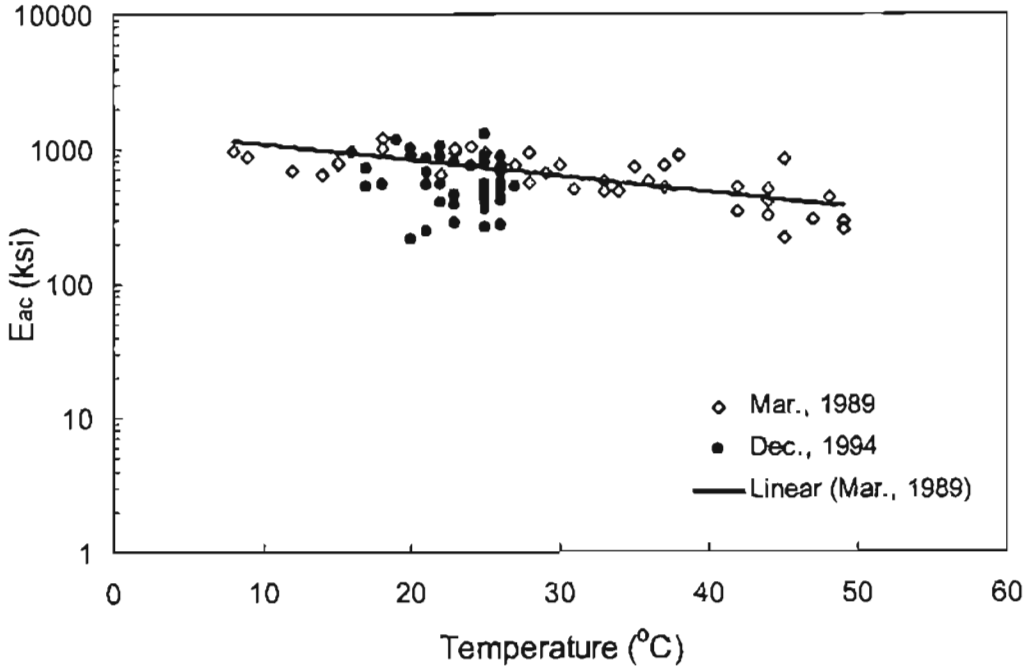

Figure 3. Predicted E_{ac} vs. temperature for pavement 4-1015

with lower subgrade strength. This hypothesis could not be tested for full-depth pavements in this study due to the lack of field data with debonding. It will be shown later in the aggregate base pavements that detection of debonding from 9 kip FWD deflections is difficult.

Cracking Potential

The tensile strain at the bottom of the AC layer, ε_{ac}, for intact pavements is an indicator for pavement cracking potential. Based on the ILLI-PAVE analysis, Garg and Thompson (7) established a simple regression equation to predict the AC tensile strain from a single deflection basin parameter *AUPP*, which is defined as follows:

$$AUPP = \frac{5 * D_0 - 2 * D_{12} - 2 * D_{24} - D_{36}}{2} \tag{12}$$

Based on the synthetic database developed from dynamic, nonlinear analysis, a better correlation (higher R-squared value) was found between the AC tensile strain and the deflection basin parameter *BDI*, which is defined as follows:

$$BDI = D_{12} - D_{24} \tag{13}$$

The relationship between ε_{ac} and *BDI* was established as:

$$\log(\varepsilon_{ac}) = 0.9977 * \log(BDI) + 1.7142 \tag{14}$$

$$R^2 = 0.987 \qquad SEE = 0.049$$

This relationship holds for various combinations of AC layer thickness, AC modulus, depth to a stiff layer, and subgrade material properties.

A temperature correction procedure for ε_{ac} was developed based on the fact that E_{ac} is a function of temperature. First, a relationship between ε_{ac} and E_{ac} was established using the synthetic database as follows:

$$\log(\varepsilon_{ac}) = -0.8189 * \log(E_{ac}) - 1.7211 * \log(H_{ac}) - 0.0906 * \log(E_{Ri}) + 6.1175 \qquad (15)$$

$$R^2 = 0.996 \qquad SEE = 0.028$$

It can be seen that the coefficient of the E_{Ri} term is very small in Eq. 15, suggesting that the subgrade condition has a minimal effect on the AC tensile strain. This observation is consistent with the conclusions drawn from the field study of Mn/ROAD test sections by Van Deusen et al. (5).

To incorporate the temperature effect on ε_{ac}, a temperature adjustment factor was developed. Using Eq. 15, the temperature adjustment factor for ε_{ac} is expressed as follows:

$$\alpha_1 = \frac{\varepsilon_{ac,T_m}}{\varepsilon_{ac,T_r}} = 10^{-0.8189*\left[\log(\varepsilon_{ac,T_m}) - \log(\varepsilon_{ac,T_r})\right]} \qquad (16a)$$

where

α_1 = temperature correction factor for ε_{ac} for full-depth pavements,

ε_{ac,T_m} = AC tensile strain in microstrain at measured temperature T_m,

ε_{ac,T_r} = AC tensile strain in microstrain at reference temperature T_r of 25°C,

E_{ac,T_m} = AC modulus in ksi at measured temperature T_m,

E_{ac,T_r} = AC modulus in ksi at reference temperature T_r of 25°C,

T_m = measured temperature in °C, and

T_r = reference temperature of 25°C.

Eq. 16*a* can be reduced to the following simpler expression based on Eq. 9:

$$\alpha_1 = 10^{-0.8189*b*(T_r - T_m)} \qquad (16b)$$

where b is the regression constant in AC modulus-temperature relationship.

Two approaches can be used to estimate the temperature adjustment factor α_1, one based on Eq. 16*a* and the other using Eq. 16*b*. To use Eq. 16*a*, AC moduli at two temperatures

(measured and reference) must be known. AC modulus at the measured temperature can be estimated using either the trained ANN or the regression-based approach (Eq. 11) as described previously. AC modulus at the reference temperature can be obtained in several ways, including (1) resilient modulus measured from laboratory testing; (2) backcalculation of FWD deflections measured at the reference temperature; or (3) assuming a typical AC modulus at the reference temperature based on the experience and material testing record of a local agency.

The second approach using Eq. 16*b* is much simpler as long as the agency knows the "*b*" value for their pavements. Many state agencies have developed their own AC modulus-temperature relationships using either laboratory resilient modulus test data or FWD test data of a wide range of pavements at different temperatures. Lukanen et al. (6) used deflections and temperatures measured from 40 Seasonal Monitoring Program sites of the LTPP program and found that "*b*" value could range from 0.01 to 0.04. The values of 0.0195 and 0.021 were recommended for the wheel-path and mid-lane data from the LTPP database, respectively.

The adjustment factor α_1 is then applied to the estimated ε_{ac} value from Eq. 14 to get the adjusted ε_{ac} for the reference temperature. That is,

$$Adjusted \quad \varepsilon_{ac} = \frac{Estimated \quad \varepsilon_{ac}}{\alpha_1} \tag{17}$$

Assuming the following phenomenological model for the fatigue cracking, the fatigue life of the tested pavement can be estimated:

$$N_f = f_1(\varepsilon_{ac})^{-f_2}(E_{ac})^{f_3} \tag{18}$$

where f_1, f_2, and f_3 are positive regression constants suggested by the Asphalt Institute to be 0.0796, 3.2191, and 0.854, respectively. This relationship can be used either by employing ε_{ac} and E_{ac} at the reference temperature for a simple comparison or by applying the cumulative

damage approach. In the cumulative damage approach, ε_{ac} and E_{ac} at different analysis periods (e. g., month or season) are estimated from the AC modulus-temperature relationship and Eq. 15.

The data from four NC 421 test sections were used to test the predictability of cracking potential using the above procedure. The ε_{ac} values were first calculated from FWD measurements recorded in February 1991 when pavements were still in good condition. The temperature adjustment procedure described above was then applied to ε_{ac} to get the adjusted ε_{ac}. The adjusted ε_{ac} values were plotted against the areas of fatigue cracking which were measured in August 1993 (Figure 4). Except Section 20, the larger area of fatigue cracking in 1993 corresponded to a larger ε_{ac} value in 1991.

Subgrade Strength

According to the sensitivity study described previously, DBPs *BDI* and *BCI* were found to be the two most sensitive parameters to subgrade stiffness. *BDI* is defined in Eq. 13 and *BCI* is defined as follows:

$$BCI = D_{24} - D_{36} \tag{19}$$

Higher values of *BDI* or *BCI* indicate poorer subgrade strength.

In addition to DBPs, stress and strain parameters, including compressive stress, deviator stress, principal stress ratio, compressive strain, and Subgrade Stress Ratio (*SSR*) on top of the subgrade, were also investigated. First, using the synthetic data from the dynamic, nonlinear analysis, the ANNs were developed to predict each of these parameters. The field data with known subgrade conditions were then used to test these parameters. Among them, the stress related parameters, such as compressive stress, deviator stress, and principal stress ratio, did not

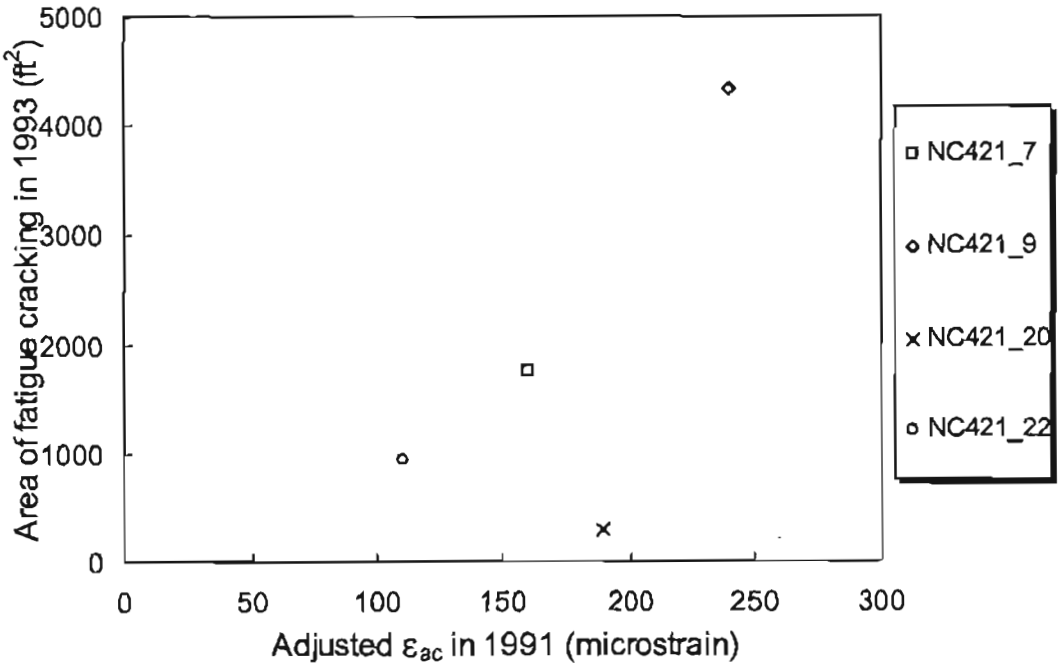

Figure 4. Adjusted ε_{ac} vs. area of fatigue cracking for full-depth pavements (NC 421)

work well for detecting subgrade condition. This is probably because subgrade performance is not only related to load induced stresses but also to the subgrade strength.

The compressive strain on top of the subgrade, ε_{sg}, is used to represent subgrade rutting potential, since the permanent deformation of subgrade is mainly controlled by subgrade vertical strain. Larger values of ε_{sg} indicate higher rutting potential. For full-depth pavements, it was found that ε_{sg} can be directly predicted from *BDI* using the following equation:

$$\log(\varepsilon_{sg}) = 0.9823 * \log(BDI) + 2.1460 \tag{20}$$

$$R^2 = 0.978 \qquad SEE = 0.063$$

This equation was developed from the synthetic database of dynamic, nonlinear analysis with various combinations of pavement structures and material properties.

The stress parameter, *SSR*, has been successfully used as a rutting potential indicator for cohesive soils by Garg and Thompson (7), and is defined as follows:

$$SSR = \frac{\sigma_d}{q_u} \tag{21}$$

Larger values of *SSR* correspond to greater subgrade rutting potential. It was found that from the ANN study that *SSR* can be directly predicted from the seven deflections and the AC thickness.

Although *BDI*, *BCI*, ε_{sg}, and *SSR* are related to subgrade condition in pavements, their values are also dependent on other layer properties such as AC thickness and AC modulus. To facilitate an evaluation procedure that is independent of the pavement structure, a "structural correction" procedure was developed to normalize these condition indicator values to a standard structure. A pavement structure with E_{ac} = 500 ksi, H_{ac} = 8 inches, and H_{sg} = infinity is used as the standard full-depth pavement structure. Initially, each condition indicator parameter was

described in terms of these structure specific properties. Using the synthetic database, the following relationships were established:

$$\log(BDI) = -0.7272 * \log(E_{ac}) - 1.8812 * \log(H_{ac}) - 0.1073 * \log(E_{Ri}) + 4.3299 \quad (22)$$

$$R^2 = 0.991 \qquad SEE = 0.044$$

$$\log(BCI) = -0.5757 * \log(E_{ac}) - 1.7014 * \log(H_{ac}) - 0.1885 * \log(E_{Ri}) + 0.1654 * \log(H_{sg}) + 3.3744 \quad (23)$$

$$R^2 = 0.979 \qquad SEE = 0.077$$

$$\log(\varepsilon_{sg}) = -0.7614 * \log(E_{ac}) - 1.7923 * \log(H_{ac}) - 0.1284 * \log(E_{Ri}) + 6.4863 \quad (24)$$

$$R^2 = 0.990 \qquad SEE = 0.043$$

$$\log(SSR) = -0.5003 * \log(E_{ac}) - 0.9302 * \log(H_{ac}) - 0.9439 * \log(E_{Ri}) + 2.2369 \quad (25)$$

$$R^2 = 0.986 \qquad SEE = 0.062$$

Several observations are made from Eqs. 22 through 25. First, E_{ac} and H_{ac} appear to have significant effects on all indicators. Secondly, the effects of the subgrade "break point" modulus, E_{Ri}, on the indicators vary with the highest effect on *SSR* and relatively low effects on ε_{sg} and *BDI*. E_{Ri} is an important material property for subgrade, which is the resilient modulus at 6 psi deviator stress in the subgrade bilinear model. The differences in the effect of E_{Ri} on the investigated indicators could result in the variation of indicator performance for detecting subgrade condition.

Using these equations, an adjustment factor for each parameter was obtained for structural correction. Similar to the temperature correction procedure described previously, the values of a parameter are estimated for the actual pavement structure and for the standard

pavement structure. The ratio of these values is then defined as an adjustment factor. Using *SSR* as an example, the unknown pavement layer properties E_{ac} and E_{Ri} are first predicted. The E_{ac} value can be estimated using either the pre-trained ANN or the regression-based approach (Eq. 11). The E_{Ri} value can be predicted from the trained ANN where the seven sensor deflections and the AC layer thickness are used as inputs. A value of *SSR* is then estimated (Eq. 25) using the predicted E_{ac} value, the actual H_{ac} value, and the predicted E_{Ri} value. This resulting value is defined as SSR_m. This is repeated for the value corresponding to the standard structure. This result is defined as SSR_r. The structural adjustment factor β_1 is then defined as:

$$\beta_1 = \frac{SSR_m}{SSR_r} \tag{26}$$

The adjustment factor is then applied to the estimated *SSR* value from measured deflections using the trained ANN described above, that is:

$$Adjusted \quad SSR = \frac{Estimated \quad SSR}{\beta_1} \tag{27}$$

This adjustment procedure is similar to the method presented by Garg and Thompson. (1) for adjusting D_0 to benchmark asphalt concrete and subgrade stiffnesses. The adjustment procedures were applied to the predicted values of *BDI*, *BCI*, and ε_{sg} to obtain structurally adjusted parameters.

Besides the above indicators, subgrade modulus is also used to represent the subgrade condition since the modulus and the unconfined compressive strength of cohesive soil are related by cohesion. Assuming a friction angle of zero for cohesive soil, the relationship between the unconfined compressive strength q_u and the cohesion c can be expressed as follows:

$$q_u = 2 * c \tag{28}$$

A correlation can also be found between the cohesion c and the modulus since they both are a function of the density, degree of saturation (or suction), grain size, and grain size distribution of cohesive soils. A higher value of cohesion corresponds to a higher value of subgrade modulus.

Two methods were investigated to predict subgrade modulus. The first method uses an ANN to relate E_{sg} with FWD measurements. An ANN representing E_{sg} in terms of the last three deflections and the AC layer thickness was developed. It was found that using only the last three deflections gave improved predictions for field measurements over using all seven deflections. This observation is meaningful because the outer sensor deflections are more affected by lower layer conditions, therefore better represent subgrade condition. The second method is based on statistical regression and uses surface modulus to describe E_{sg}. Using the synthetic database from dynamic, linear elastic analysis, the following relationships between the minimum surface modulus E_{smin}, calculated using Eqs. 6 and 7, and E_{sg} were developed:

For $H_{sg} \geq 160$ inches,

$$E_{sg} = \frac{E_{s\min} - 0.1406 * F_{ac}^{\ 2} - 7.2188 * F_{ac} + 2.2688}{0.1139 * F_{ac}^{\ 2} - 0.4112 * F_{ac} + 1.1551} \tag{29}$$

$$R^2 = 0.999 \qquad SEE = 0.34$$

For $H_{sg} < 160$ inches,

$$E_{sg} = \frac{E_{s\min} - 0.0186 * F_{ac}^{\ 2} - 5.4088 * F_{ac} + 1.0637}{0.108 * F_{ac}^{\ 2} - 0.1944 * F_{ac} + 39.5426 * \frac{F_{ac}}{D_{sg}^{\ 3}} + 1.033} \tag{30}$$

$$R^2 = 0.981 \qquad SEE = 0.87$$

where D_{sg} is H_{sg} in foot and F_{ac} is defined as follows:

$$F_{ac} = \frac{H_{ac} \sqrt[3]{E_{ac}}}{100} \tag{31}$$

Based on Eqs. 29 and 30, when the AC layer is weak (F_{ac} is small), the difference between E_{sg} and E_{smin} becomes negligible. Further information about the surface modulus and its application to E_{sg} prediction is provided in Appendix C.

Field data from NC 421 and NC 2427 test sections were used to study the performance of the proposed indicators in evaluating subgrade conditions. The field observations include information on FWD testing and Dynamic Cone Penetration (DCP) testing. The values from the DCP test, which was used to determine soil strength, were correlated to *CBR* strength using the following equation developed by the NCDOT:

$$\log(CBR) = 2.6 - 1.07 * \log(DCP) \tag{32}$$

The *CBR* values were then compared against the predicted values of subgrade condition indicators to evaluate their validity. A critical value for each condition indicator was then determined based on the critical value of *CBR*: a value less than 10 is typically considered to represent poor soils. Figure 5 shows the relationship between *CBR* and adjusted *BDI* values. A higher *CBR* value usually corresponds to a lower adjusted *BDI* value, and an adjusted *BDI* value of greater than 3.4 (corresponding to *CBR* less than 10) is identified as the criterion for poor subgrade. Similar trends are seen in Figures 6 through 9 for the other subgrade condition indicators. For full-depth pavements, Table 10 shows the identified criteria for poor subgrade.

It is noted that performances of the different criteria for assessing subgrade condition are different. Since detecting poor subgrade is the main concern for state highway agencies, the performance of different criteria can be evaluated by counting what percentage of pavements with measured *CBR* values less than 10 indeed meet the criteria. Even though the performance difference is not significant among the indicators, the adjusted *SSR* seems to work the best for

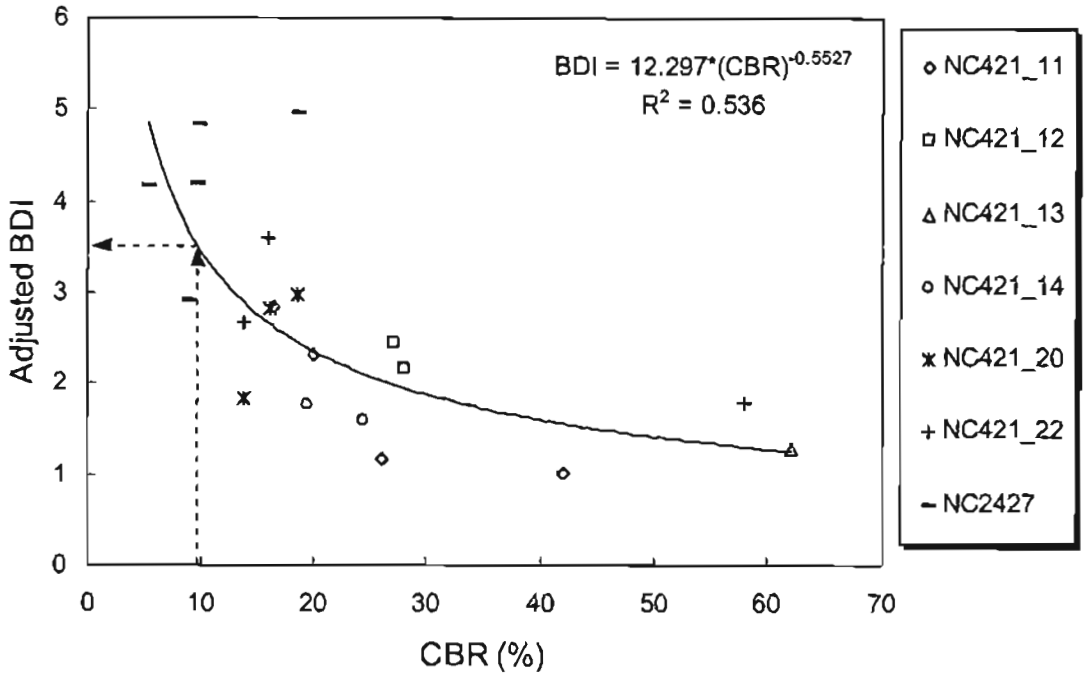

Figure 5. Adjusted BDI as subgrade condition indicator for full-depth pavement (NC 421 and NC 2427)

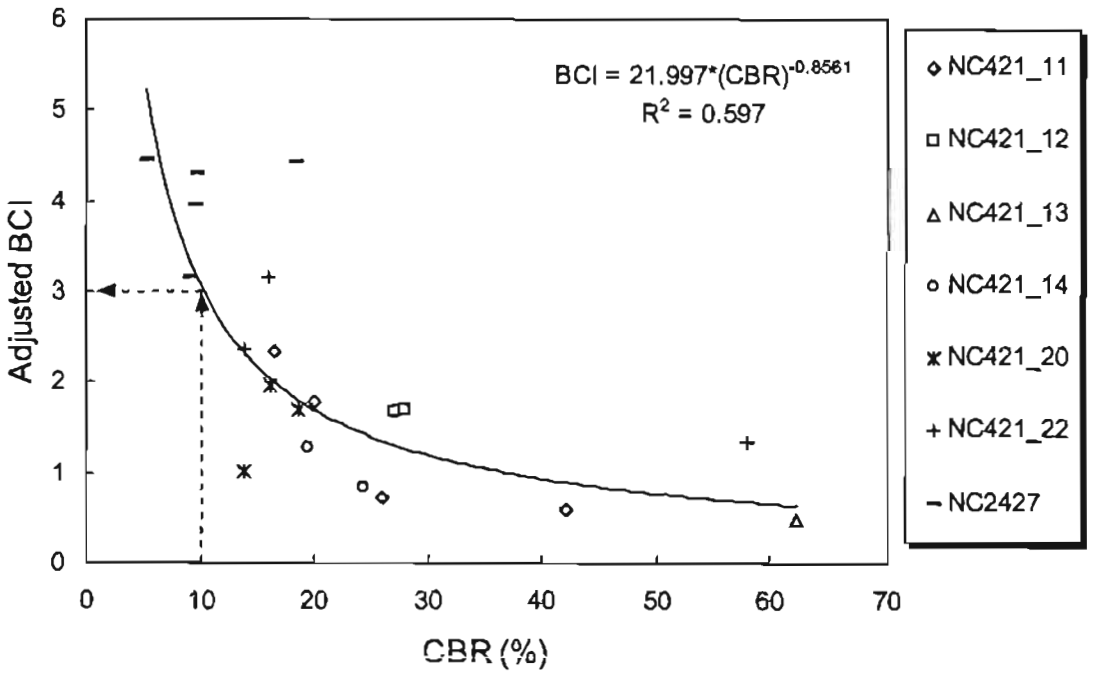

Figure 6. Adjusted BCI as subgrade condition indicator for full-depth pavement (NC 421 and NC 2427)

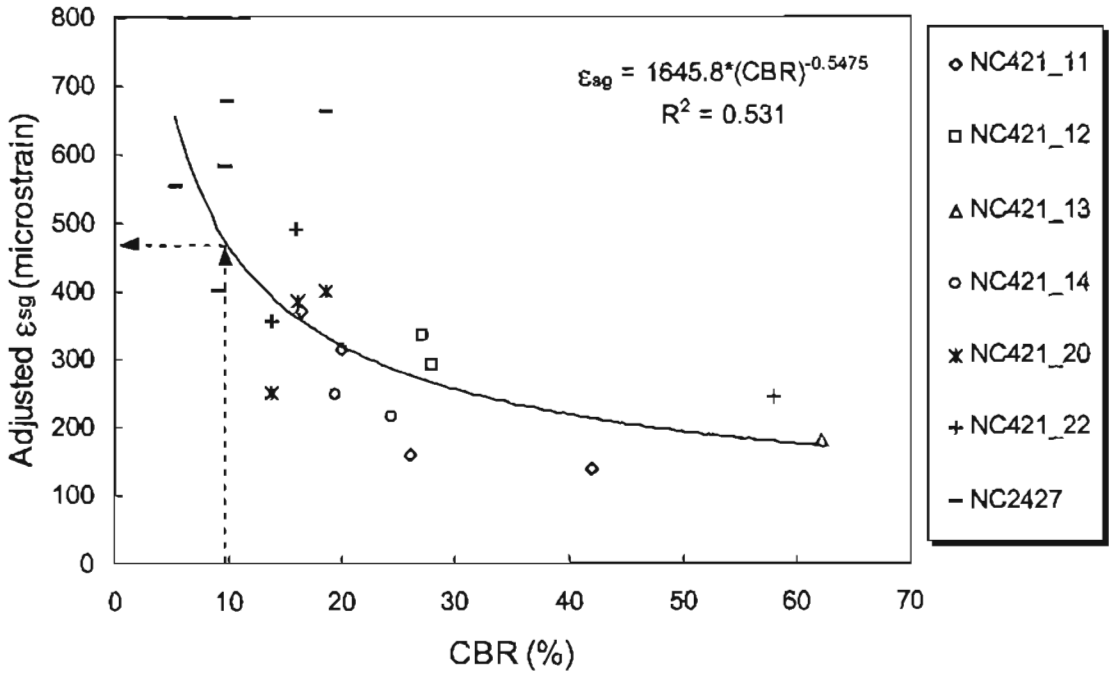

Figure 7. Adjusted ε_{sg} as subgrade condition indicator for full-depth pavement (NC 421 and NC 2427)

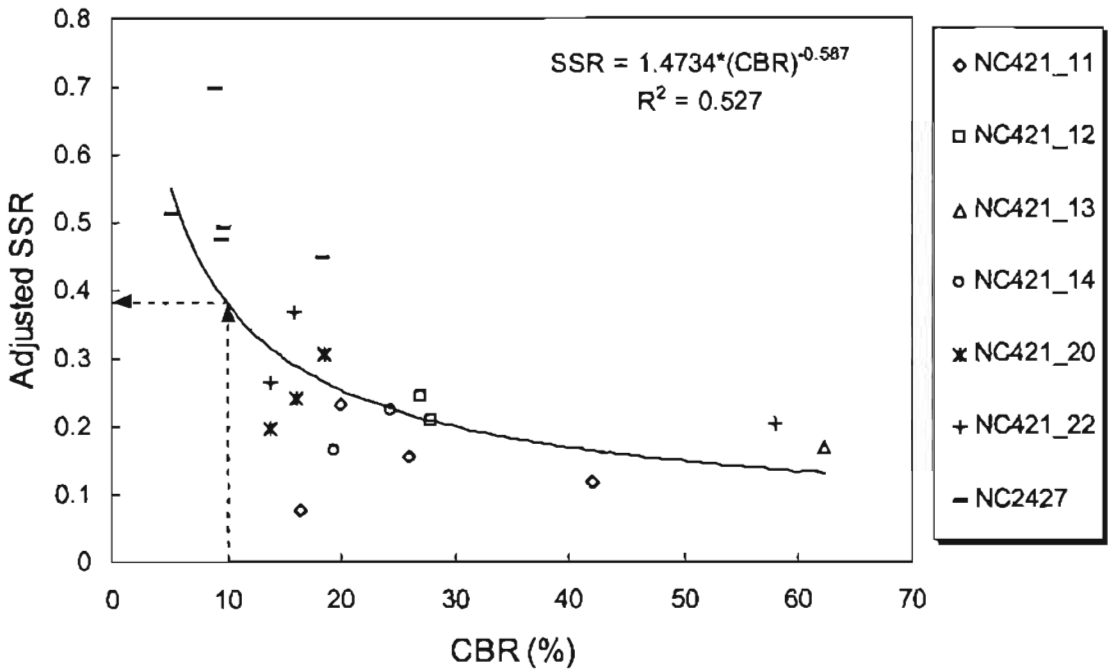

Figure 8. Adjusted SSR as subgrade condition indicator for full-depth pavement (NC 421 and NC 2427)

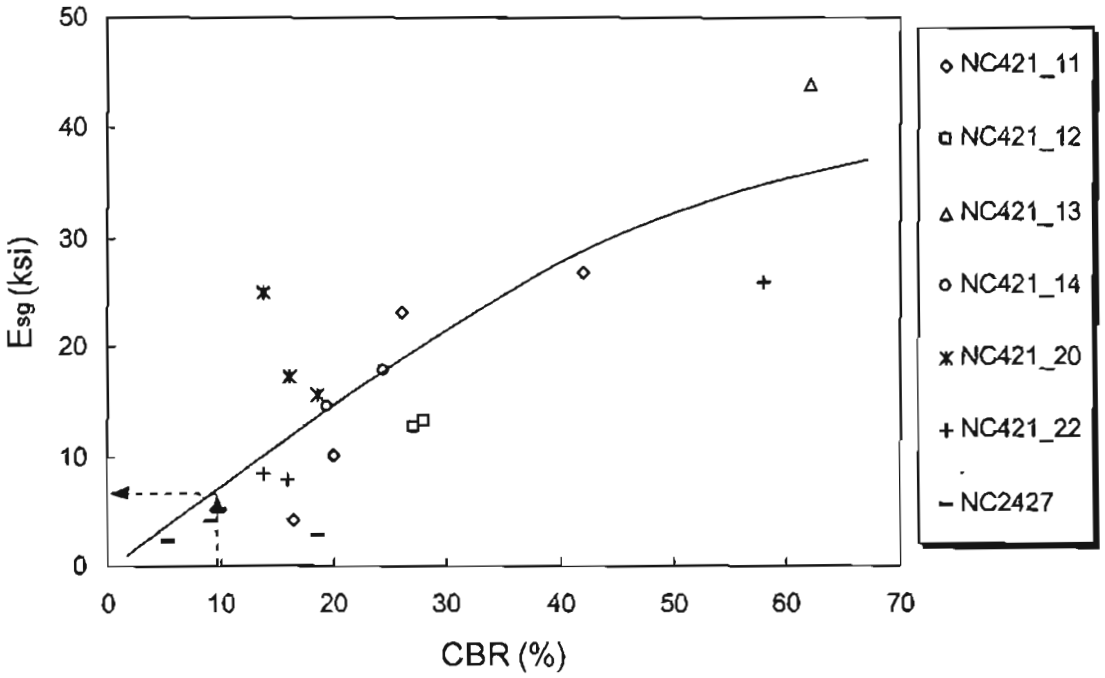

Figure 9. E_{sg} as subgrade condition indicator for full-depth pavement (NC 421 and NC 2427)

Table 10. Suggested criteria for poor subgrade in full-depth pavements

Subgrade condition indicators	Criteria for poor subgrade
Adjusted *BDI*	≥3.4 mils
Adjusted *BCI*	≥3 mils
Adjusted ε_{sg}	≥470 microstrain
Adjusted *SSR*	≥0.38
E_{sg}	≤7 ksi

detecting subgrade condition since its criterion failed in only one out of four pavements with weak subgrade. This is probably because E_{Ri} has the greatest effect on the *SSR* value, as shown in Eq. 25.

It should be noted that the adjusted ε_{sg} value after structural correction represents only the strength or rutting potential of subgrade. Overall rutting potential of a pavement is not only related to the material strength of all layers but also to the pavement structure. The actual ε_{sg} value, instead of the structurally corrected ε_{sg}, should be used to represent the contribution of the subgrade to the pavement's overall rutting potential. Considering the temperature effect on AC modulus, the actual ε_{sg} value has to be corrected to a reference AC modulus corresponding to a reference temperature at 25°C. Based on Eq. 24, the temperature adjustment factor for ε_{sg} can be expressed as:

$$\alpha_2 = \frac{\varepsilon_{sg,T_m}}{\varepsilon_{sg,T_r}} = 10^{-0.7614*\left[\log(E_{ac,T_m})-\log(E_{ac,T_r})\right]} \qquad (33a)$$

where α_2 = temperature correction factor for ε_{sg} for full-depth pavements,

ε_{sg,T_m} = subgrade compressive strain in microstrain at measured temperature T_m,

ε_{sg,T_r} = compressive strain in microstrain at reference temperature T_r of 25°C,

E_{ac,T_m} = AC modulus in ksi at measured temperature T_m,

E_{ac,T_r} = AC modulus in ksi at reference temperature T_r of 25°C,

T_m = measured temperature in °C, and

T_r = reference temperature of 25°C.

Eq. 33a can be reduced to the following simpler expression based on Eq. 9:

$$\alpha_2 = 10^{-0.7614*b*(T_r-T_m)} \qquad (33b)$$

where b is the regression constant in AC modulus-temperature relationship.

This adjustment factor is then applied to the ε_{sg} value predicted from Eq. 20 to get the adjusted ε_{ac} for the reference temperature. The limiting number of cycles to rutting of subgrade N_d can then be estimated based on ε_{sg} using the following equation:

$$N_d = f_5(\varepsilon_{sg})^{-f_6} \tag{34}$$

where f_5 and f_6 are positive regression constants. This relationship can be used either by employing the temperature-adjusted ε_{sg} value at the reference temperature for a simple comparison or by applying the cumulative damage approach. In the cumulative damage approach, ε_{sg} values at different analysis periods (e. g., month or season) are estimated from the AC modulus-temperature relationship and Eq. 24.

Depth to a Stiff Layer

A shallow depth to a stiff layer has a great impact on pavement surface deflections. The miscalculation of a shallow stiff layer depth could result in errors in predicting layer condition, especially subgrade. For instance, if a pavement has an actual stiff layer depth of 5 feet, a miscalculation of this depth to 10 feet could cause up to 40% overestimation of subgrade strength. The effect of stiff layer on surface deflections decreases as stiff layer depth increases. Figures 10 and 11 show the deflection basins computed from the dynamic finite element analysis on weak and strong pavements with varying depths of a stiff layer, respectively. It can be seen that, when stiff layer depth is greater than 15 feet, there is almost no change in deflection basins.

Three approaches were examined in this research to predict the depth to a stiff layer: the direct R_0 method, the Modulus 5.1 method, and the ANN-based approach developed from

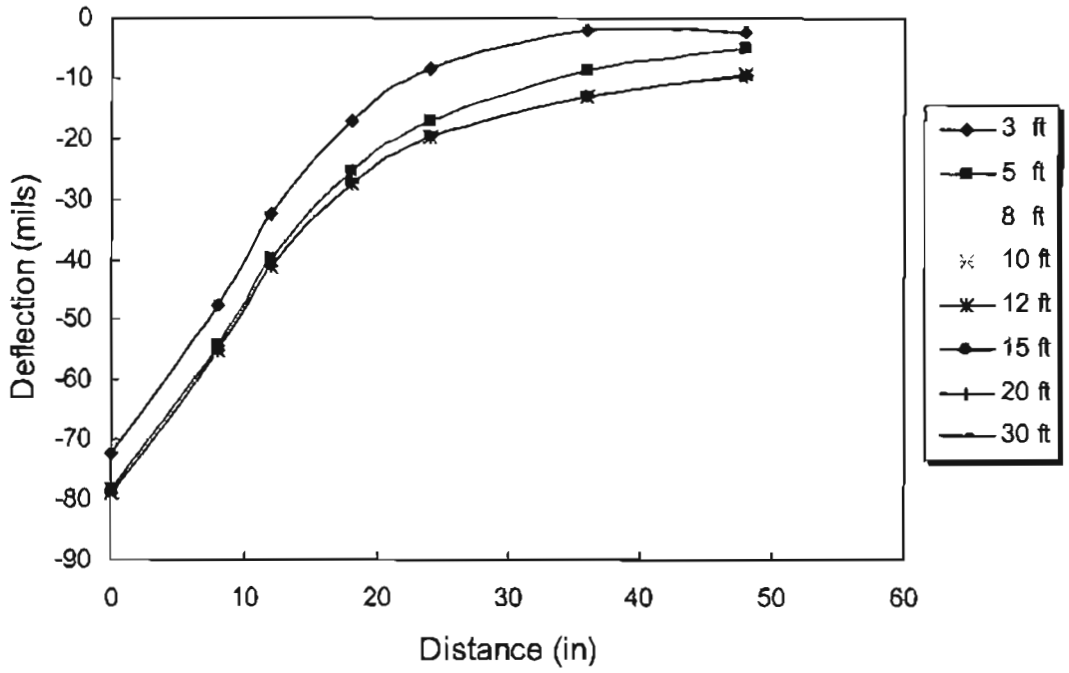

Figure 10. Computed peak surface deflections with various DSLs for a weak pavement

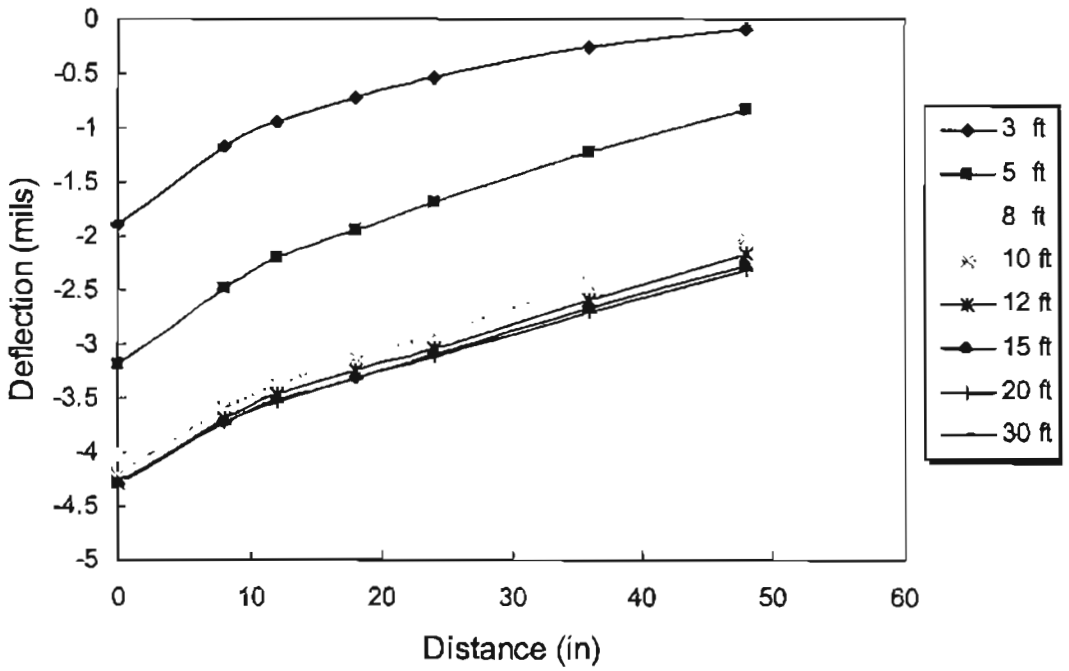

Figure 11. Computed peak surface deflections with various DSLs for a strong pavement

dynamic, linear elastic analysis. The R_0 method is based on the premise that the majority of the measured surface deflection at any offset is a result of the deflection below a certain depth in the pavement. If a stiff layer exists at some depth, then no surface deflection will occur beyond the offset at which the stress zone and the stiff layer intercept. The method to predict the apparent depth to a stiff layer is based on the hypothesis that the position of zero surface deflection should be strongly related to the depth in the pavement at which no deflection occurs. A plot of the measured surface deflection against the inverse of the distance from the center of the applied load (1/r) is used to estimate the depth at which zero deflection occurs. In actual pavements the deflection versus 1/r plot is only linear over the mid part of the curve. Nonlinearities associated with stiff upper layers and stress-sensitive subgrades tend to curve both the upper and lower portions of the deflection versus 1/r plot. In these cases, the zero deflection point is estimated by extrapolating the linear portion of the 1/r curve to the x-axis intercept.

The Modulus 5.1 method utilizes an improved version of the R_0 theory. Improvements were made by accounting for the stiffness and thickness of the upper layers. This was done by using the basin shape factors SCI, BCI, and BDI in a series of theoretically generated equations relating known depth to a stiff layer to these basin parameters and the 1/r intercept.

Seven deflections, AC layer thickness, and DBPs F_2 and F_3 are used as inputs in the ANN approach. F_2 and F_3, as defined in Table 2, were selected because they are the two most sensitive parameters to thickness of subgrade based on the sensitivity study. Their addition as inputs of the ANN improved prediction performances. The DSL prediction values, actual DSL values , and Root-Mean-Square-Errors (RMSEs) of five SMP pavements are shown in Figures 12 through 16.

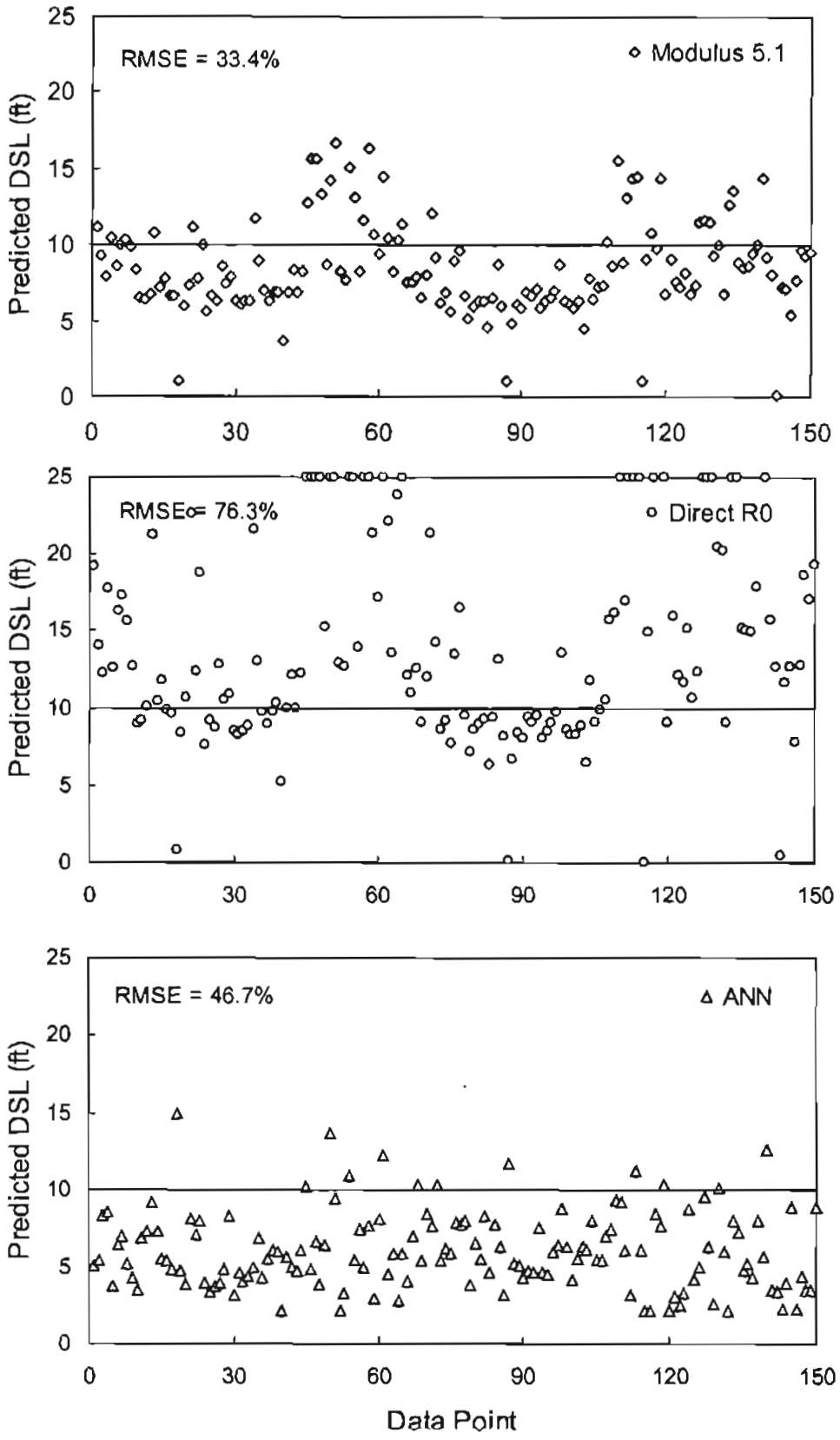

Figure 12. Comparison of DSL prediction from different approaches for full-depth pavement 21-1034 (Actual DSL = 10 ft)

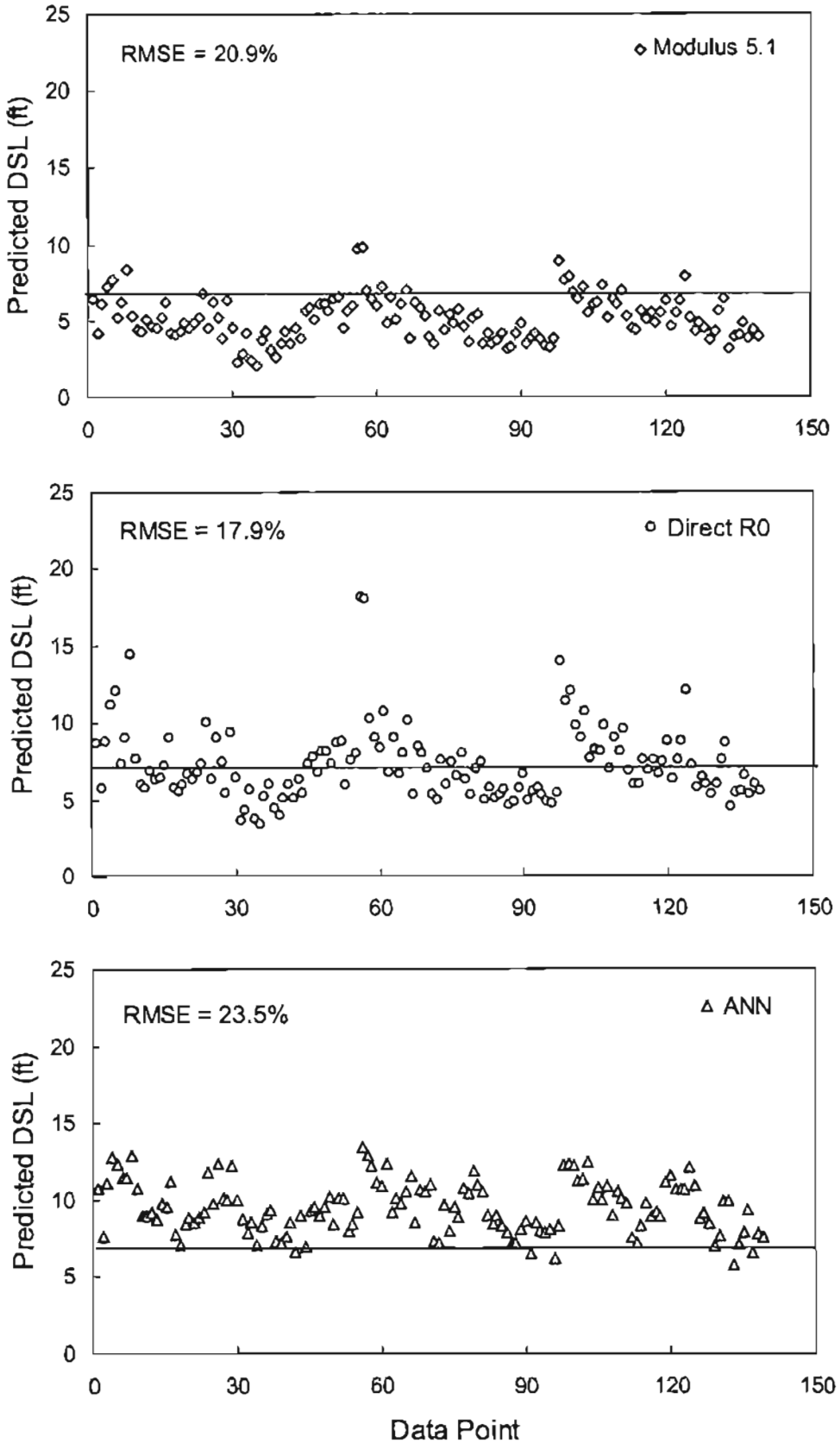

Figure 13. Comparison of DSL prediction from different approaches for full-depth pavement 4-1025 (Actual DSL = 7 ft)

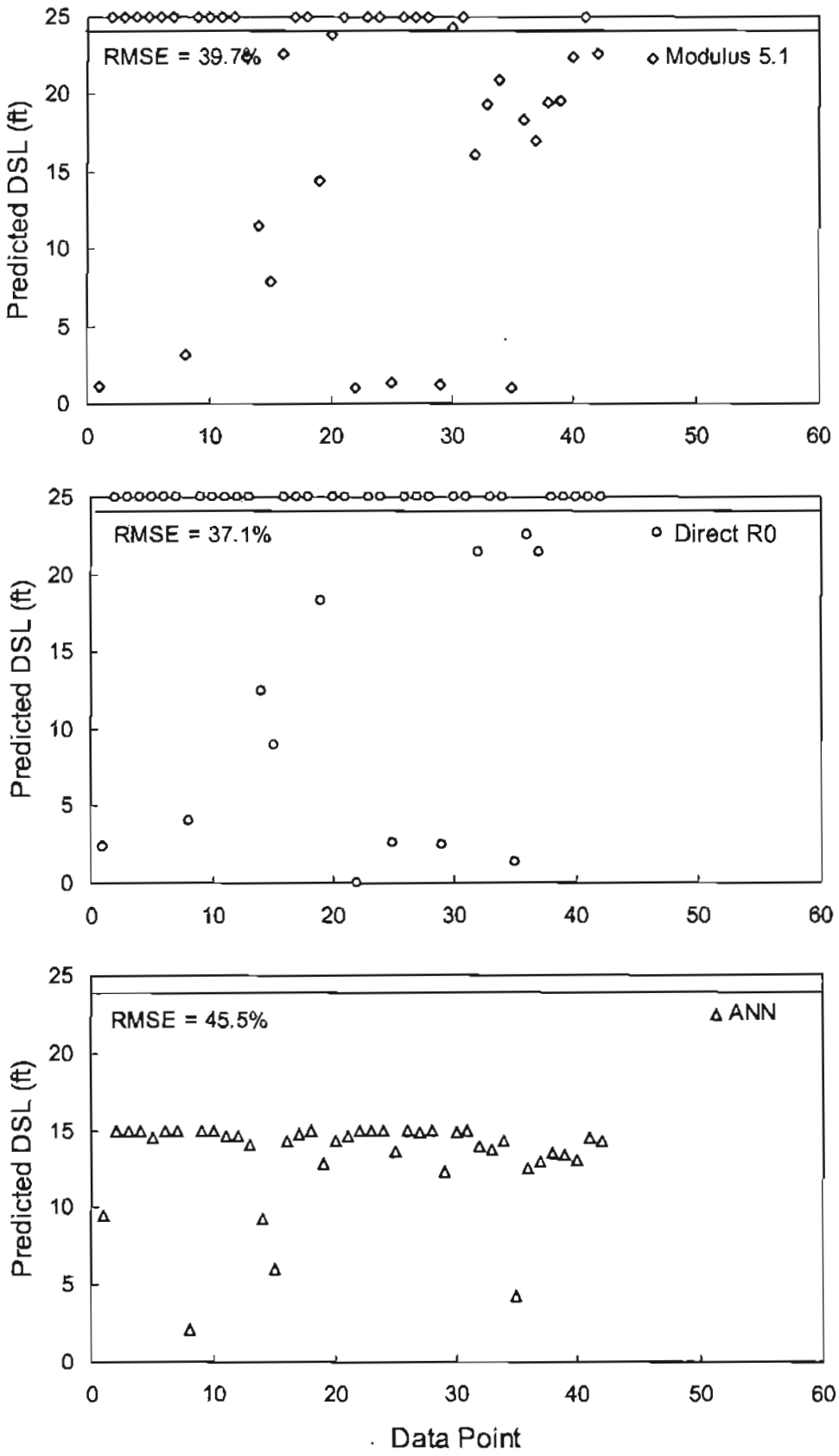

Figure 14. Comparison of DSL prediction from different approaches for full-depth pavement 46-9106 (Actual DSL = 24 ft)

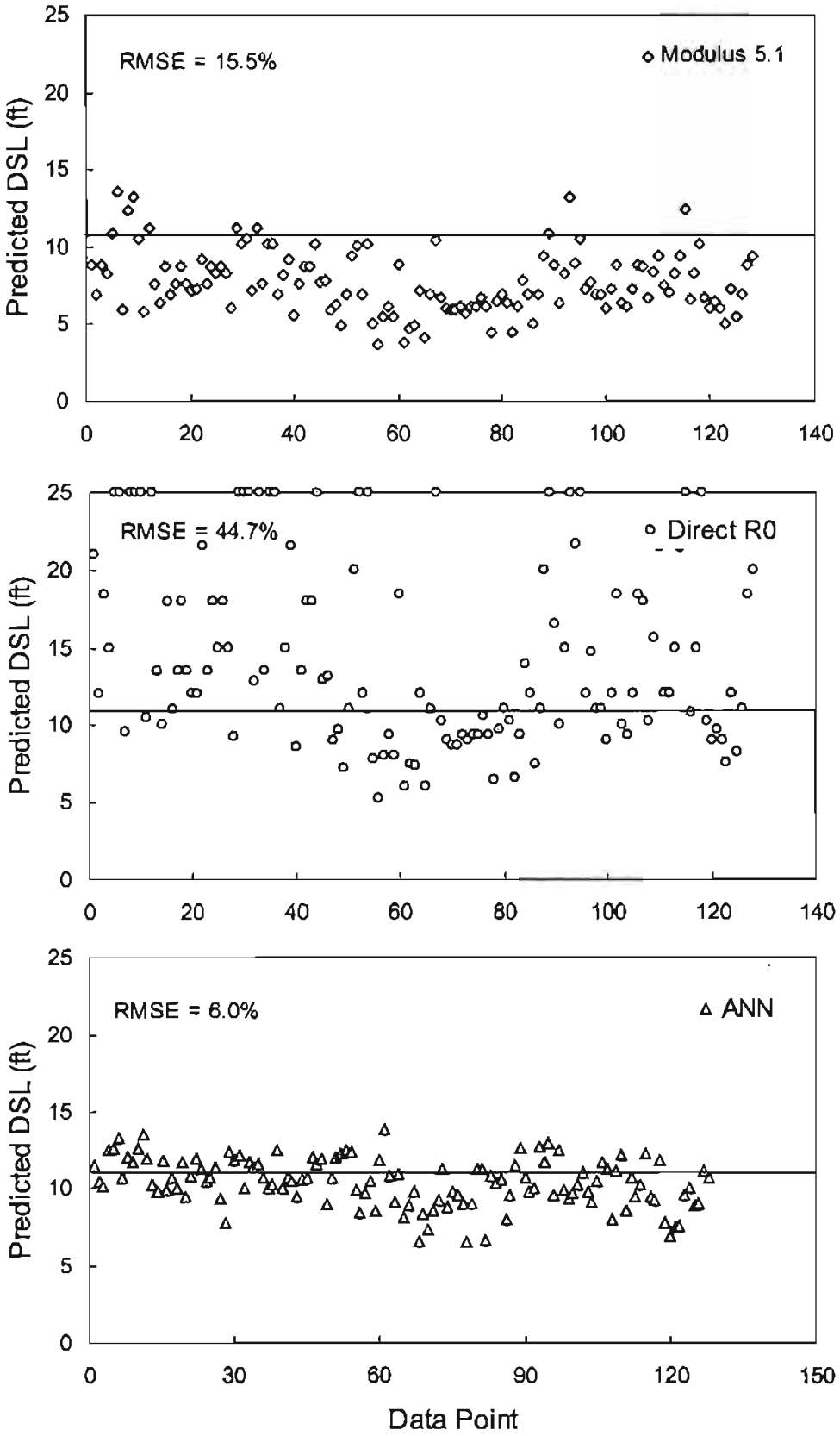

Figure 15. Comparison of DSL prediction from different approaches for full-depth pavement 47-9024 (Actual DSL = 11 ft)

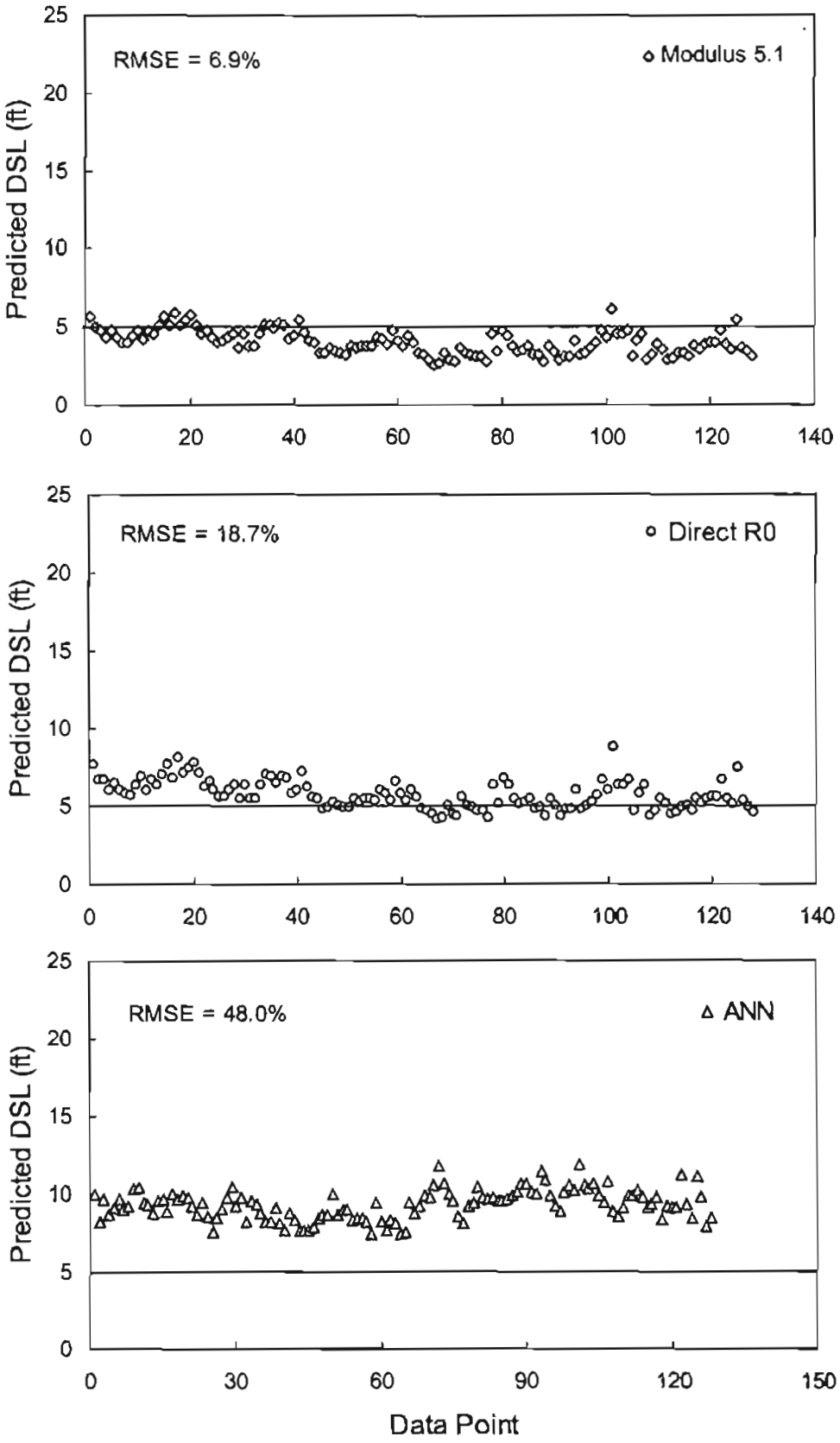

Figure 16. Comparison of DSL prediction from different approaches for full-depth pavement 81-8529 (Actual DSL = 5 ft)

The Modulus 5.1 approach has better prediction performances than the direct R0 approach, which is to be expected, since the Modulus 5.1 approach is a modified version of the R_0 method. Although the ANN-based approach was developed from the dynamic analysis, which is believed to better simulate the actual FWD loading and the effect of stiff layer on deflections, no significant improvement was observed in the DSL predictions when using the ANN approach. It should be noted that the ranges of predictable DSL for each approach are different. A value of 25 ft is the maximum DSL prediction for both the direct R0 approach and the Modulus 5.1 approach, while the range of the DSL is up to 15 feet for the ANN approach. The large prediction error from the ANN in Figure 14 should not be a concern because the effect of stiff layer on pavement evaluation is insignificant after 15 feet. That is, in Figure 14, how many predictions fall below 15 feet should be a concern instead of the ability to predict the actual DSL value around 24 feet. It can be seen that the ANN approach results in the least number of points predicted below around 15 feet. Another observation from these figures is that the results from the direct R_0 method seemed to be more scattered than those from the other two approaches, while the results from the ANN approach seemed to be more consistent.

AGGREGATE BASE PAVEMENTS

The following sections describe the efforts made in determining the condition of aggregate base pavements as listed in the research plan. For distressed pavements, the cracking, stripping, and debonding in AC layer, base strength, subgrade strength, and depth to a stiff layer were investigated. Fatigue cracking and rutting potentials were also studied for intact pavements. The DBPs chosen from the sensitivity study were investigated along with optimized ANN structures.

A set of regression equations correlating the DBPs to layer condition indicators was also developed from the synthetic data. The final results of these investigations are presented below.

AC Layer Condition

Cracking and Stripping

For aggregate base pavements, Eqs. 4 and 5 as well as the SLIC method can be used to detect unusual deflections that result from severe cracking and stripping in AC layer. Also, similar to the approach described for the full-depth case, AC modulus can be used to detect cracking and stripping in the AC layer by comparing the predicted modulus value with the appropriate modulus value from the modulus-temperature relationship of intact pavements.

The ANN and regression based approaches were developed to predict E_{ac}. These approaches were developed using the synthetic database from dynamic, nonlinear finite element analysis. In the ANN-based approach, the deflections from the five sensors closest to the load center, *SCI* and *BDI*, and thicknesses of AC and base layers were used as inputs. In the regression-based approach, the following equations were developed to predict E_{ac}:

For $H_{ac} \geq 6$ inches,

$$\log(E_{ac}) = -1.1435 * \log(SCI) - 2.5435 * \log(H_{ac}) + 0.0498 * H_{ac} + 5.2005 \qquad (35)$$

$$R^2 = 0.988 \qquad SEE = 0.039$$

For $H_{ac} < 6$ inches,

$$\log(E_{ac}) = -2.4527 * \log(SCI) + 1.4116 * \log(BDI) - 2.1621 * \log(H_{ac}) + 0.0013 * H_{abc} + 5.1230 \qquad (36)$$

$$R^2 = 0.965 \qquad SEE = 0.099$$

The data from four sections of the Mn/ROAD test facility were used to verify this procedure. These four sections were constructed between Fall 1992 and Summer 1993. Traffic

was introduced in mid-June 1994. Different types of distresses, such as fatigue cracking, thermal cracking, and rutting, had appeared at test locations by mid-1998. The AC modulus for each FWD test conducted between March and June 1994 was predicted using the regression based approach. Figure 17 compares these predictions as a function of mid-depth temperature. While these predictions for the different sections, which were assumed to be intact during the 1994 tests, show similar modulus vs. temperature trends, a corresponding set of predictions for tests carried out in 1998 (Figure 18) shows appreciable variations. Section 28 was the most distressed pavement, according to the visual condition survey performed in 1998 and shows the smallest values of E_{ac}.

The data from Arizona pavement 04-0902 were also used to check the above procedure in detecting distresses in AC layer. FWD measurements as well as air and pavement temperatures of this pavement were stored in DataPave 2.0. It was also recorded from DataPave 2.0 that the pavement was intact in 1994 and stripping was observed after 1995. Figure 19 shows the predicted AC moduli as a function of surface temperature in 1994, 1995, and 1998. It can be seen that the AC modulus values in 1995 and 1998 were significantly lower than those in 1994, indicating distresses in the AC layer.

Debonding

As mentioned for the full-depth pavement case, a single FWD measurement is not sufficient to distinguish between a debonded pavement and an intact pavement with lower strength. The data from US 220 test sections were used to demonstrate this difficulty. FWD testing was performed on US 220 pavements in both 1995 and 1996. Backcalculated moduli values from these deflections suggested that the subgrade was weak. However, coring and DCP

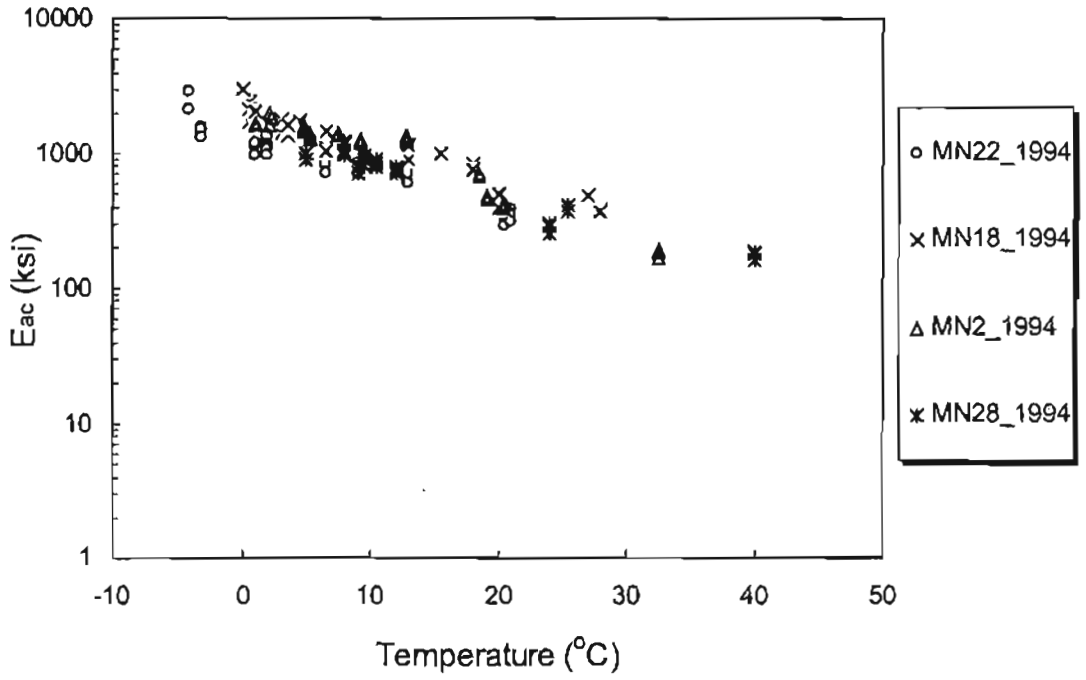

Figure 17. Predicted E_{ac} vs. temperature for aggregate base pavements from Mn/ROAD intact pavements, 1994

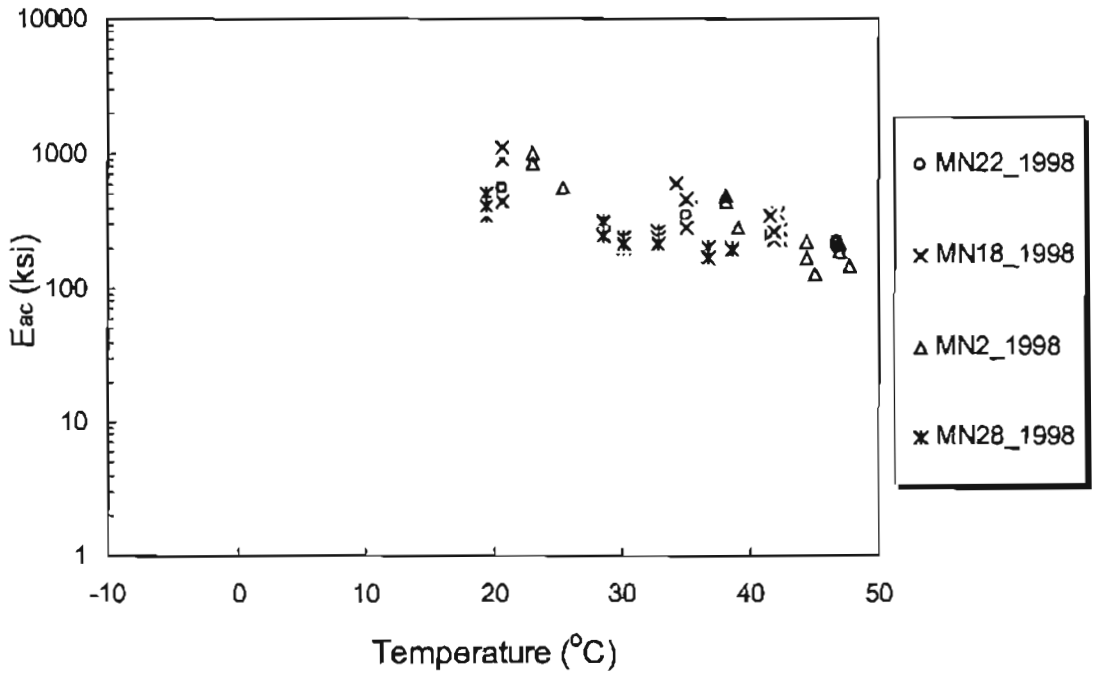

Figure 18. Predicted E_{ac} vs. temperature for aggregate base pavements from Mn/ROAD distressed pavements, 1998

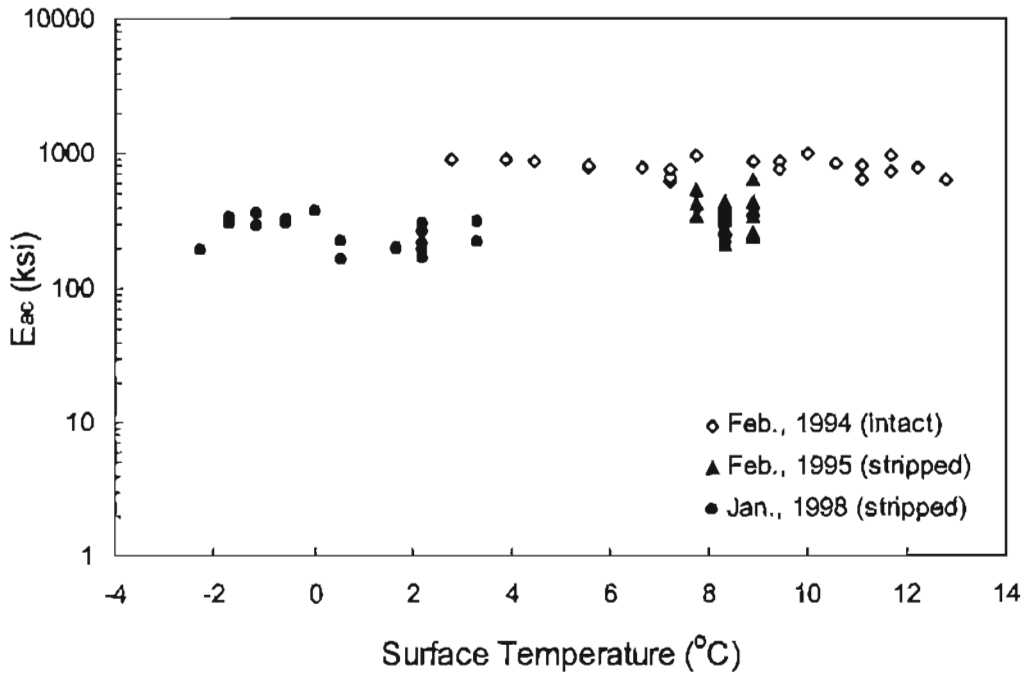

Figure 19. Predicted E_{ac} vs. temperature for pavement 4-0902

testing of this pavement in 1996 revealed that the subgrade was strong. In 1995, debonding in AC layer began to be reported from the core information. By 1996, debonding had already become a serious problem for pavement performance. It was evident from the backcalculated moduli and the coring and DCP test results that larger outer sensor deflections due to debonding were incorrectly attributed to a weak subgrade by the backcalculation program. This misprediction has a significant implication in terms of rehabilitation cost. If debonding could be detected and subgrade was estimated strong, the resulting rehabilitation strategy will not include the repair of subgrade. However, the backcalculation results would incorrectly suggest a full-depth repair of this section.

To test the accuracy of the condition evaluation methods developed in this research, several condition indicators were predicted for AC layer and subgrade, including layer moduli and adjusted BCI, ε_{sg}, and SSR for subgrade. The definitions and evaluation methods of the subgrade condition indicators will be presented later under "Subgrade Strength" section. As will be demonstrated in that section, the field verification of these indicators based on DCP results was fairly good.

Figure 20 shows predicted AC moduli as a function of pavement temperatures for both 1995 and 1996. It can been seen that the E_{ac} values in 1996 are lower than those values in 1995, although the pavement temperatures in 1996 are much lower than 1995. This indicates some possible distresses in the AC layer, which agrees with the known condition of AC layer. Figure 21 shows predicted E_{sg} values versus position for both 1995 and 1996. It can been seen that in 1996 the effect of debonding on deflections was mistakenly identified as poor subgrade (mostly less than 7 ksi of E_{sg}). Similar predictions are made in Figures 22 through 24 based on other subgrade condition indicators (adjusted *BCI*, ε_{sg}, and *SSR*). Although general conclusions cannot

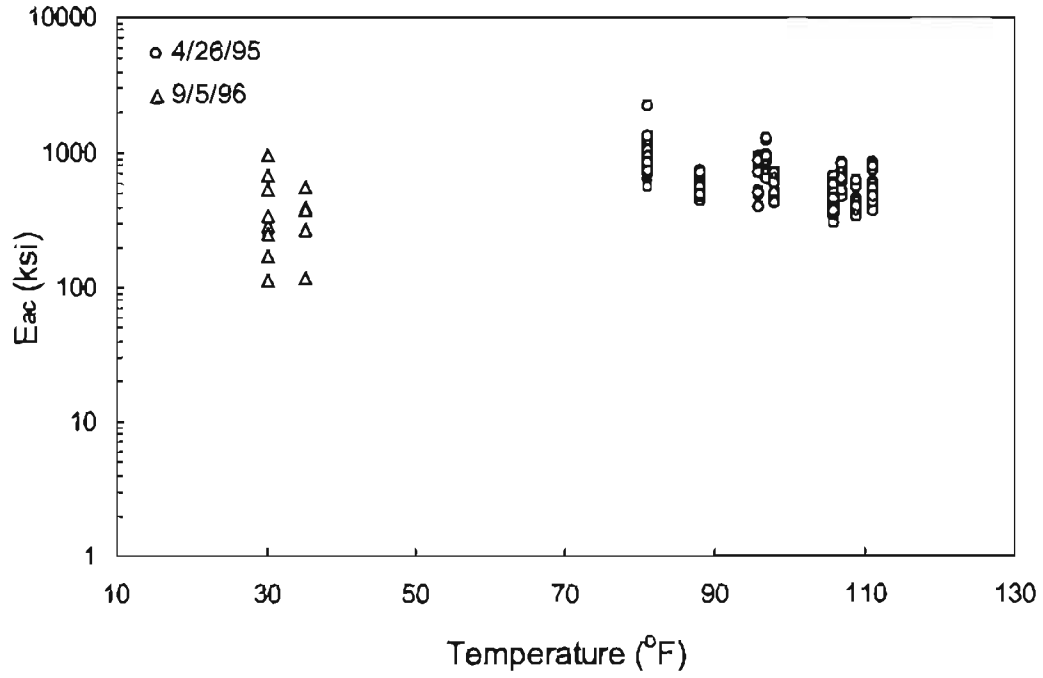

Figure 20. E_{ac} vs. temperature for aggregate base pavements from US 220 debonded pavements

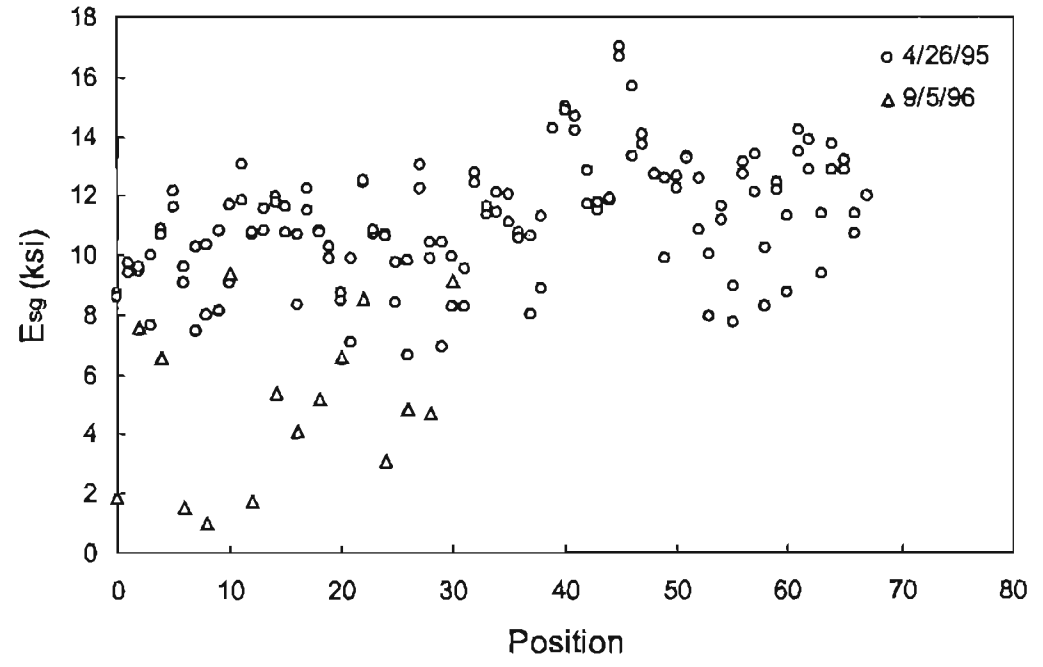

Figure 21. E_{sg} position for aggregate base pavements from US 220 debonded pavements

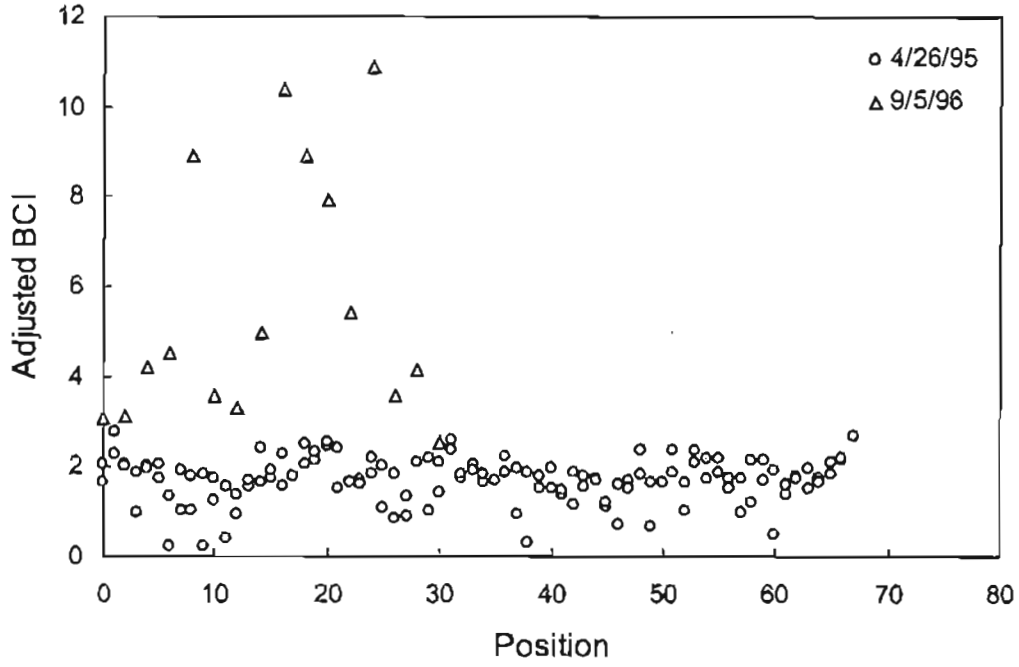

Figure 22. Adjusted BCI vs. position for aggregate base pavements from US 220 debonded pavements

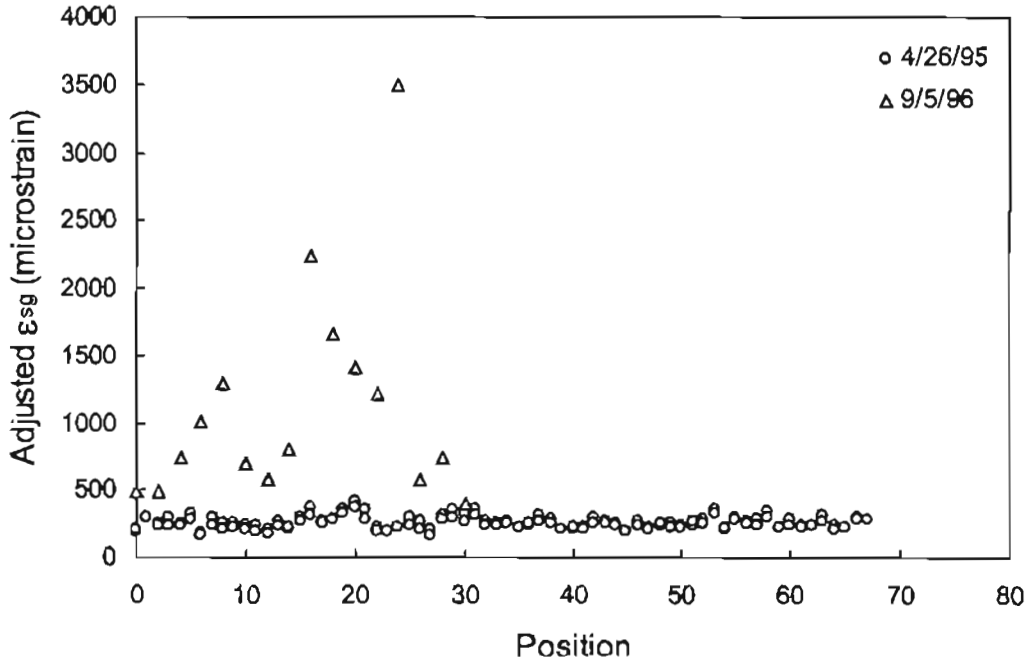

Figure 23. Adjusted ε_{sg} vs. position for aggregate base pavements from US 220 debonded pavements

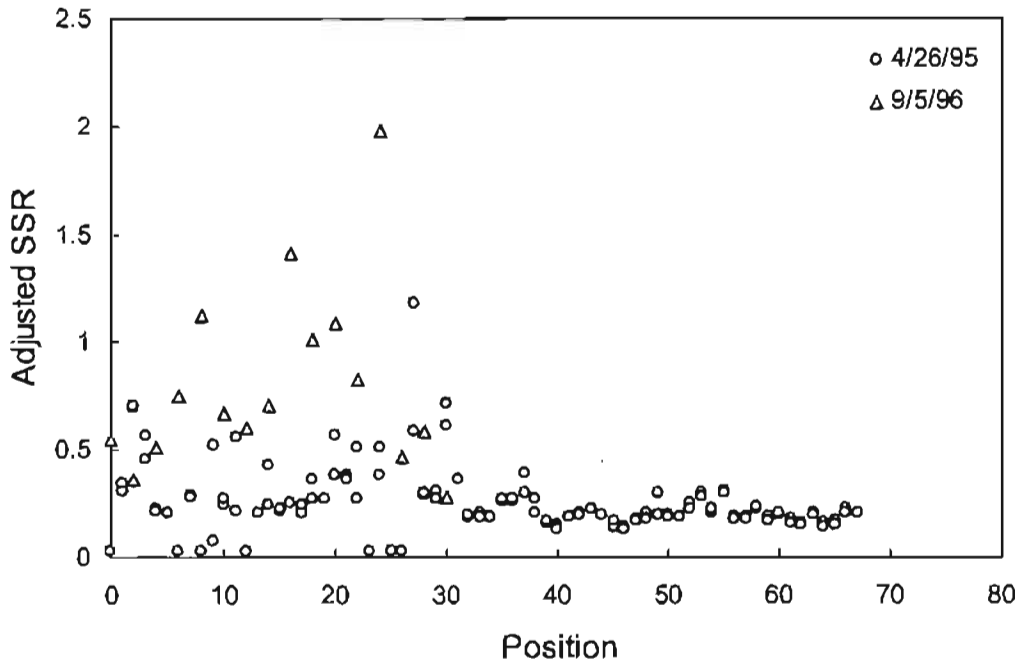

Figure 24. Adjusted *SSR* vs. position for aggregate base pavements from US 220 debonded pavements

be made based on one case, this example demonstrates the difficulty of distinguishing between debonding and weak subgrade from FWD 9-kip deflections.

Cracking Potential

For aggregate base pavements, the tensile strain at the bottom of the AC layer was found to be a good indicator for pavement cracking potential. This parameter is predicted from the following equations that were developed from the nonlinear synthetic database:

For $H_{ac} \geq 6$ inches,

$$\log(\varepsilon_{ac}) = 1.0230 * \log(BDI) + 1.7227 \tag{37}$$

$$R^2 = 0.981 \qquad SEE = 0.052$$

For $H_{ac} < 6$ inches,

$$\log(\varepsilon_{ac}) = 0.7798 * \log(SCI) + 0.2279 * \log(BDI) + 0.5736 * \log(H_{ac}) + 0.0410 * \log(H_{abc}) + 1.1604 \tag{38}$$

$$R^2 = 0.969 \qquad SEE = 0.041$$

Similar to the temperature adjustment procedure for ε_{ac} described in the "Cracking Potential" section for full-depth pavements, the effect of temperature on ε_{ac} is adjusted by considering the temperature effects on E_{ac}. To achieve this, the following relationship between ε_{ac} and E_{ac} was developed:

$$\log(\varepsilon_{ac}) = -0.6411 * \log(E_{ac}) - 0.6267 * \log(H_{ac}) - 0.0346 * H_{ac} - 0.0882 * \log(H_{abc}) - 0.0317 * \log(E_{Rl}) + 4.8664 \tag{39}$$

$$R^2 = 0.973 \qquad SEE = 0.071$$

Using Eq. 39, the temperature adjustment factor for ε_{ac} is expressed as follows:

$$\alpha_3 = \frac{\varepsilon_{ac,T_m}}{\varepsilon_{ac,T_r}} = 10^{-0.6411*\left[\log(E_{ac,T_m})-\log(E_{ac,T_r})\right]} \quad (40a)$$

Eq. 40a can be reduced to the following simpler expression based on Eq. 9:

$$\alpha_3 = 10^{-0.6411*b*(T_r-T_m)} \quad (40b)$$

where b is the regression constant in AC modulus-temperature relationship. This adjustment factor is then applied to the ε_{ac} value predicted from Eq. 37 or 38 to get the adjusted ε_{ac}. Pavement fatigue life can also be estimated from temperature adjusted ε_{ac} using Eq. 18.

The data from Mn/ROAD test sections were used to verify the predictability of cracking potential using the above procedure. Areas of fatigue cracking were available from MnDOT for April and October 1998. Also available was the deflections and temperatures measured from these sections when they were intact in 1994. The temperature adjustment procedure described above was applied to ε_{ac} values determined from the deflections, and the adjusted ε_{ac} values were plotted against the fatigue cracking areas measured in 1998 (Figure 25). A general trend was found that the larger area of fatigue cracking in 1998 corresponded to a larger ε_{ac} value in 1994. This conclusion was further supported by the fact that the traffic on Section 28 was lighter than the other three sections.

Base Strength

Prediction of base layer condition was a challenging task in this research. Based on the analysis of synthetic data, it was found that only a small portion of pavement surface deflections from FWD testing is affected by the base layer properties. Garg and Thompson (7) also concluded, based on an analysis of field measurements from Mn/ROAD test sections, that the

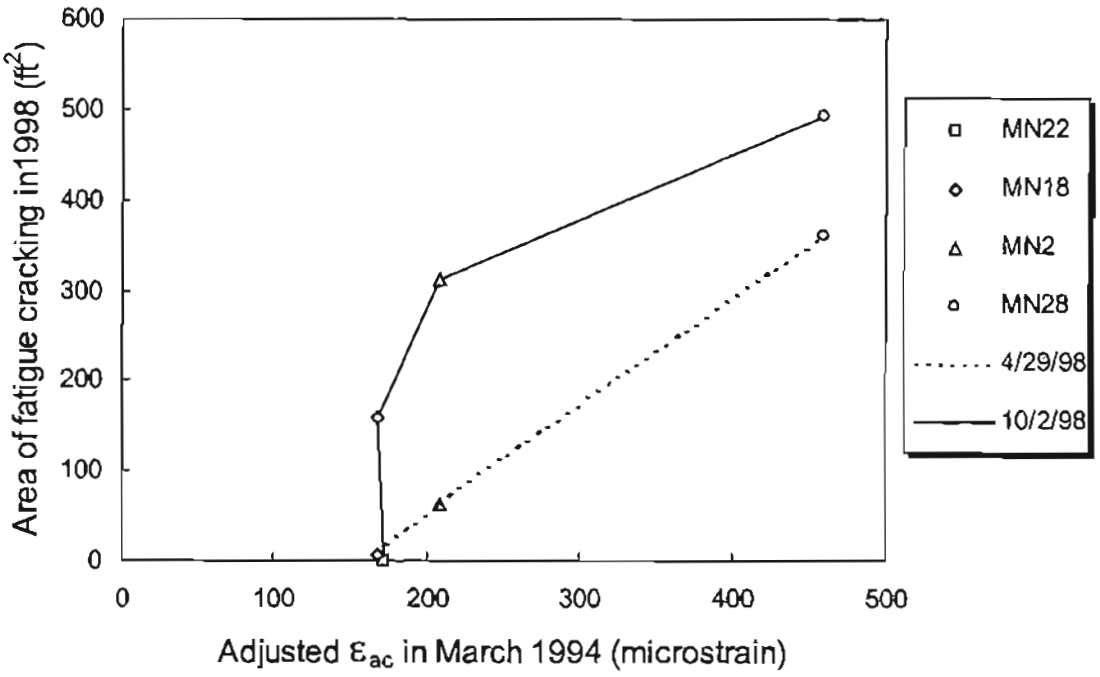

Figure 25. Adjusted ε_{ac} vs. area of fatigue cracking for aggregate base pavements from Mn/ROAD test sections

quality of base layer has no significant effect on pavement surface deflections; it has, however, a significant effect on the long-term performance of the pavements. Investigation of aggregate base pavements concluded that the compressive strain on top of base layer, ε_{abc}, and the *BDI* value are good indicators for long-term performance as represented by base strength or rutting potential.

A regression analysis of the synthetic data resulted in the following equations for ε_{abc} in microstrain:

For $H_{ac} \geq 6$ inches,

$$\log(\varepsilon_{abc}) = 0.9958 * \log(BDI) + 2.1955 \tag{41}$$

$$R^2 = 0.976 \qquad SEE = 0.052$$

For $H_{ac} < 6$ inches,

$$\log(\varepsilon_{abc}) = 0.7357 * \log(SCI) + 0.1043 * \log(BDI) + 0.1240 * \log(H_{ac}) + 0.0648 * \log(H_{abc}) + 2.073 \tag{42}$$

$$R^2 = 0.963 \qquad SEE = 0.054$$

Higher values of *BDI* and ε_{abc} represent poorer base quality. As described previously, *BDI* and ε_{abc} are dependent on the pavement structure, and therefore a structural correction approach is needed. These indicators can be described in terms of structural parameters by the following equations:

$$\log(BDI) = -0.5169 * \log(E_{ac}) - 0.9696 * \log(H_{ac}) - 0.0252 * H_{ac} - 0.1576 * \log(H_{abc}) - 0.0531 * \log(E_{Ri}) + 3.1552 \tag{43}$$

$$R^2 = 0.983 \qquad SEE = 0.087$$

$$\log(\varepsilon_{abc}) = -0.5700 * \log(E_{ac}) - 0.8404 * \log(H_{ac}) - 0.0322 * H_{ac} - 0.0170 * \log(H_{abc}) - 0.0045 * \log(E_{Ri}) + 5.2106 \tag{44}$$

$$R^2 = 0.971 \qquad SEE = 0.078$$

Using these equations, the indicators *BDI* and ε_{abc} are estimated for the pavement structure in question and for a standard structure. The following standard structure was used: H_{ac} = 6 inch, E_{ac} = 500 ksi, H_{abc} = 10 inch, E_{Rj} = 7 ksi, and H_{sg} = infinite. Using a similar approach previously, an adjustment factor is computed and then applied to the *BDI* and ε_{abc} that are estimated from Eqs. 13, 41, and 42.

The data from NC 421 and NC 2026 test sections were used to validate the prediction performances of the above procedures for detecting base strength. Both FWD and DCP test data were available for seven NC 421 test sections and NC 2026 test sections. Among them, NC 421 sections 2 and 5 have very strong cement stabilized subgrade, and NC 421 sections 17 and 24 have lime stabilized subgrade. Figures 26 and 27 show the adjusted values of the condition indicators *BDI* and ε_{abc} versus the estimated *CBR* values of the base material from DCP measurements. The trend lines in these figures show an expected behavior, i.e., increasing values of the indicators with decreasing *CBR* values. For the same data set, the base modulus, E_{abc}, predicted from the ANN are plotted against the *CBR* values (Figure 28). As expected, no meaningful relationship could be found because the stiffness of the base layer, if within a reasonable range, has no significant effect on pavement surface deflections. Using the commonly accepted criterion that $CBR \leq 100$ (corresponding to DCP > 2.6 mm/blow) represents a poor base condition, the criteria for *BDI* and ε_{abc} are established as shown in Table 11.

Similar to the temperature adjustment procedure for ε_{sg} described previously, the temperature adjustment factor for ε_{abc} is expressed as follows:

$$\alpha_4 = \frac{\varepsilon_{abc,T_m}}{\varepsilon_{abc,T_r}} = 10^{-0.57*\left|\log(E_{ac,T_m}) - \log(E_{ac,T_r})\right|} \qquad (45a)$$

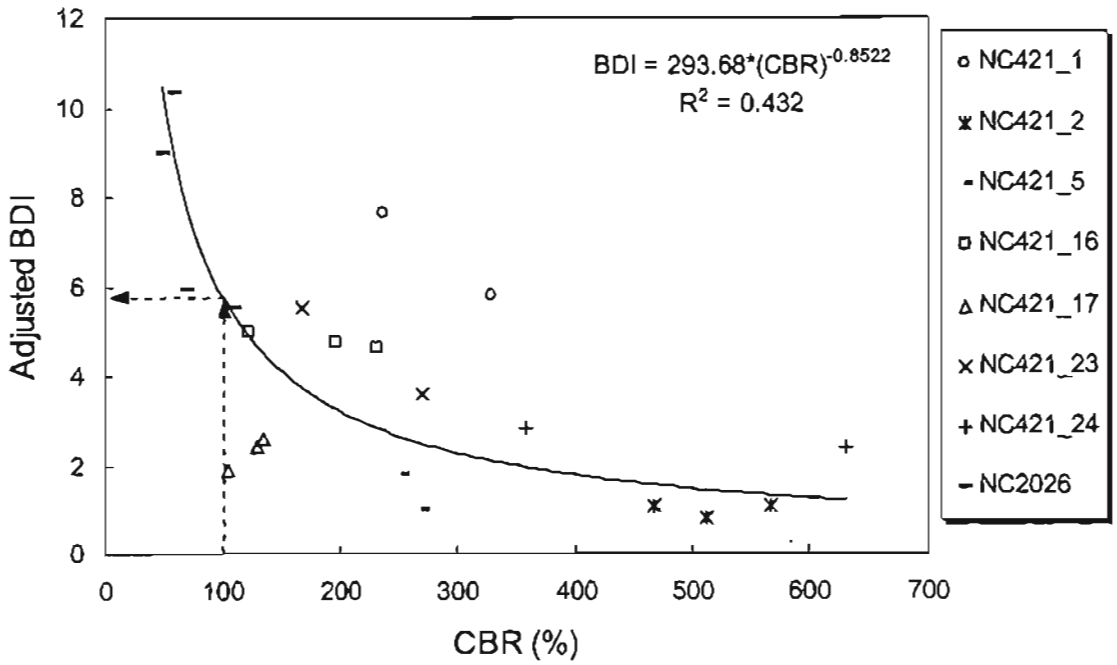

Figure 26. Adjusted BDI as base layer condition indicator for aggregate base pavements (NC 421 and NC 2026)

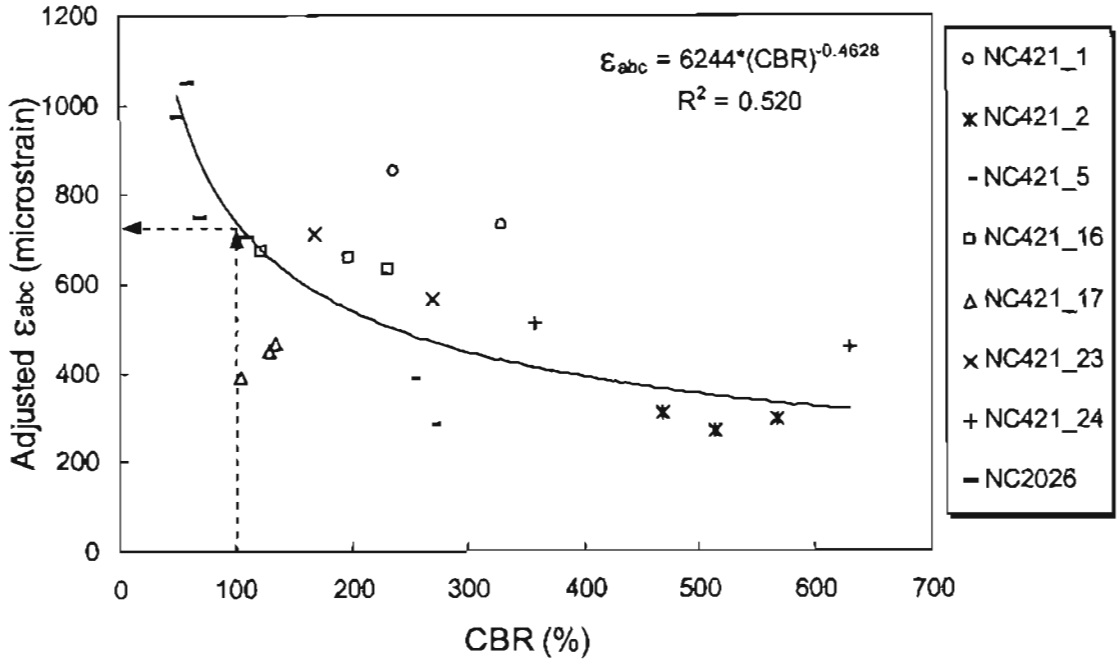

Figure 27. Adjusted ε_{abc} as base layer condition indicator for aggregate base pavements (NC 421 and NC 2026)

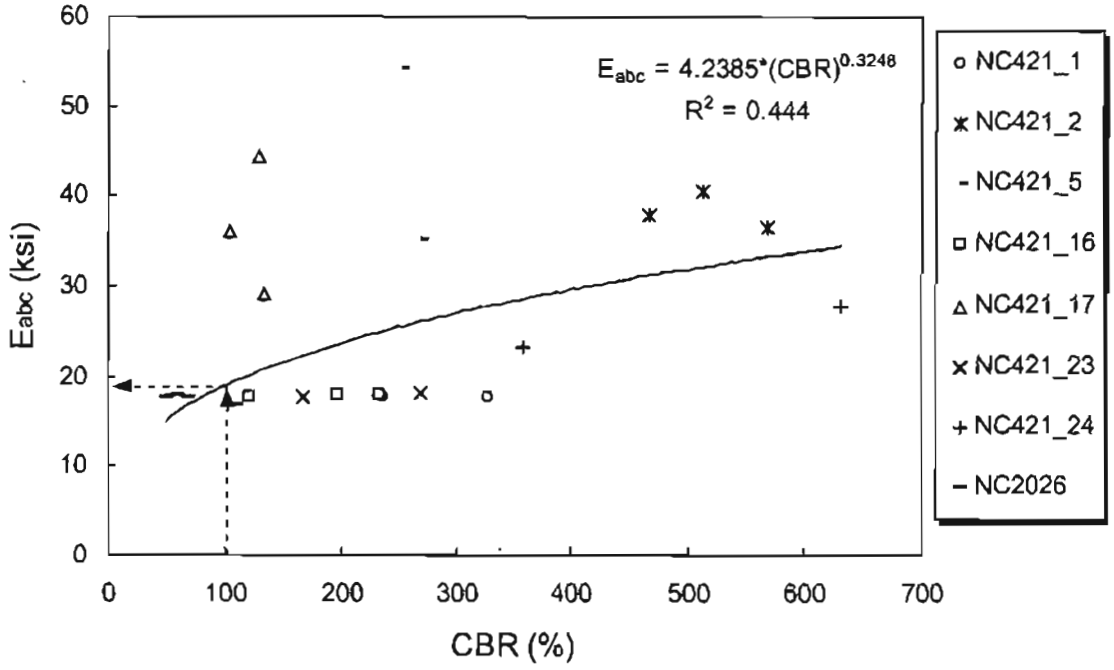

Figure 28. Adjusted E_{abc} as base layer condition indicator for aggregate base pavements (NC 421 and NC 2026)

Table 11. Suggested criteria for poor base in aggregate base pavements

Base condition indicators	Criterion for poor base condition
Adjusted ε_{abc}	$\geq$ 720 microstrain
Adjusted *BDI*	$\geq$ 5.8 mils

$$\alpha_4 = 10^{-0.57*b*(T_r - T_m)} \quad (45b)$$

where

α_4 = temperature correction factor for ε_{abc} for aggregate base pavements,

ε_{abc,T_m} = compressive strain on top of base layer in microstrain at measured temperature T_m,

ε_{abc,T_r} = compressive strain on top of base layer in microstrain at reference temperature T_r of 25°C.

The other variables in the above equations are defined previously. This adjustment factor is then applied to the ε_{abc} value predicted from Eq. 41 or 42 to get the adjusted ε_{abc}. The temperature adjusted ε_{abc} can then be used to estimate the limiting number of cycles to cause rutting in the base layer using Eq. 34.

The data from Mn/ROAD test sections were used to verify the proposed procedure in predicting pavement overall rutting potential. The temperature adjusted ε_{abc} value for each section was calculated from 1994 data and then compared to the pavement rut depths measured in 1998, as plotted in Figure 29. It can be seen that the higher adjusted initial ε_{abc} corresponds to the larger rut depth. It should be noted that although all pavement layers contribute to rut depth on the pavement surface, it was reported by Garg and Thompson (7) that in Mn/Road test sections, the base layer contributes most to the rutting.

Subgrade Strength

Similar to full-depth pavements, by investigating the DBPs, the stress and strain parameters, and subgrade modulus, *BCI*, ε_{sg}, *SSR*, and E_{sg} were found to be good indicators of the condition of subgrade for aggregate base pavements. Based on the sensitivity study, *BCI*

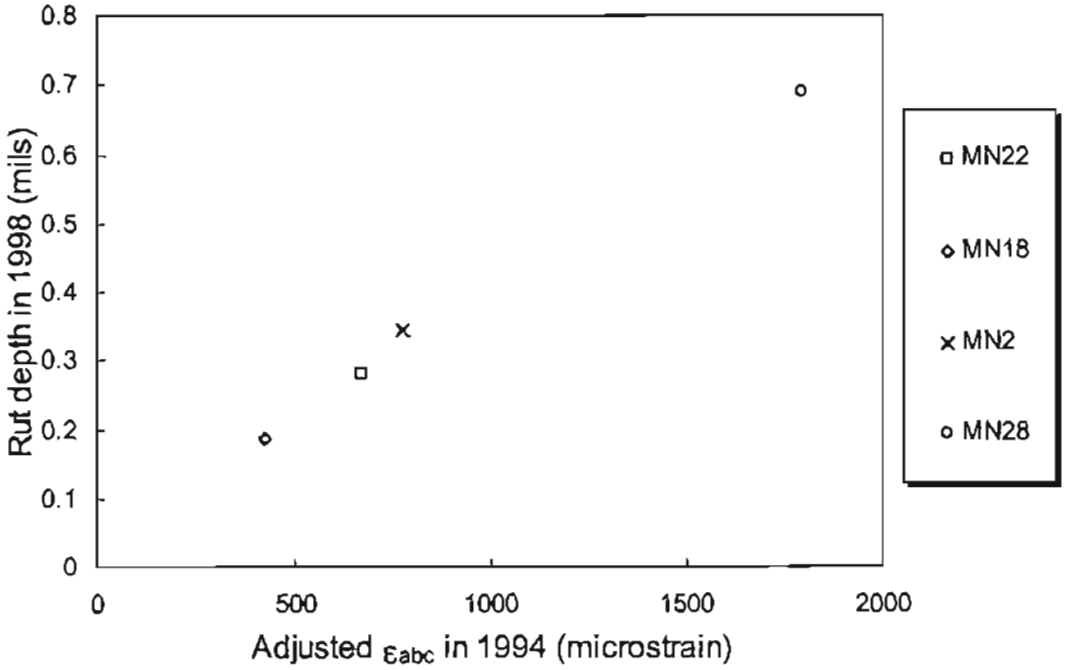

Figure 29. Adjusted ε_{abc} vs. rut depth for aggregate base pavements from Mn/ROAD test sections

appeared to be sensitive to subgrade stiffness. *SSR*, which represents the subgrade rutting potential, is predicted using the trained ANN in which seven deflections and thicknesses of AC and base layers were used as inputs. The following equations were developed to estimate ε_{sg} value in microstrain:

For $H_{ac} \geq 6$ inches,

$$\log(\varepsilon_{sg}) = 0.2811 * \log(BDI) + 0.6788 * \log(BCI) - 0.0135 * \log(H_{ac}) - 0.0123 * H_{abc} + 2.2083 \quad (46)$$

$$R^2 = 0.988 \qquad SEE = 0.016$$

For $H_{ac} < 6$ inches,

$$\log(\varepsilon_{sg}) = 0.8835 * \log(BDI) + 0.1526 * \log(BCI) - 0.0995 * \log(H_{ac}) - 0.0185 * H_{abc} + 2.2461 \quad (47)$$

$$R^2 = 0.976 \qquad SEE = 0.010$$

To enable general application of the indicators *BCI*, ε_{sg}, and *SSR* to different structures of aggregate base pavements, the values of these condition indicators are normalized to a standard structure. First, the nonlinear synthetic database was used to represent these indicators in terms of structural parameters as follows:

$$\log(\varepsilon_{sg}) = -0.4080 * \log(E_{ac}) - 1.2613 * \log(H_{ac}) - 0.0129 * H_{abc} - 0.1310 * \log(H_{abc}) - 0.2980 * \log(E_{Ri}) + 5.0937 \quad (48)$$

$$R^2 = 0.962 \qquad SEE = 0.108$$

$$\log(SSR) = -0.2222 * \log(E_{ac}) - 0.4946 * \log(H_{ac}) - 0.0953 * \frac{H_{ac}}{H_{abc}} - 0.3818 * \log(H_{abc}) - 1.0461 * \log(E_{Ri}) + 1.5633 \quad (49)$$

$$R^2 = 0.966 \qquad SEE = 0.089$$

$$\log(BCI) = -0.3286 * \log(E_{ac}) - 0.2621 * \log(H_{ac}) - 0.0404 * H_{ac} - 0.2287 * \log(H_{abc}) - 0.1267 * \log(E_{Ri}) + 0.0503 * \log(H_{sg}) + 2.0187 \quad (50)$$

$$R^2 = 0.955 \qquad SEE = 0.110$$

Using these equations, the indicators *BCI*, ε_{sg}, and *SSR* are estimated for the pavement structure in question and for a standard structure. The following standard structure was used: H_{ac} = 6 inch, E_{ac} = 500 ksi, H_{abc} = 10 inch, and H_{sg} = infinite. Using a similar approach to the one described previously, the values of an indicator are estimated for both the actual pavement structure and the standard pavement structure. A ratio of these values is then defined as an adjustment factor. The adjustment factor is then applied to each of the predicted *BCI*, ε_{sg}, and *SSR* values.

Another subgrade condition indicator investigated in this study is the modulus of subgrade (E_{sg}). Two methods were developed in this research to predict E_{sg}. One method uses an ANN in which the deflections of the three sensors farthest from the load center and thicknesses of AC and base layers are used as inputs. The other method is based on a relationship developed between E_{sg} and the minimum surface modulus, E_{smin}, which is described in details in Appendix C. The resulting functional equations from the surface modulus approach are as follows:

For $H_{sg} \geq 160$ inches,

$$E_{sg} = \frac{E_{s\min} - 0.2860 * F_{ac}^{\ 2} - 6.1389 * F_{ac} + 1.7244}{0.0861 * F_{ac}^{\ 2} - 0.3233 * F_{ac} + 1.1059} \quad (51)$$

$$R^2 = 0.978 \qquad SEE = 1.021$$

For $H_{sg} < 160$ inches,

$$E_{sg} = \frac{E_{s\min} - 0.0145 * F_{ac}^{\ 2} - 5.6922 * F_{ac} + 0.2353}{0.045 * F_{ac}^{\ 2} - 0.115 * F_{ac} + 23.2748 * \frac{F_{ac}}{D_{sg}^{\ 3}} + 1.0091} \tag{52}$$

$$R^2 = 0.901 \qquad SEE = 1.545$$

where D_{sg} is H_{sg} in foot and F_{ac} is defined as:

$$F_{ac} = \frac{H_{ac}\sqrt[3]{E_{ac}} + cH_{abc}}{100} \tag{53}$$

where c is a constant, which is assigned a value of 3, 4, and 5 for poor, marginal, and strong base, respectively.

Field data from NC 421 pavements were used to evaluate the performance of condition indicators in predicting subgrade strength of aggregate base pavements. The results of both FWD and DCP tests were available from five test sections. Among them, Sections17 and 24 have lime stabilized subgrade. Using the FWD measurements, the adjusted condition indicators were calculated from the procedures described above. These values were plotted against subgrade *CBR* values from the DCP tests in Figures 30 through 33. The trend lines in these figures show reasonable correlation between each indicator and *CBR* values. Using the commonly accepted criterion that $CBR \leq 10$ represents a poor subgrade condition, the criteria for the condition indicators are established in Table 12.

Similar to the temperature correction procedure for ε_{abc}, the following two equations can be derived from Eqs. 48 and 9 as the temperature adjustment factor α_5 for ε_{sg}:

$$\alpha_5 = \frac{\varepsilon_{sg,T_m}}{\varepsilon_{sg,T_r}} = 10^{-0.408*\left|\log(\varepsilon_{ac,T_m}) - \log(\varepsilon_{ac,T_r})\right|} \tag{54a}$$

$$\alpha_5 = 10^{-0.408*b*(T_r - T_m)} \tag{54b}$$

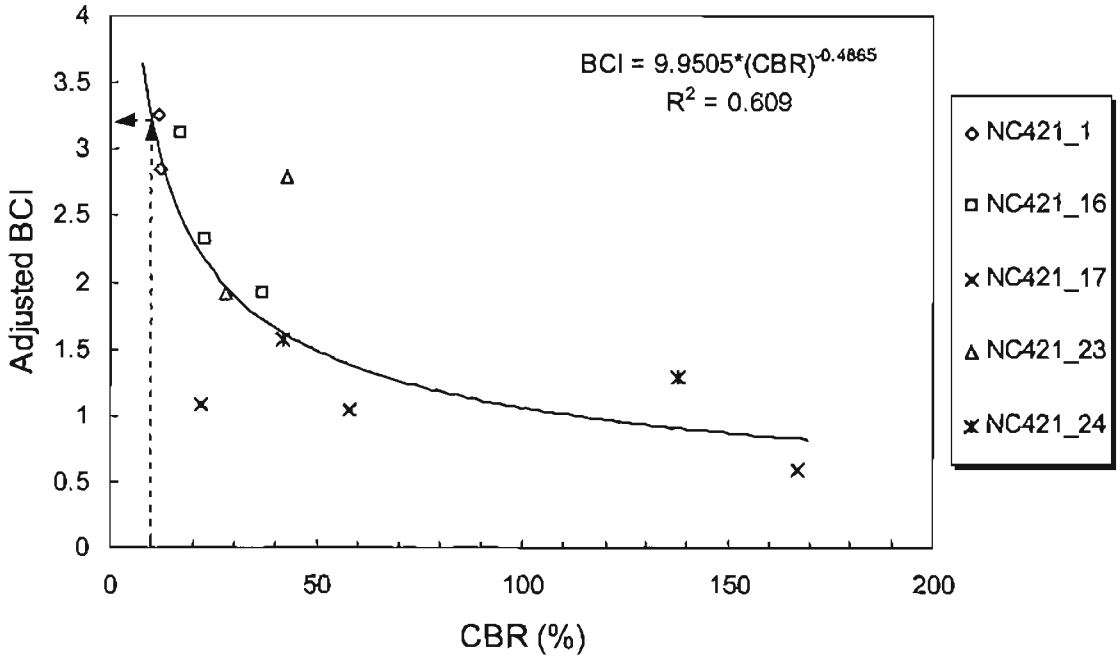

Figure 30. Adjusted BCI as subgrade condition indicator for aggregate base pavements (NC 421)

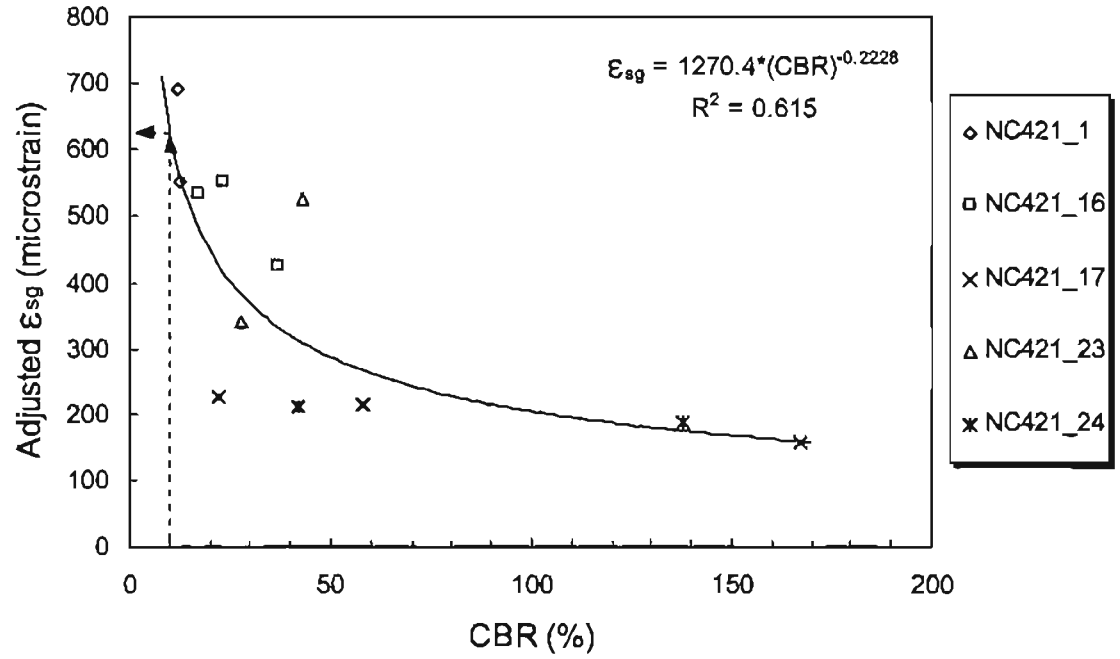

Figure 31. Adjusted ε_{sg} as subgrade condition indicator for aggregate base pavements (NC 421)

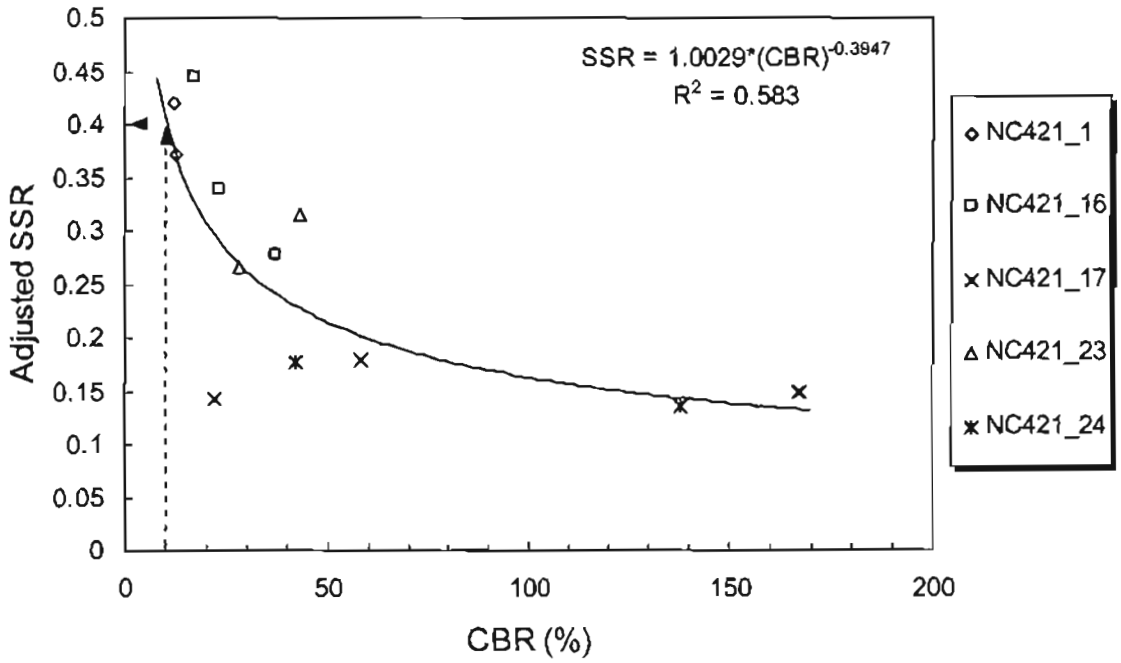

Figure 32. Adjusted SSR as subgrade condition indicator for aggregate base pavements (NC 421)

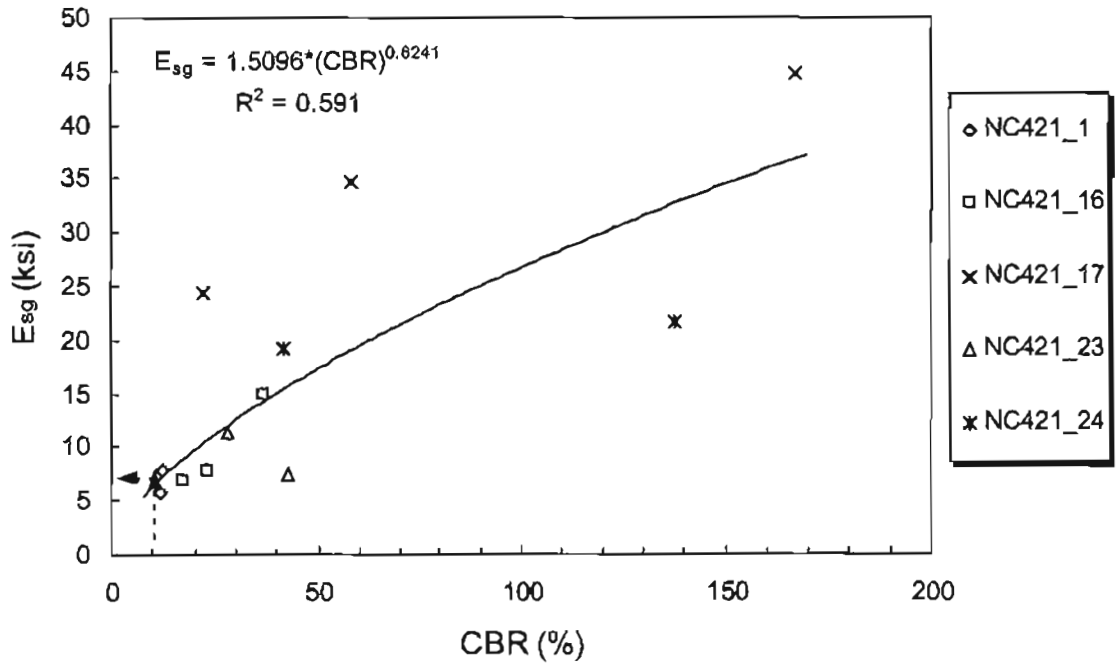

Figure 33. Adjusted E_{sg} as subgrade condition indicator for aggregate base pavements (NC 421)

Table 12. Suggested criteria for poor subgrade in aggregate base pavements

Subgrade condition indicators	Criterion for poor subgrade
Adjusted *BCI*	$\geq$ 3.2 mils
Adjusted ε_{sg}	$\geq$ 620 microstrain
Adjusted *SSR*	$\geq$ 0.40
E_{sg}	$\leq$ 7 ksi

This temperature adjusted ε_{sg} represents the contribution of subgrade to the pavement's overall rutting potential. The limiting number of cycles to rutting of subgrade can then be estimated based on the temperature-adjusted ε_{sg} using Eq. 34.

Surface treated pavements are not included in the scope of this research. Most procedures developed in this research cannot be applied for surface treated pavements due to their AC thickness is beyond the range of the synthetic data used in developing the ANNs and the governing equations. However, the minimum surface modulus approach can be used in predicting E_{sg} regardless of pavement type. When the pavement is weak, i.e., F_{ac} is smaller than 0.5, E_{smin} can be approximately considered equal to E_{sg} based on Eqs. 51 and 52. With relatively thin thicknesses of AC and base layers, the typical value of F_{ac} for a surface treated pavement is usually less than 0.5, suggesting that E_{smin} can be directly used to represent subgrade stiffness. This observation is very useful since it allows one to easily estimate subgrade stiffness from the calculated surface modulus profile without knowing thickness and modulus information of upper layers.

The data from seven secondary roads in Davidson County, North Carolina, were used to validate this concept. These sites were selected because they were low volume surface treated pavements, and constructed with varying thicknesses of aggregate base. Both DCP and FWD tests were performed at each site. Table 13 shows the thickness information for each section, first presented by Gabr et. al. (8). Calculated *CBR* values from DCP tests and predicted average E_{sg} values from FWD measurements are also shown in Table 13.

Figure 34 gives the relationship between *CBR* values and predicted E_{sg} values from FWD measurements. A reasonable trend can be found in this figure, suggesting that the minimum

Table 13. Summary information of test sites in Davidson County, North Carolina

Section	2111	2117	2352	2487	2529	2572	2751
H_{ac} (in)	0.5	5/8	1	1.39	1	5/8	1.39
H_{abc} (in)	9.4	6.7	5.5	3.5	5.5	7.9	3.5
CBR for Subgrade (%)	12.3	32.4	6.5	7.0	21.1	47.2	6.1
Average Predicted E_{sg} (ksi)	14.3	20.2	5.3	6.4	12.2	22.7	3.5

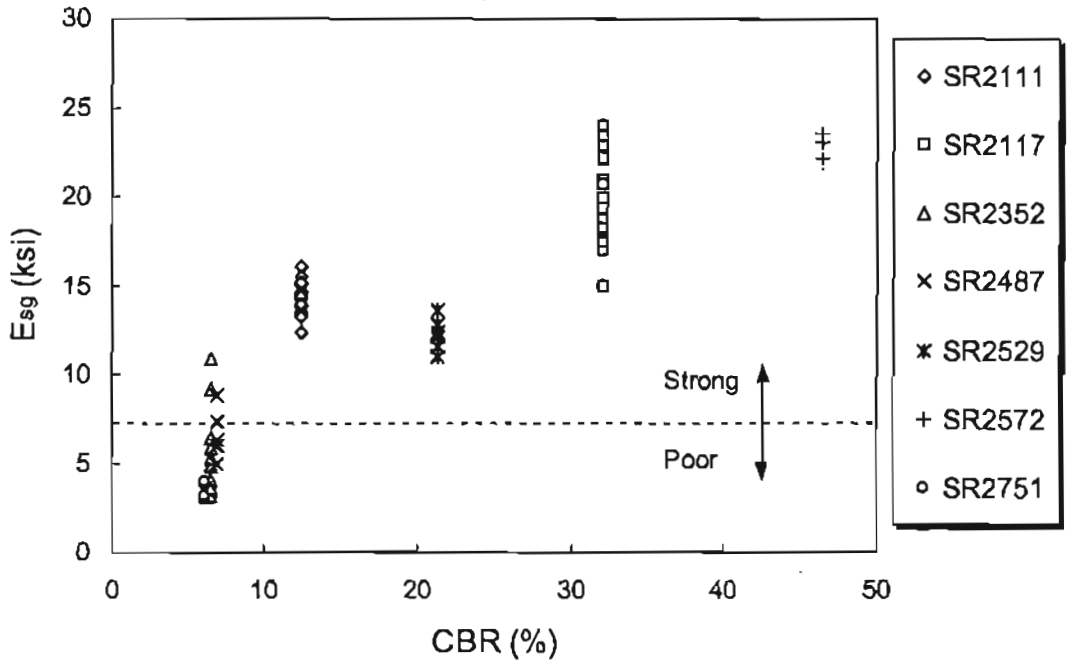

Figure 34. E_{sg} vs. subgrade CBR value for surface treated pavements in Davidson County

surface modulus method may be applicable to predicting subgrade modulus of surface treated pavements.

Depth to a Stiff Layer

For aggregate base pavements, an ANN was trained using the dynamic, linear elastic database to predict the depth to a stiff layer. Seven deflections, thicknesses of AC and base layers, and DBPs F_2 and F_3 are used as inputs for the ANN. The prediction performance of the ANN was then examined using the field data with known stiff layer depth. The direct R0 approach and the Modulus 5.1 approach were also applied to the field data to find the method most suitable for DSL predictions. The first set of field data used is from four CRREL test pavements, which were constructed and closely monitored in an indoor facility. Stiff layer depths of the CRREL pavements were known since the pavements were actually built on top of a concrete pad. Two test sites had a stiff layer 5 feet deep, while the other two test sites had a stiff layer 12 feet deep. Figure 35 shows the predicted DSL values versus the actual DSL values from the different approaches. The Modulus 5.1 method seemed to do the best job for the shallow DSL predictions and the predictions from the ANN approach were also acceptable. For the pavements with a stiff layer 12 feet deep, the ANN approach gave the closest prediction to the actual values. In general, the ANN approach yielded good results for the CRREL pavements.

Three more pavements selected from DataPave 2.0 were also used to test the performances of different approaches and the results are shown in Figures 36 through 38. For pavement 21-1010, all approaches appear to underestimate the DSLs, resulting in overestimation of subgrade strength. For other pavements, the ANN approach yielded the most accurate and consistent predictions.

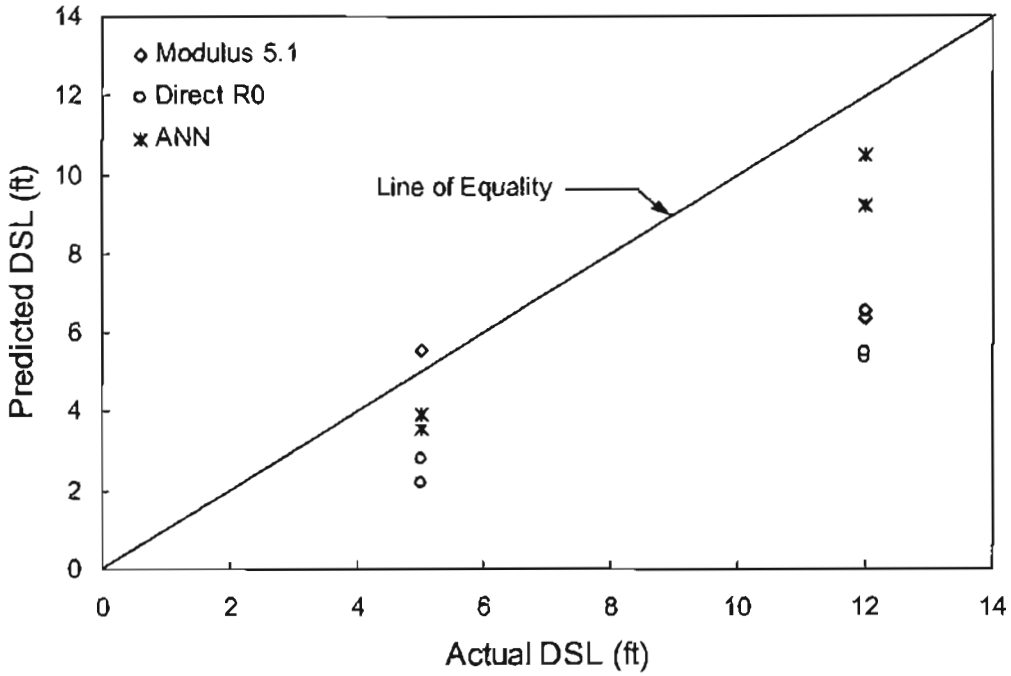

Figure 35. Comparison of DSL predictions from different approaches for CRREL pavements

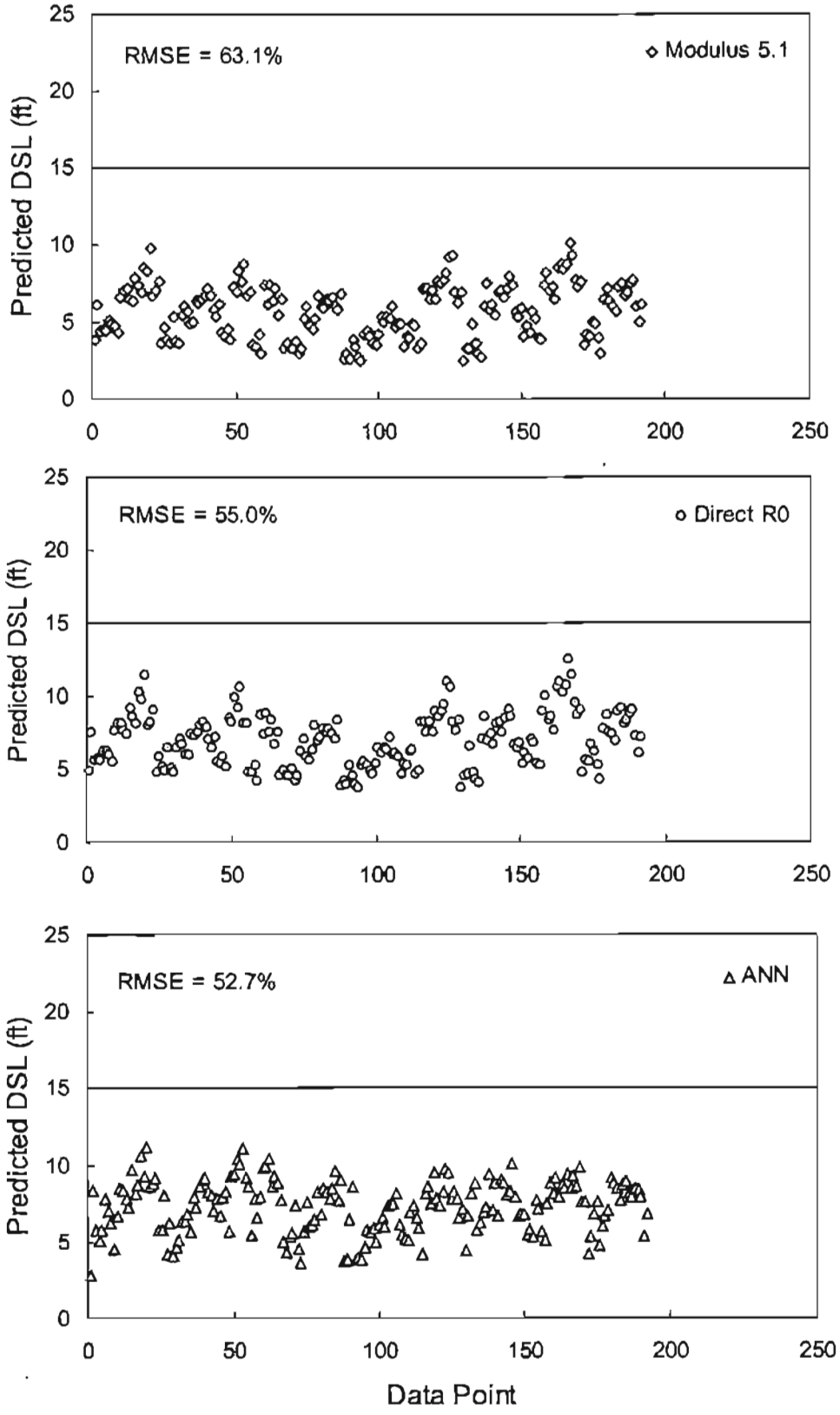

Figure 36. Comparison of DSL predictions from different approaches for pavement 21-1010 (Actual DSL = 15 ft)

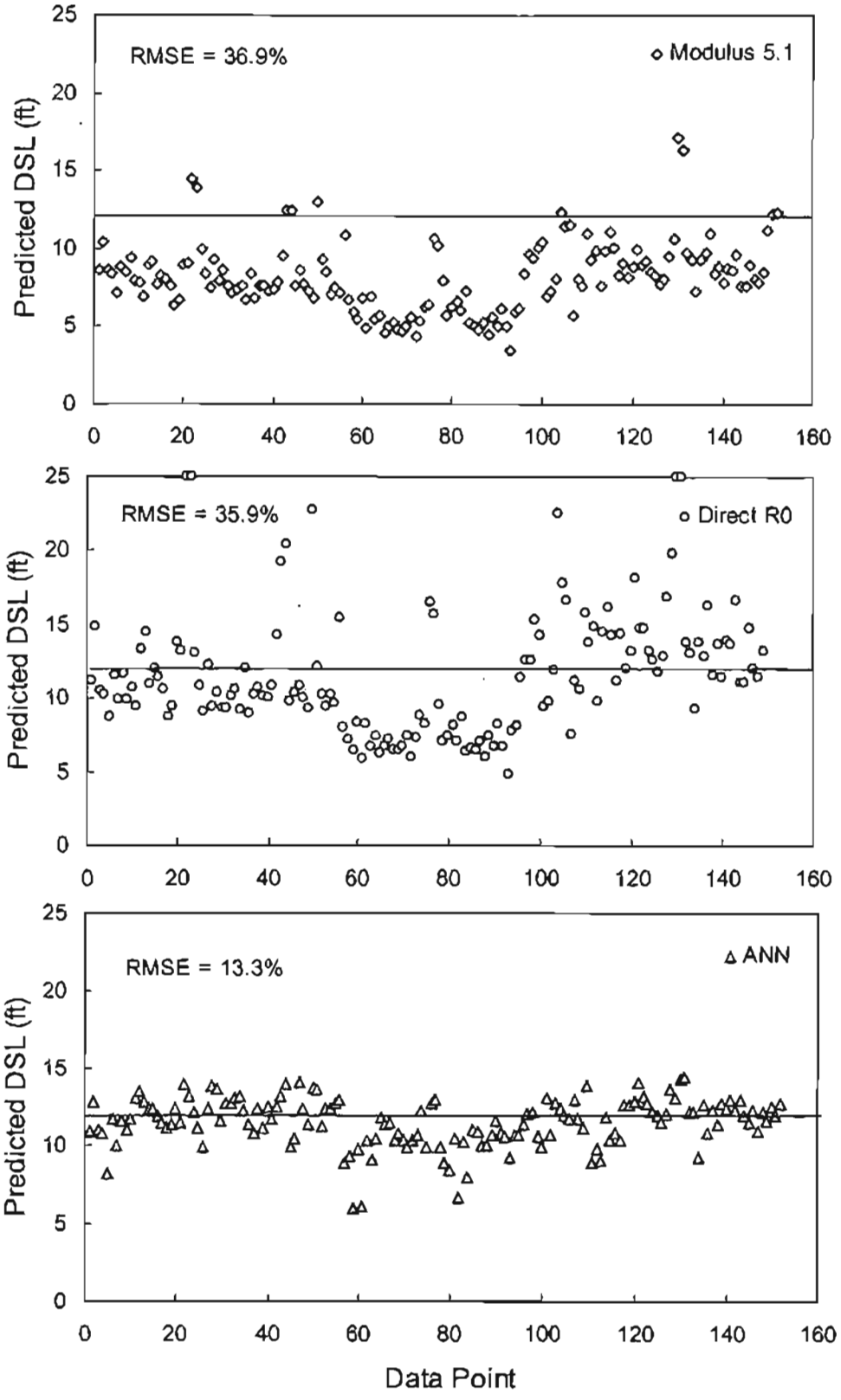

Figure 37. Comparison of DSL predictions from different approaches for pavement 47-3101 (Actual DSL = 12 ft)

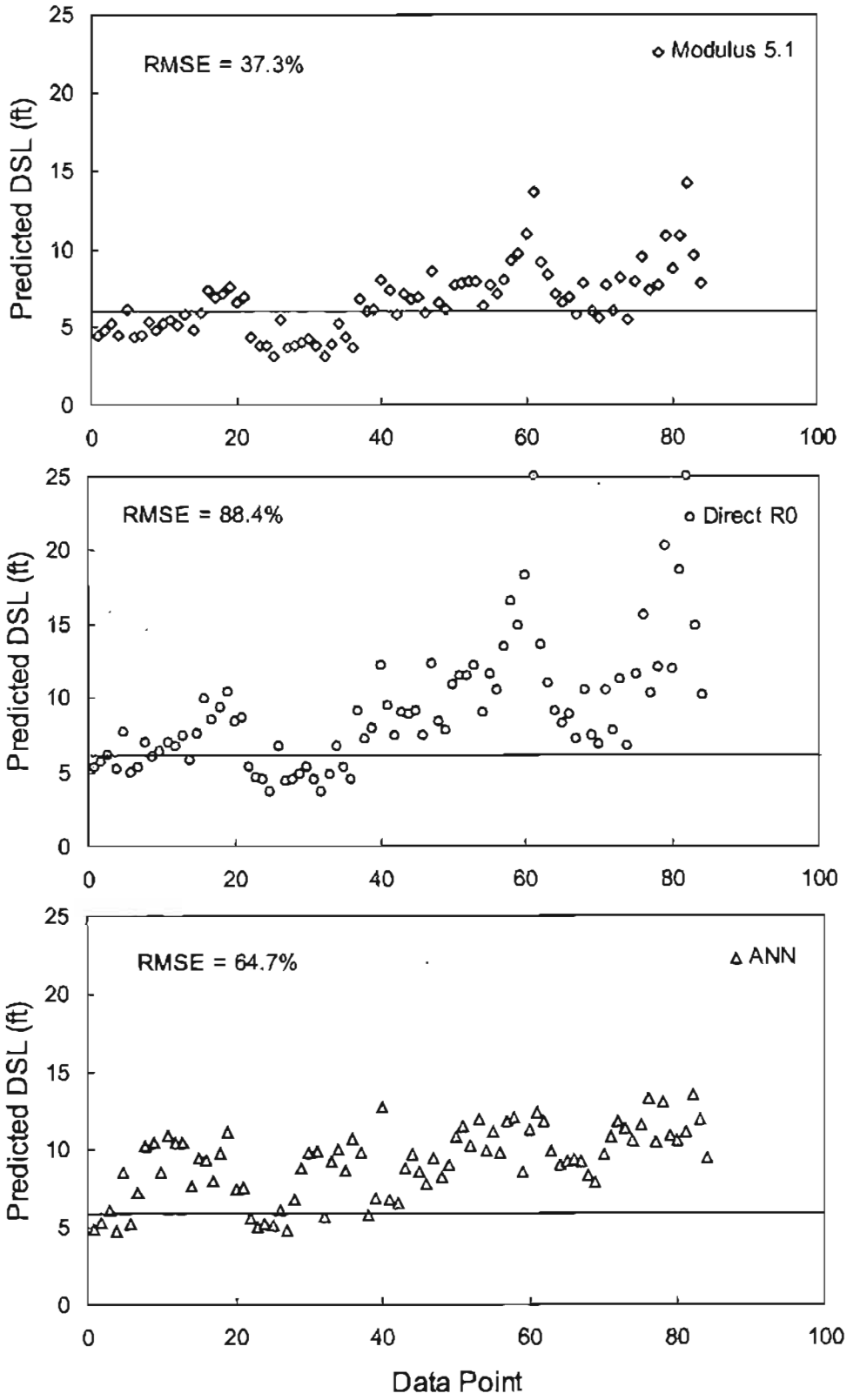

Figure 38. Comparison of DSL predictions from different approaches for pavement 51-1002 (Actual DSL = 6 ft)

CEMENT TREATED BASE (CTB) PAVEMENTS

The following sections describe the efforts of the research team in determining the condition of CTB pavement layers as listed in the research plan. Debonding in the asphalt layer, cracking in the base layer, strength of subgrade, and depth to a stiff layer were investigated and the results are presented in subsections one through four. As was discussed in the "Parametric Sensitivity Study" section, the linear elastic synthetic database was used to select promising DBPs and to develop Artificial Neural Network (ANN) structures. These DBPs and the ANN structures were investigated further, and the final results of that investigation are presented below.

Debonding in AC Layer

Limited field data was available to study debonding in the asphalt layer of CTB pavements. This data came from the test of Arrowood Road in Charlotte, NC from NC 49 to I-77. From the parametric study discussed previously, BDI was found to best detect the condition of the asphalt layer.

Figure 39 shows a plot of computed BDI values for intact test sections from NC 49, NC 58, and Ohio, debonded test sections from NC 49, and cracked CTB test sections from NC 49. It can be seen that the debonded sections have the highest calculated BDI values.

Also included in this figure is a line labeled "envelope" to distinguish between intact and distressed pavement cases. In this case, an FWD deflection bowl with BDI value greater than 2.5 is considered to represent a distressed pavement. These observations from the synthetic and field databases suggest that BDI of 2.5 is a promising criterion for detecting the condition of the

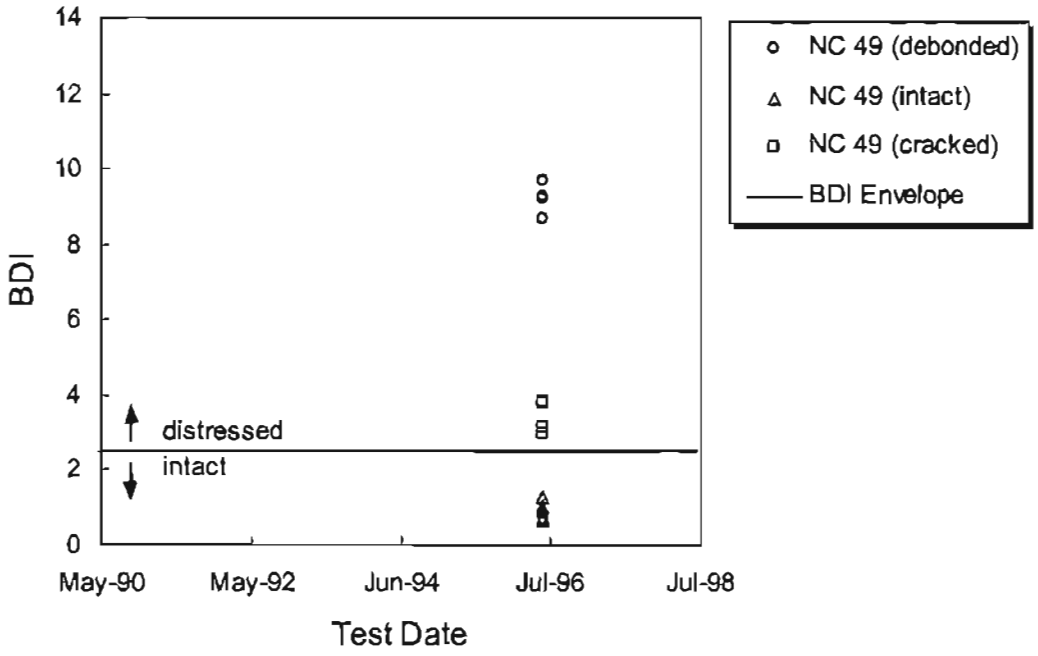

Figure 39. BDI vs. test date for the determination of debonding in the asphalt layer in CTB field data

asphalt layer in CTB pavements. Further details of the BDI envelope are provided in Appendix C.

Cracking in Cement Treated Base Layer

Distress due to cracking in the base layer of a CTB pavement is identified using the BDI envelope described above. This envelope was verified by sections from NC 421 and NC 49, field data with cracking in the CTB layer. Field tests performed on intact CTB cores from these test sites, described in the "Field Data" section indicated 1500 ksi was an average tested moduli value. BDI values were computed for deflection bowls in the synthetic database. These BDI values were separated according to their prescribed CTB effective modulus values. The plot of BDI values in synthetic cases with a CTB effective modulus of 1500 ksi, or higher, all fell below 2.5. Cracked data from NC 49 and NC 421 data are plotted in Figure 40. The field data and synthetic study results suggest that BDI is the best indicator of base layer condition in CTB pavements.

Subgrade Strength

The best indicator for the determination of strength of the subgrade in CTB pavements is D_{48}, which represents the deflection at the sensor located four feet from the load center. Field data collected from NC 421 test sections were used to study subgrade condition. This data includes cores from the FWD test locations in two or more locations in each test section and corresponding Dynamic Cone Penetrometer (DCP) test results. DCP tests have been used for many years to determine the strength of subgrade and aggregate base pavement layers.

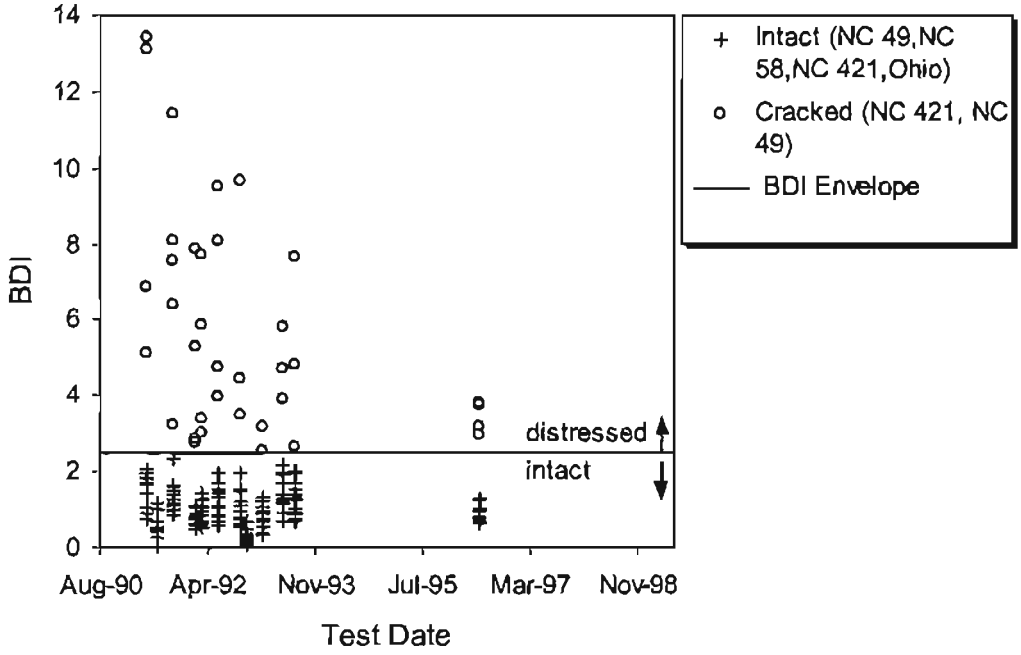

Figure 40. BDI vs. test date for the determination of cracking in the base layer in CTB field data

Extensive research has been performed to relate DCP test results to CBR values, and was defined as Eq. 32. The relationship between D_{48} and CBR (shown in Figure 41) was obtained by fitting a curve using regression. The resulting relationship, when rearranged, is of the form given below, with an R-squared value of 0.5.

$$CBR = \left(\frac{D_{48}}{83.4}\right)^{-0.82} \tag{55}$$

Based on a CBR value of 10, which is well accepted as a criterion for weak subgrade condition, a D_{48} value of 5.07 is identified as the subgrade condition criterion, i.e., a value of $D_{48} > 5.07$ indicates a poor subgrade in CTB pavements.

Depth to a Stiff Layer

Results from the parametric study described previously indicated F_3 would best characterize depth to a stiff layer in CTB pavements. F_3 describes the shape of the tail of the deflection basin and is defined in Table 2. FWD test data recovered from DataPave and Ohio test records were used in the DSL study. The reported DSL in the Ohio section was greater than 25 feet, while the DataPave sections in Florida, Nevada, and Texas had estimated DSLs of 1.3-2 feet, 10.3 feet, and 9.5-10 feet, respectively. No core information was available to confirm these estimates, and therefore the stiff layer depth is known with little certainty. Figure 42 shows F_3 versus estimated DSL for all available field data. The linear regression analysis of the data in Figure 42 resulted in the following relationship with R^2=0.78:

$$DSL = \frac{0.7631 - F_3}{0.0002} \tag{56}$$

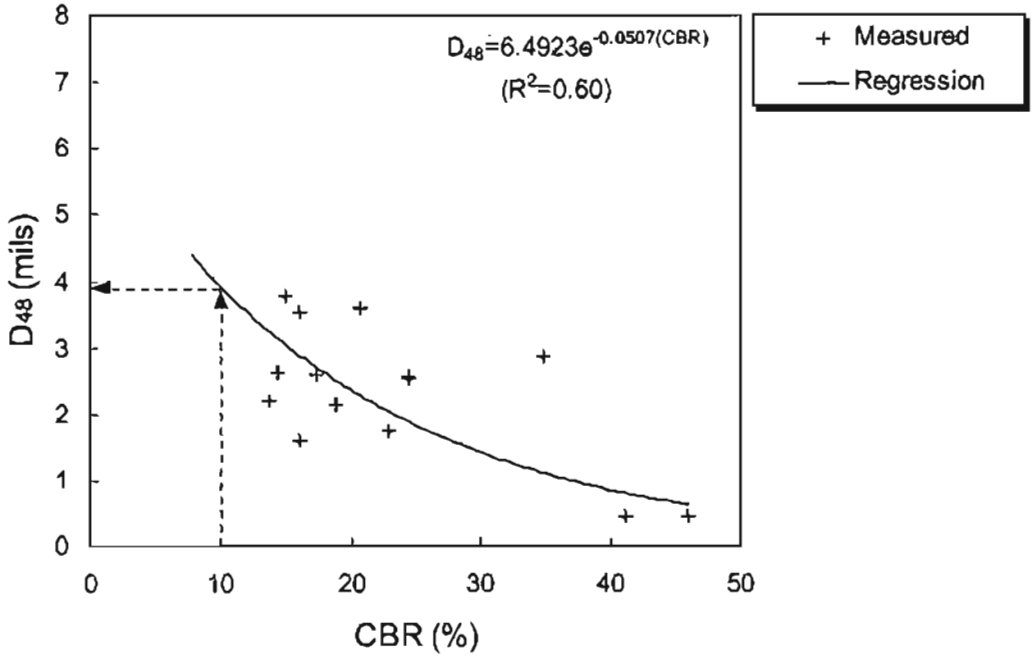

Figure 41. D_{48} vs. CBR of subgrade from CTB field data

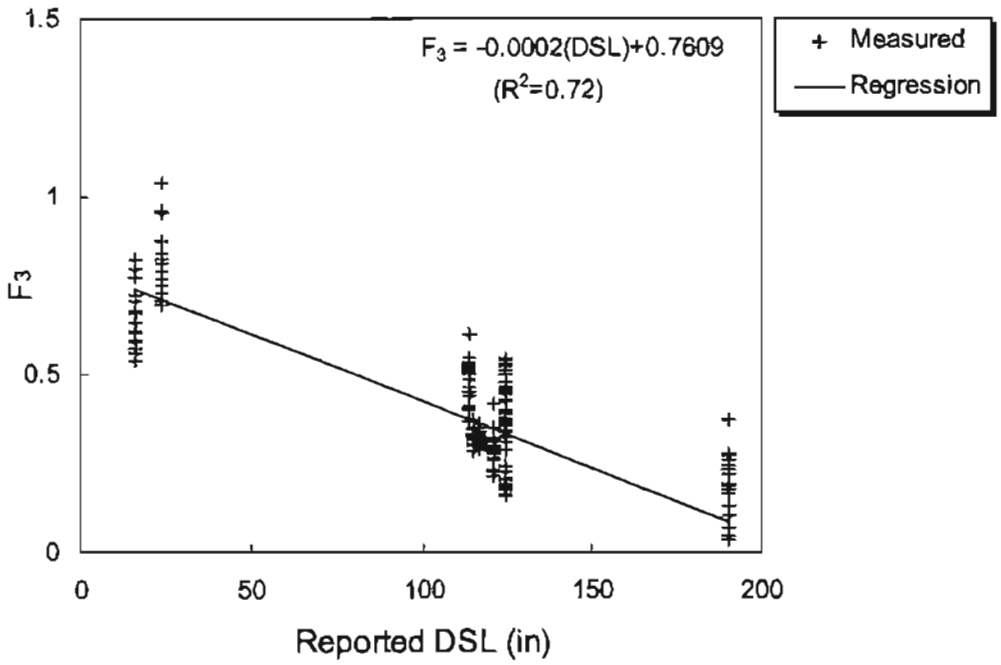

Figure 42. F_3 vs. reported DSL from CTB field data.

ASPHALT CONCRETE OVERLAIN PORTLAND CEMENT CONCRETE PAVEMENTS

The following sections describe efforts of the research team in determining AC/PCC pavement layer conditions specified in the research plan. Debonding in the asphalt layer, voids beneath PCC slab, subgrade strength, and depth to a stiff layer were investigated and the results are given in sections one through four below. As was discussed in the "Parametric Sensitivity Study" section, the linear elastic synthetic database was used to select promising DBPs and to develop Artificial Neural Network (ANN) structures. These DBPs and ANN structures were investigated further. The voids under PCC slab condition was also investigated. The final results of all investigations are shown below.

Debonding in AC Layer

The field data representing known debonding in the asphalt layer was not available. Neither a DataPave database search, nor a state Department of Transportation request for field data produced any information. Synthetic data with debonding in the asphalt layer was also considered. As described previously, the FEM model for debonding in the axisymmetric case gave no unique solutions and therefore could not be included in this study. For this reason, the research team was unable to make any progress in finding a procedure useful for detecting the presence of debonding in the asphalt layer.

Voids beneath PCC slab

Detection of voids beneath PCC slabs can be achieved through a comparative examination of subgrade k-values estimated for an interior loading condition, an edge loading

condition, or a corner loading condition. The equation for estimating the k-value for either case is:

$$\Delta_j = \left(\frac{\delta_j k l^2}{P} \right) \tag{57}$$

where j equals i for an interior loading condition, e for an edge loading condition, or c for a corner loading condition. For each case, a best-fit curve using regression was determined. The equations with the R-squared value of the fit are given below:

For center loading (0.999):

$$\Delta_i = 0.52 + 693(a/l)^6 - 1200(a/l)^5 + 855(a/l)^4 - 322(a/l)^3 + 68(a/l)^2 - 8(a/l) \tag{58}$$

For edge loading (0.999):

$$\Delta_i = 2.2 + 4382(a/l)^6 - 7476(a/l)^5 + 5202(a/l)^4 - 1892(a/l)^3 + 381(a/l)^2 - 41(a/l) \tag{59}$$

For corner loading (0.991):

$$\Delta_i = 1.265 - 8.507(a/l) + 49.043(a/l)^2 - 137.84(a/l)^3 - 0.2423(LTE) \tag{60}$$

where LTE is a joint load transfer efficiency parameter defined as:

$$LTE = \frac{\delta_u / \delta_l}{0.95} \tag{61}$$

For center loading (R^2=0.999):

$$l = 0.0007(AREA)^3 - 0.0566(AREA)^2 + 2.2285(AREA) - 14.792 \tag{62}$$

For edge loading (R^2=0.999):

$$l = 0.0006(AREA)^3 - 0.0539(AREA)^2 + 2.3194(AREA) - 19.037 \quad (63)$$

For corner loading (R^2=0.999):

$$l = 0.0008(AREA)^3 - 0.0565(AREA)^2 + 2.2586(AREA) - 15.057 \quad (64)$$

The AREA parameter in these equations is defined as:

$$AREA = \left(\frac{1}{D_1}\right)\sum_{i=1}^{n}\left[(R_{i+1} - R_i)\frac{(D_i + D_{i+1})}{2}\right] \quad (65)$$

In addition, the concrete modulus of elasticity can be defined as:

$$l^4 = \frac{Eh^3}{12(1-\nu^2)k} \quad (66)$$

If a loading offset exists, the deflections and AREA values must be corrected using the following equations:

For deflections:

$$D_{iOD} / D_{i0} = k_1\left(\left(\frac{OD}{l}\right)^{k_2} - k_3 \exp\left(\frac{OD}{l}\right)^{k_4}\right) \quad (67)$$

A list of regression parameters (k_1-k_4) and their respective R-squared values are shown in Table 14.

For AREA:

$$AREA_{OD} / AREA_0 = k_1\left(1 - \left(\frac{OD}{l}\right)^{k_2} + k_3 \exp\left(\frac{OD}{l}\right)^{k_4}\right) \quad (68)$$

The regression parameters in Eq. 68 are (R^2=0.978) k_1=0.68227, k_2=0.70424, k_3=0.46806, k_4=0.48343.

Once the k-values are estimated for both center slab and corner slab locations, the ratio of k-values is calculated for each test location in a given test section. The results are then plotted

Table 14. Regression parameters (k_1, k_2, k_3, and k_4) for use in deflection modification

Sensors	k_1	k_2	k_3	k_4	R^2
D_0	-2.2230	0.56552	0.45114	0.39979	0.997
D_{12}	-2.2531	0.57103	0.44572	0.40785	0.996
D_{24}	-2.2844	0.58125	0.44029	0.41933	0.995
D_{48}	-2.3580	0.60296	0.42826	0.44503	0.991
D_{60}	-2.4060	0.61229	0.42097	0.45829	0.986
D_{72}	-2.4673	0.61200	0.41240	0.46333	0.975

versus test locations to find a control value of the k ratio that corresponds to the lower bound of k ratios where sound support conditions are expected. Lower bounds of k ratios are determined based on the trend of k ratios along the whole test section. This control value is then compared to each of the k ratios along the pavement test section. Observations in a field case study led to the conclusion that a local void or weakened subgrade condition is to be expected if the calculated k ratio is less than 20% of the control value. For detailed information concerning the development of the void detection relationships, refer to Appendix E.

Subgrade Strength

Deflection Value Based Approach Using ANN

The first method of determining subgrade strength is to directly predict E_{sg} based on the deflections D_{24}, D_{36}, D_{48}, and the asphalt and PCC layer thicknesses using an ANN. As described in Appendix D, many combinations of DBPs and deflections were tested to arrive at the optimum ANN structure of the last three deflections, and layer thicknesses. Synthetic data developed through FEM analysis was used to train the ANN. Of the tested field data, only two cases (from the Ohio data set) included an accurate subgrade strength measure, i.e., resilient modulus data determined from cores. These two field data cases from Ohio were added to the synthetic database for training of the ANN. Field data from Ohio, Montana, and Washington were used to test the procedure.

Figures 43 and 44 show the ANN prediction of E_{sg} for the two Ohio test sections with known subgrade strength. Also included are the prediction results from the existing method presented in the AASHTO 1993 Guide for determining subgrade strength in asphalt overlaid PCC pavements. The field report from these Ohio test sections included an average, a minimum,

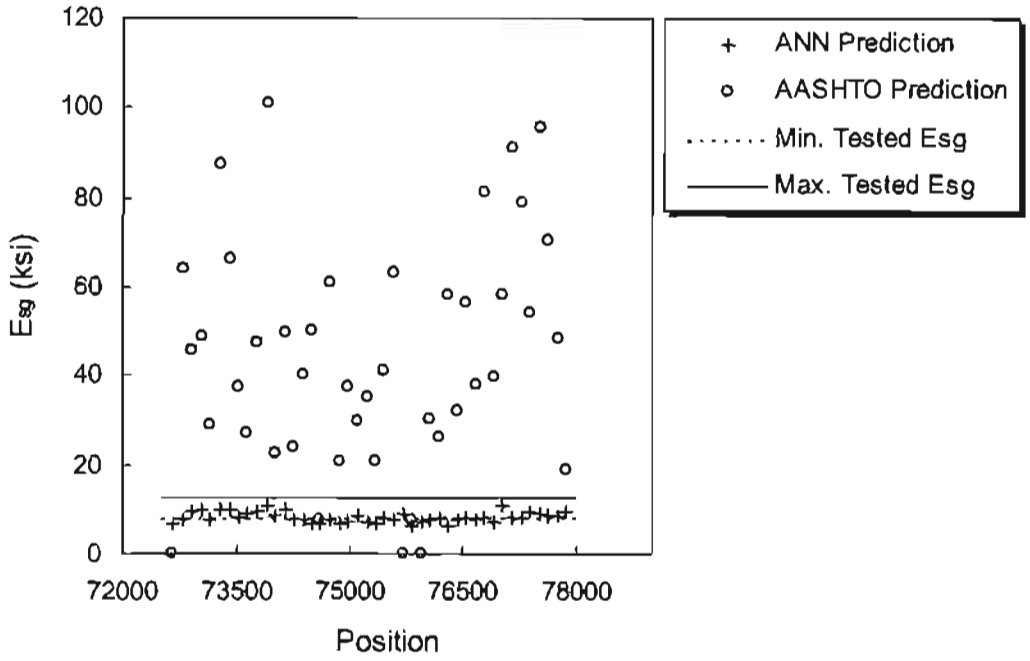

Figure 43. E_{sg} as an indicator of subgrade condition in AC/PCC pavements (Ohio test section 0107192)

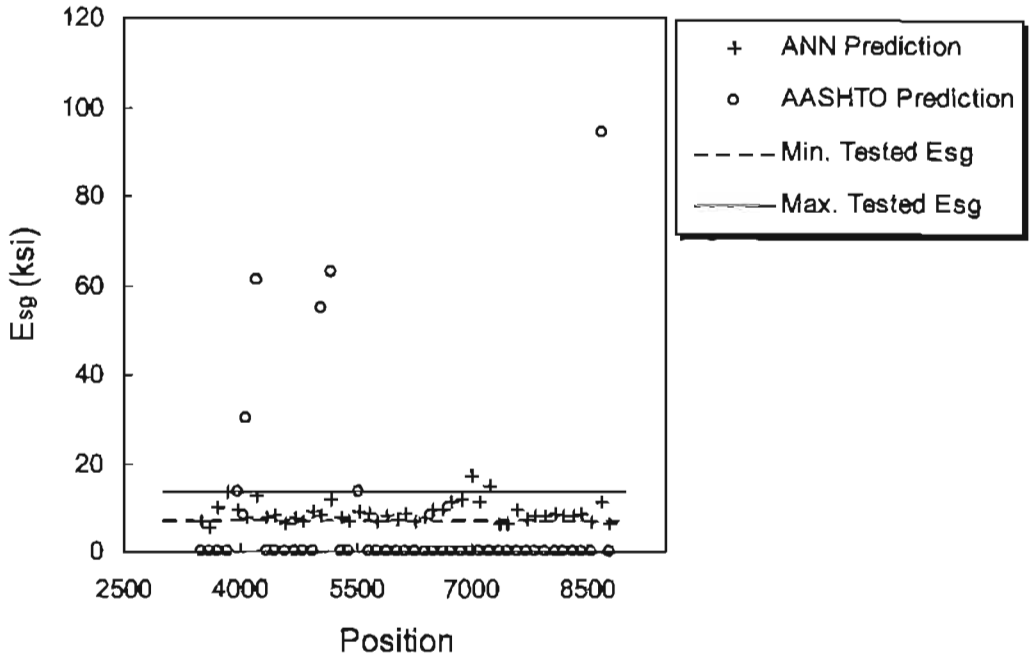

Figure 44. E_{sg} as an indicator of subgrade condition in AC/PCC pavements (Ohio test section 0407912)

and a maximum resilient modulus values for each section tested as shown in the figures. The ANN predicted values fall within the reported range, which is expected since the tested cases were used in developing the ANN. The AASHTO '93 results are more sporadic and deviate from the actual field measurements. Some field data could not be predicted using the AASHTO '93 method. For AC/PCC pavements, the AASHTO '93 procedure requires the modification of the center deflection so that it will represent the deflection on top of the PCC layer. This equation, for bonded JRCP pavements is given as:

$$d_{0_{compress}} = -0.0000328 + 121.5006\left(\frac{D_{ac}}{E_{ac}}\right)^{1.0798} \tag{69}$$

This modified center deflection is then used in the calculation of AREA. This computed value represents the AREA of the PCC slab, corrected for the AC overlay, and is shown below:

$$AREA_{pcc} = 6\left[1 + 2\left(\frac{d_{12}}{d_{0_{pcc}}}\right) + 2\left(\frac{d_{24}}{d_{0_{pcc}}}\right) + \left(\frac{d_{36}}{d_{0_{pcc}}}\right)\right] \tag{70}$$

where $d_{0_{pcc}} = d_0 - d_{0_{compress}}$. In some cases, the $d_{0_{pcc}}$ values were small enough to force the calculated $AREA_{pcc}$ to exceed 36, the maximum value of AREA. These cases in the AASHTO '93 prediction set are shown to have an E_{sg} value of 0.

Deflection Basin Parameter Approach

An alternate method for predicting subgrade condition is to use D_{48} as a subgrade condition indicator. D_{48} is the deflection located four feet from the load center. Figures 45 and 46 show the D_{48} values versus position for the same Ohio field data points used in previous predictions. For the Ohio sections with low subgrade modulus, the calculated D_{48} values are above the indicated good/poor line. In both cases the D_{48} values are fairly consistent.

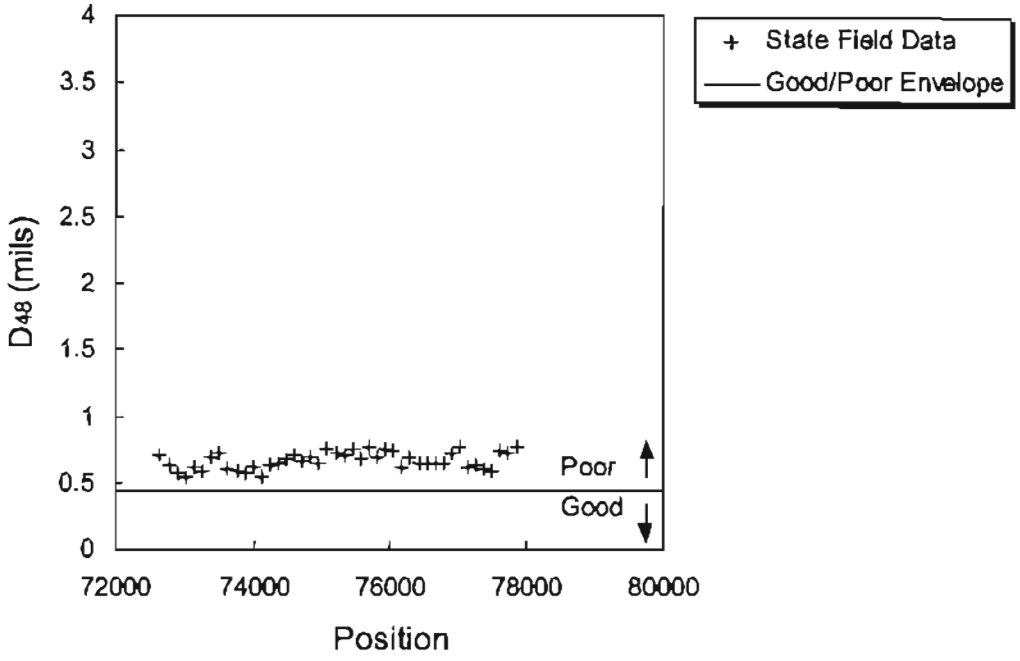

Figure 45. D_{48} as an indicator of subgrade condition in AC/PCC pavements (Ohio test section 0107192)

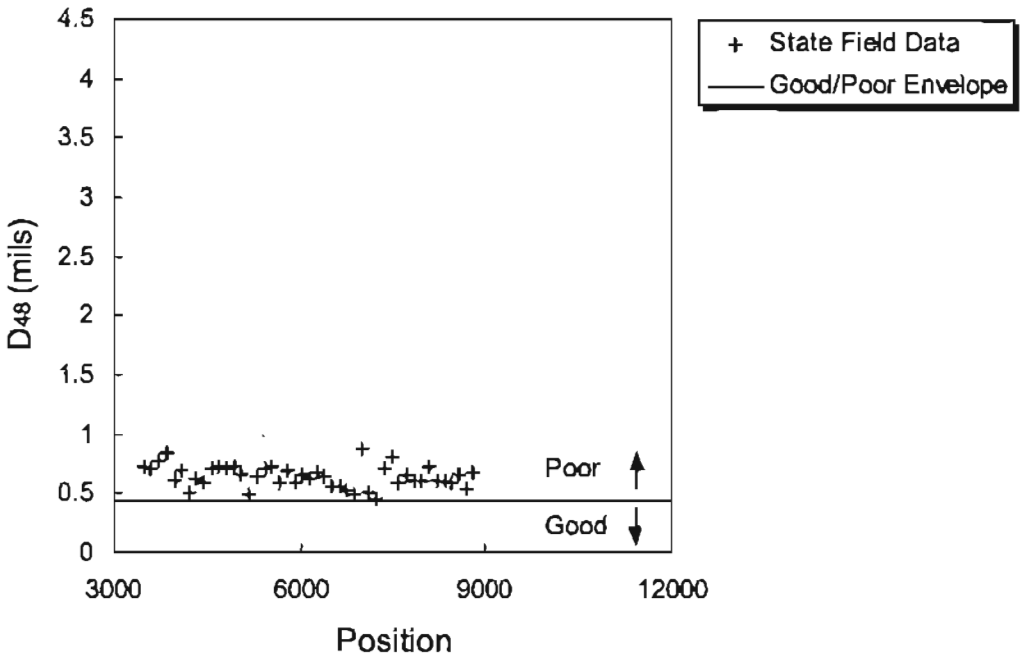

Figure 46. D_{48} as an indicator of subgrade condition in AC/PCC pavements (Ohio test section 0407912e)

Depth to a Stiff Layer

Deflection Value Based Approach Using ANN

The first method is to directly predict DSL from the trained ANN using all seven deflections, using a sensor spacing configuration of 0, 8, 12, 18, 24, 36, and 48 inches, F_2 and F_3, and the asphalt and PCC layer thicknesses. Figures 47 and 48 show the predicted DSL values versus test position. Although a few outlying points are present in both test sections, the predictions for a majority of the data falls close to the actual values.

Deflection Basin Parameter Approach

The second method developed by the research team in predicting stiff layer depth employs the deflection basin parameter F_3, as was found promising from the parametric study. Synthetic data was analyzed and a best fit curve of F_3 vs. DSL generated. Figures 49 through 51 show F_3 versus DSL for the same field data points used in the ANN prediction analysis. The best fit curve from the synthetic database was extended to fit field data cases by adding upper layer thicknesses to H_{sg} values to attain DSL. The figures show that the calculated F_3 shape factor values match the synthetic regression curve quite well. Theory and the preliminary synthetic database investigations would suggest that higher F_3 values would describe shallower stiff layer depth. However, no field data with shallow stiff layer information was available to verify this hypothesis.

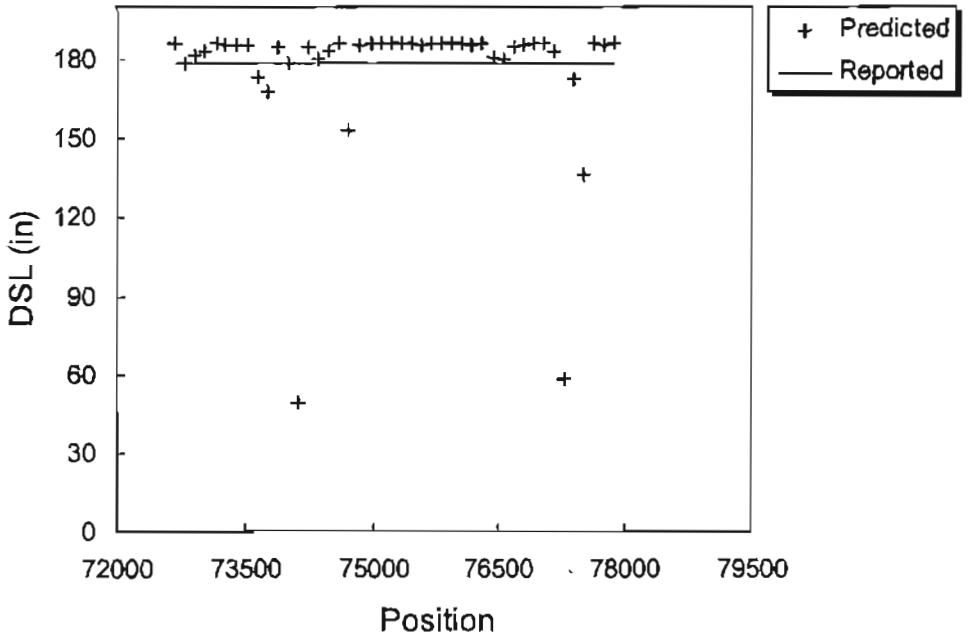

Figure 47. Predicted DSLs in AC/PCC pavements
(Ohio test section 0107192e)

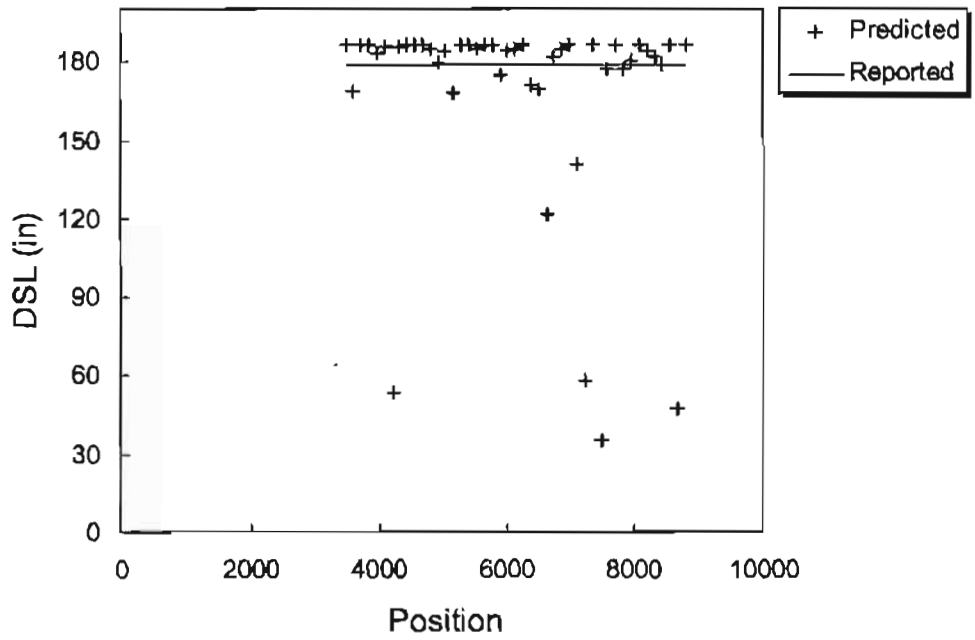

Figure 48. Predicted DSLs in AC/PCC pavements
(Ohio test section 0407912e)

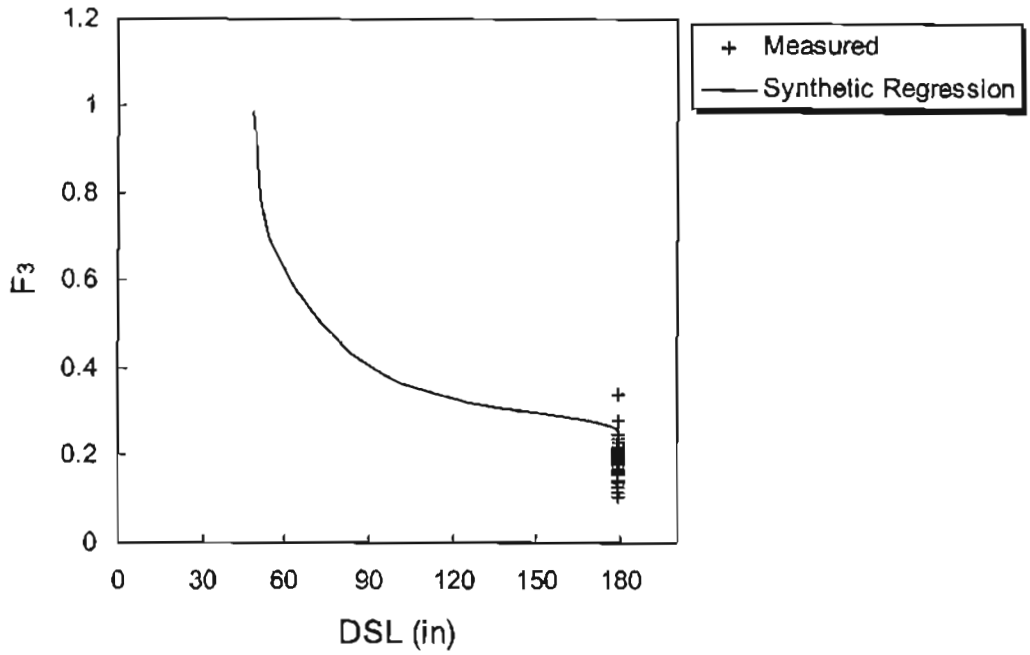

Figure 49. F_3 as an indicator of depth to a stiff layer in AC/PCC pavements (Ohio test section 0107192e)

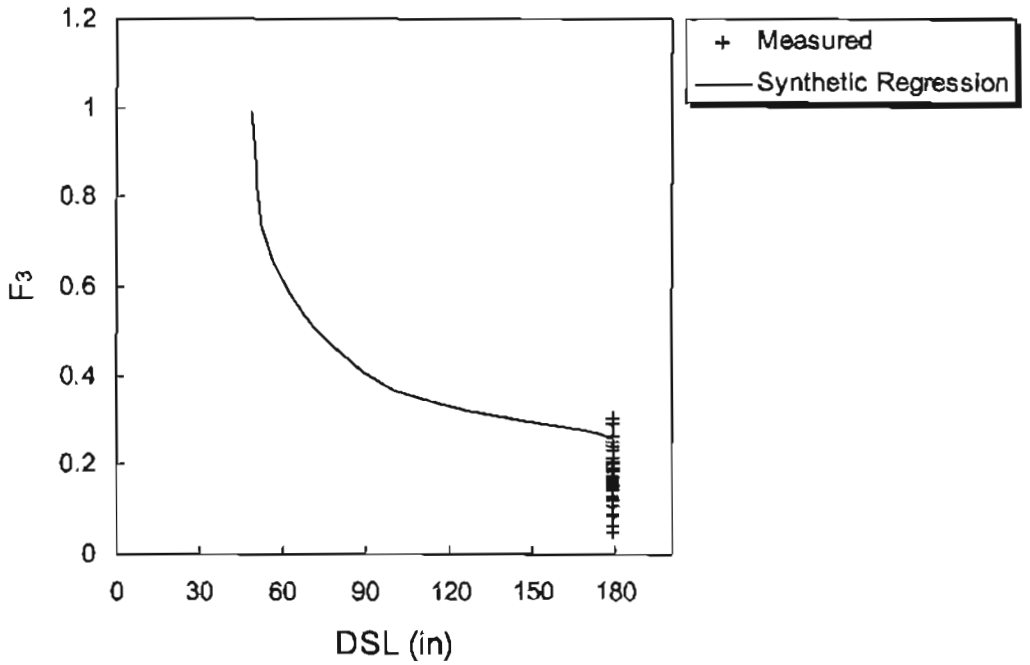

Figure 50. F_3 as an indicator of depth to a stiff layer in AC/PCC pavements (Ohio test section 0407912e)

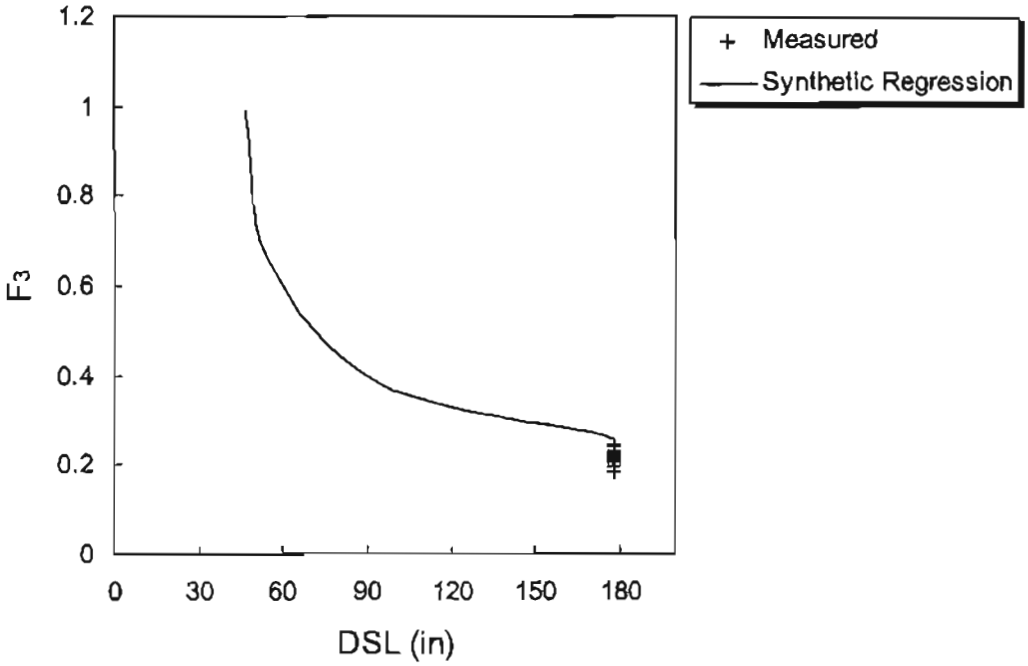

Figure 51. F_3 as an indicator of depth to a stiff layer in AC/PCC pavements (Ohio test section 0107091f)

CHAPTER 3

INTERPRETATION, APPRAISAL, AND APPLICATIONS

FULL-DEPTH AND AGGREGATE BASE PAVEMENTS

The challenge presented here was to determine the overall procedures for pavement layer condition assessment using condition indicators predicted from FWD measurements. As presented previously, E_{ac} and ε_{ac} seem to be good condition indicators for AC layer, while *BDI* and ε_{abc} show promising results for the prediction of base layer. *BCI*, ε_{sg}, *SSR*, and E_{sg} were found to effectively represent subgrade layer conditions. Tables 15 and 16 summarize all these indicators and their prediction methods for full-depth pavements and aggregate base pavements, respectively.

These condition indicators can be categorized into four groups: critical stresses, strains, DBPs, and layer moduli. Among them, the stress, strain, and deflection related indicators are not only affected by layer material properties but also affected by pavement structure and environmental conditions, such as temperature and moisture content. Thus, structure and temperature corrections are necessary for these pavement response parameters to be used in various pavements. As described in the "Findings", a set of temperature adjustment factors for various strain related indicators was developed from the synthetic database based on dynamic, nonlinear analysis, which can be written in a general form as:

$$\alpha = 10^{-f*b*(T_m - T_r)} \tag{71}$$

where f is the coefficient of temperature adjustment factor.

Table 17 gives the values of f used for different condition indicators. It is noted that f becomes smaller when the temperature adjustment is applied for the condition indicators of

Table 15. Proposed methods for layer condition assessment using condition indicators for full-depth pavements

Layer	Condition	Indicator	Proposed Method	Required Inputs	Criteria for Poor Condition
AC	Cracking Stripping	E_{ac}[b]	ANN approach and regression based approach (Eq. 11)	D_0-D_{18}, *SCI*, H_{ac}, E_{ac}-Temperature model, AC mid-depth temperature	E_{ac} is less than "intact" E_{ac} up to 30%
	Cracking potential	ε_{ac}[b]	Regression approach (Eq. 14)	*BDI*, H_{ac}	*N/A*[c]
Subgrade	Strength	*BDI*[a]	By definition (Table 2)	D_{12}-D_{24}	*BDI*[a] $\geq$ 3.4 mils
		BCI[a]	By definition (Table 2)	D_{24}-D_{36}	*BCI*[a] $\geq$ 3 mils
		ε_{sg}[a]	Regression approach (Eq. 20)	*BDI*, *BCI*, H_{ac}	ε_{sg}[a] $\geq$ 470 micro.
		SSR[a]	ANN approach	D_0-D_{48}, H_{ac}	*SSR*[a] $\geq$ 0.38
		E_{sg}	ANN approach and surface modulus approach (Eq. 30)	D_{24}-D_{48}, H_{ac}, AI_4, *BCI*, E_{ac}	$E_{sg} \leq 7$ ksi
	Rutting potential	ε_{sg}[b]	Regression approach (Eq. 20)	*BDI*, *BCI*, H_{ac}	*N/A*[c]

[a]After structural adjustment;

[b]After temperature adjustment;

[c]Not available.

Table 16. Proposed methods for layer condition assessment using condition indicators for aggregate base pavements

Layer	Condition	Indicator	Proposed Method	Required Inputs	Criteria for Poor Condition
AC	Cracking Stripping	E_{ac}[b]	ANN approach and regression based approach (Eq. 35 or 36)	D_0-D_{24}, *SCI*, *BDI*, H_{ac}, H_{abc}, E_{ac}-Temperature model, AC mid-depth temperature	E_{ac} is less than "intact" E_{ac} up to 30%
	Cracking potential	ε_{ac}[b]	Regression approach (Eq. 37 or 38)	*BDI*, H_{ac}	*N/A*
Base layer	Strength	*BDI*[a]	By definition (Table 2)	D_{12}-D_{24}	*BDI*[a] $\geq$ 5.8 mils
		ε_{abc}[a]	Regression approach (Table 2)	*BDI*, H_{ac}, H_{abc}, *BCI*	ε_{abc}[a] $\geq$ 720 micro.
	Rutting potential	ε_{abc}[b]	Regression approach (Eq. 41 or 42)	*BDI*, H_{ac}, H_{abc}, *BCI*	*N/A*[c]
Subgrade	Strength	*BCI*[a]	By definition (Table 2)	D_{24}-D_{36}	*BCI*[a] $\geq$ 3.2 mils
		ε_{sg}[a]	Regression approach (Eq. 46 or 47)	*BDI*, *BCI*, H_{ac}, H_{abc}	ε_{sg}[a] $\geq$ 620 micro.
		SSR[a]	ANN approach	D_0-D_{48}, H_{ac}, H_{abc}	*SSR*[a] $\geq$ 0.4
		E_{sg}	ANN approach and surface modulus approach (Eq. 52)	D_{24}-D_{48}, H_{ac}, H_{abc}, AI_4, *BCI*, E_{ac}	$E_{sg} \leq$ 7 ksi
	Rutting potential	ε_{sg}[b]	Regression approach (Eq. 46 or 47)	*BDI*, *BCI*, H_{ac}, H_{abc}	*N/A*[c]

[a]After structural adjustment;

[b]After temperature adjustment.

[c]Not available.

Table 17. Coefficient f for various temperature adjustments

f	E_{ac}	ε_{ac}	ε_{abc}	ε_{sg}
Full-Depth Pavements	1.0	0.898	----	0.761
Aggregate Base Pavements	1.0	0.641	0.570	0.408

lower layers, which is to be expected since the effect of temperature on the pavement response decreases with depth. To validate the developed temperature adjustment factors, the temperature correction procedure was applied to the AC tensile strain of pavement 9-1803. Figures 52 and 53 show the seasonal variations of predicted E_{ac} and ε_{ac} values, respectively. The reasonable trends for E_{ac} and ε_{ac} can be observed: in summer, E_{ac} values are low, while the tensile strains are high, and in winter, higher E_{ac} and lower tensile strain values were found. Figure 54 shows the temperature adjusted ε_{ac} values versus testing dates. It can be seen that after applying the temperature adjustment, the AC tensile strains are fairly consistent during different seasons.

Structural correction is needed when structurally dependent condition indicators are used for layer condition assessment. After the structural correction, the condition indicators will be a function of the layer material strength in question. Table 18 gives the standard structures used in this research for different structural corrections. For base layer correction, only base layer thickness is included in the standard structure. This is due to the difficulty in using a single material property to represent the base layer condition when a nonlinear model was assumed for base materials. Considering the base layer quality has a minor effect on pavement deflection responses, this simplification is deemed to be acceptable.

The following sections describe some important issues concerning the application of the proposed procedures in detecting layer conditions. The limitations of the proposed procedures are also presented.

Distresses in AC layer

According to the findings, the method to detect cracking and stripping in AC layer is to first predict the value of E_{ac} from FWD measurements, and then compare it with the appropriate

Table 18. Standard structures used for assessing layer conditions

	E_{ac} (ksi)	H_{ac} (in)	H_{abc} (in)	E_{Ri} (ksi)	H_{sg} (in)
Subgrade of full-depth pavements	500	8	---	various	infinite
Base layer of aggregate base pavements	500	6	10	7	infinite
Subgrade of aggregate base pavements	500	6	10	various	infinite

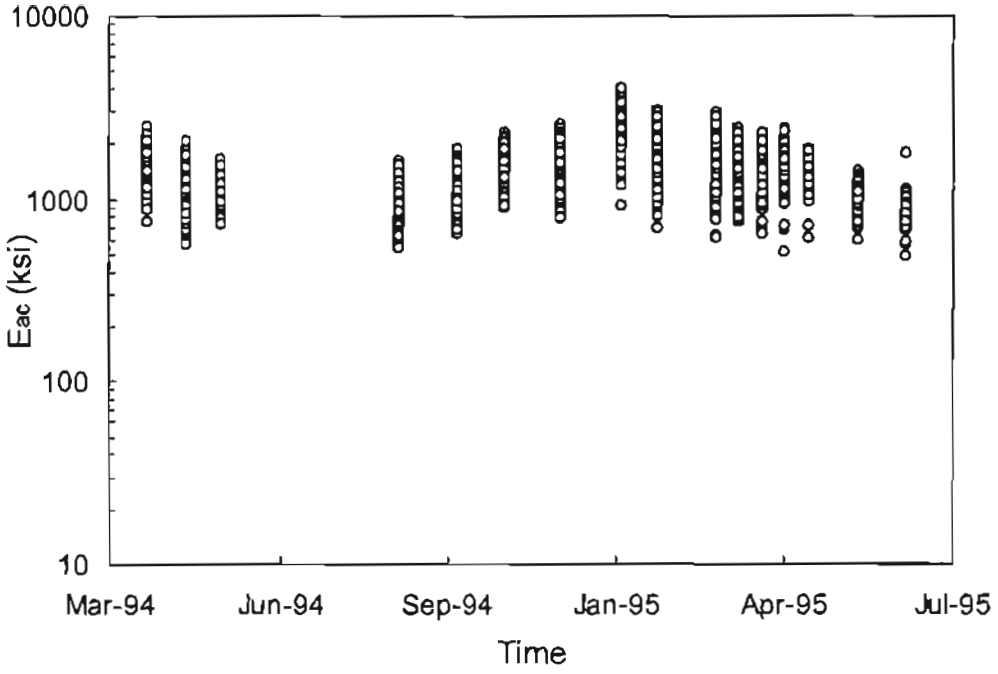

Figure 52. Seasonal variation of predicted E_{ac} for aggregate base pavement 9-1803

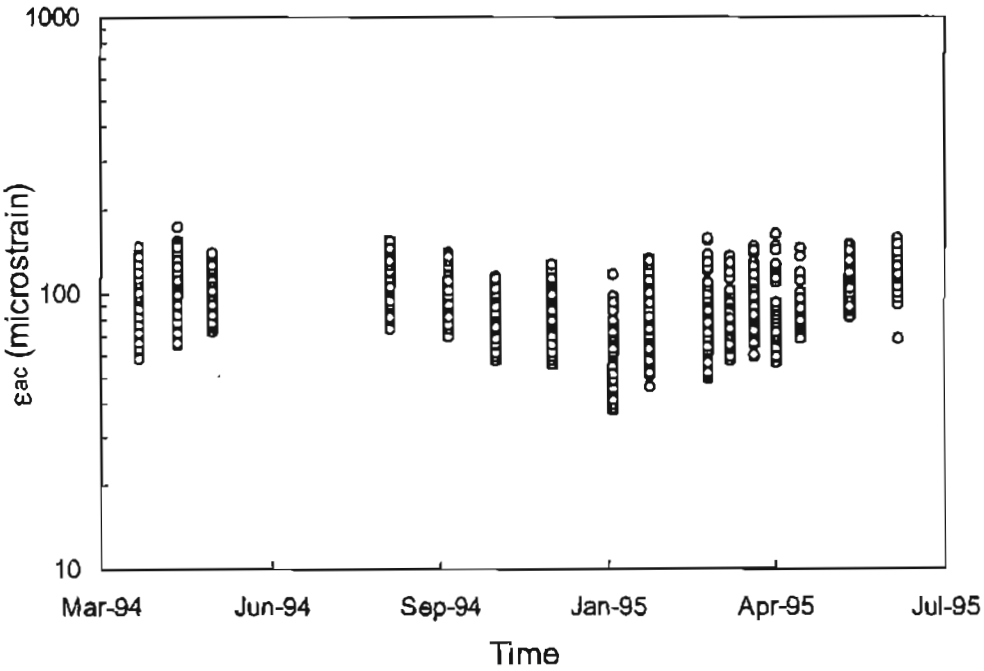

Figure 53. Seasonal variation of predicted ε_{ac} for aggregate base pavement 9-1803

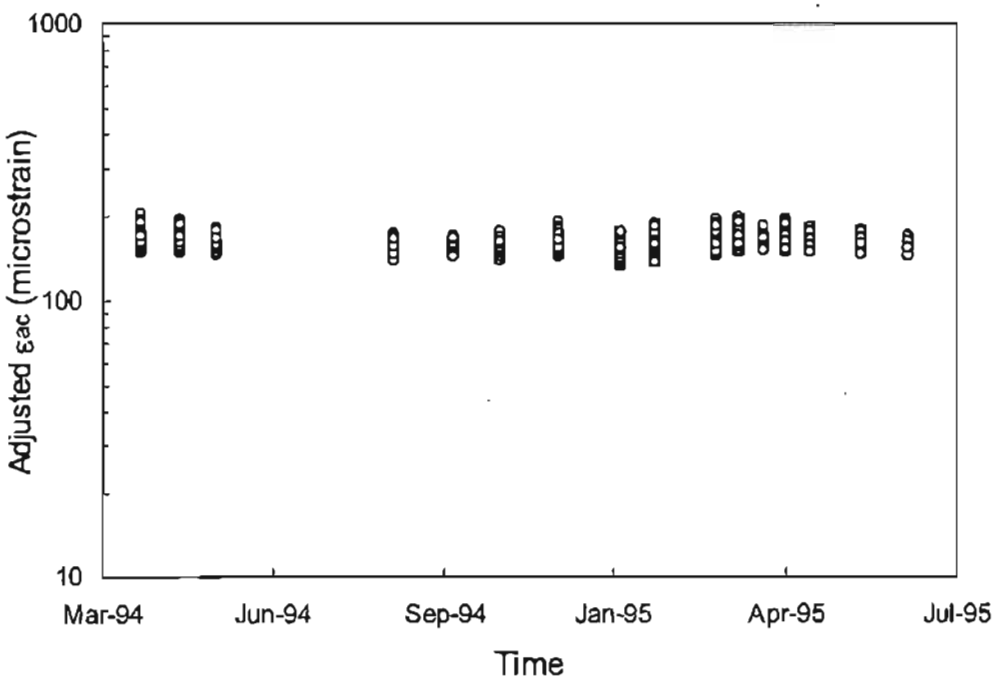

Figure 54. Adjusted ε_{ac} vs. time for aggregate base pavement 9-1803

intact AC modulus from the AC modulus-temperature relationship. Presence of any distress will result in lower AC modulus values. The degree of distress in the AC layer is indicated by the amount of deviation of the predicted value from that of an intact AC layer. The accuracy of applying the above procedure depends on three factors: (1) the correct prediction of AC mid-depth temperature; (2) the reliable backcalculation of effective AC modulus; and (3) the proper establishment of AC modulus-temperature relationship.

The following equation for the *BELL3* method proposed by Lukanen et al. (6) is used to predict the AC mid-depth temperature based on the time of testing, the pavement surface temperature, and the average air temperature the day before testing:

$$T_d = 0.95 + 0.892 * IR + 0.042 * IR * \sin(hr_{18} - 13.5) + \{\log(d) - 1.25\}\{-0.448 * IR + 0.621 * (1 - day) + 1.83 * \sin(hr_{18} - 15.5)\} \quad (72)$$

where

T_d = AC temperature at depth d, °C,

IR = infrared surface temperature, °C,

d = depth at which temperature is to be predicted, mm,

1-day = average air temperature the day before testing,

log = base 10 logarithm,

sin = sine function in 18-hour clock system, with 2π radians equal to one 18-hour cycle,

hr_{18} = time of day, in 24-hour system, but calculated using an 18-hour AC temperature rise and fall time cycle, as indicated below:

When using the $\sin(hr_{18}-15.5)$ function, only use times from 11:00 to 05:00 hrs. If the actual time is not within this time range, consider 11:00 hrs as the actual time. If the actual time is between 0:00 and 5:00 hrs, add 24 to the actual time. The calculate as follows: If the time is 13:15, then in decimal form, 13.25-15.50=-2.25; -2.25/18=-0.125; -0.125 x 2π =-0.785 radians; sin(-0.785)=0.707.

When using the $\sin(hr_{18}-13.5)$ function, only use times from 09:00 to 03:00 hrs. If the actual time is not within this time range, consider 09:00 hrs as the actual time. If the actual time is between 0:00 and 3:00 hrs, add 24 to the actual time.

The *BELL3* method was developed from the large database of the SMP pavements in the LTPP program, where actually measured asphalt temperatures and corresponding deflection responses were stored. This method accounts for the variation of the temperature gradient in the asphalt concrete during the rising and fall cycles of the day. The shading effect of FWD routine testing is also taken into account.

As shown in Tables 15 and 16, the regression-based approach and ANN approach are used to predict AC modulus in this research. Since there are no laboratory data available to test the prediction performance of the proposed method, the accuracy of the AC modulus prediction must be checked by plotting the predicted values against the temperatures to see whether a reasonable trend can be found. It should be noted that the intact AC modulus vs. temperature relationship is not unique. It may vary from region to region due to variations in the physical properties of the asphalt concrete used. Thus, a study was conducted to evaluate the prediction performance of the proposed method and to develop the AC modulus-temperature models for different climate regions, including Wet-No Freeze (WN), Wet-Freeze (WF), Dry-No Freeze (DN), and Dry-Freeze (DF) regions, based on the data from SMP pavements in the LTTP program. FWD deflections as well as actually measured AC mid-depth temperatures were available for these pavements from DataPave 2.0.

Since not all SMP pavements were intact, only newly constructed SPS-1 pavements were included in this study. Thus, only eight pavements were accepted, of which none were full-depth

pavements. Table 19 shows basic information such as layer thickness and asphalt type of these pavements. For each of the four climate regions, at least one pavement was selected. The models resulting from the regression-based approach, the Modulus 5.1 program, and the ANN approach were presented for comparison. Figures 55 through 78 show the plots of AC modulus vs. temperature for each pavement using all three methods.

It can be seen from these figures that the prediction performances of the regression-based approach and the ANN approach are similar in general. For some pavements, such as 1-0101 and 1-0102, the prediction performances of the regression-based approach and the Modulus 5.1 approach are similar. However, for the other pavements, significant improvements were found when applying the regression-based approach to build AC modulus-temperature relationships. Focusing on those pavements with similar prediction results from both approaches gives the comparisons shown in Figures 79 and 80. Modulus 5.1 techniques seemed to yield slightly lower E_{ac} values than the regression-based approach. This is probably due to the different forward modeling involved: Modulus 5.1 is based on a static, linear elastic analysis, while the regression-based approach is based on a dynamic, nonlinear elastic analysis. The static analysis based program could underestimate the AC modulus when deflections obtained from dynamic tests are used. To test AC modulus predictions for distressed pavements, the data from Mn/ROAD test sections in both 1994 and 1998 were analyzed and agreement was found between both approaches, as shown in Figure 81. Since the ANN based approach to predict E_{ac} is also proposed in this research, the comparisons were then made between the ANN based approach and the regression based approach, as shown in Figures 82 and 83. In general, both approaches agreed well with each other, although the resulted values from the ANN were slightly higher

Table 19. Information about the pavements used in developing AC modulus-temperature models

State ID	Pavement ID	H_{ac} (in)	H_{abc} (in)	Asphalt Type	Climate Region
1	0101	6.6	7.9	AC-20	WN
1	0102	3.9	11.9	AC-20	WN
51	0113	4	13.9	AC-20	WN
51	0114	6.8	17.9	AC-20	WN
10	0102	5.5	50.8	AC-20	WF
4	0113	4.2	7.5	AC-30	DN
4	0114	7.1	12	AC-30	DN
32	0101	7.1	31.3	AC-20P	DF

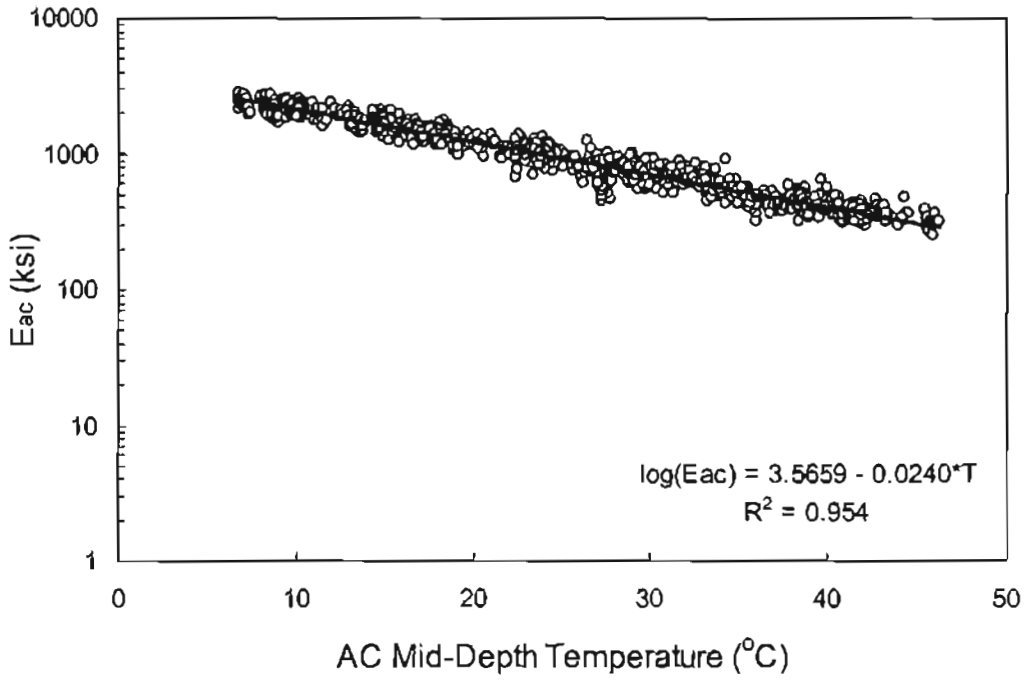

Figure 55. Predicted E_{ac} from the regression-based approach vs. temperature for WN pavement 1-0101

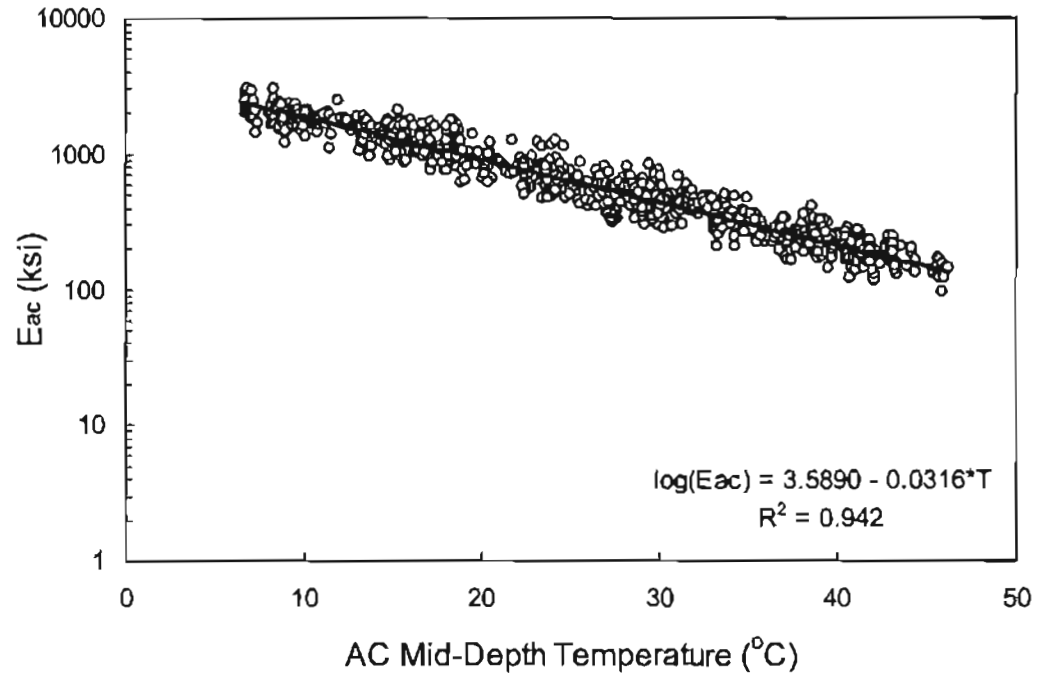

Figure 56. Predicted E_{ac} from Modulus 5.1 vs. temperature for WN pavement 1-0101

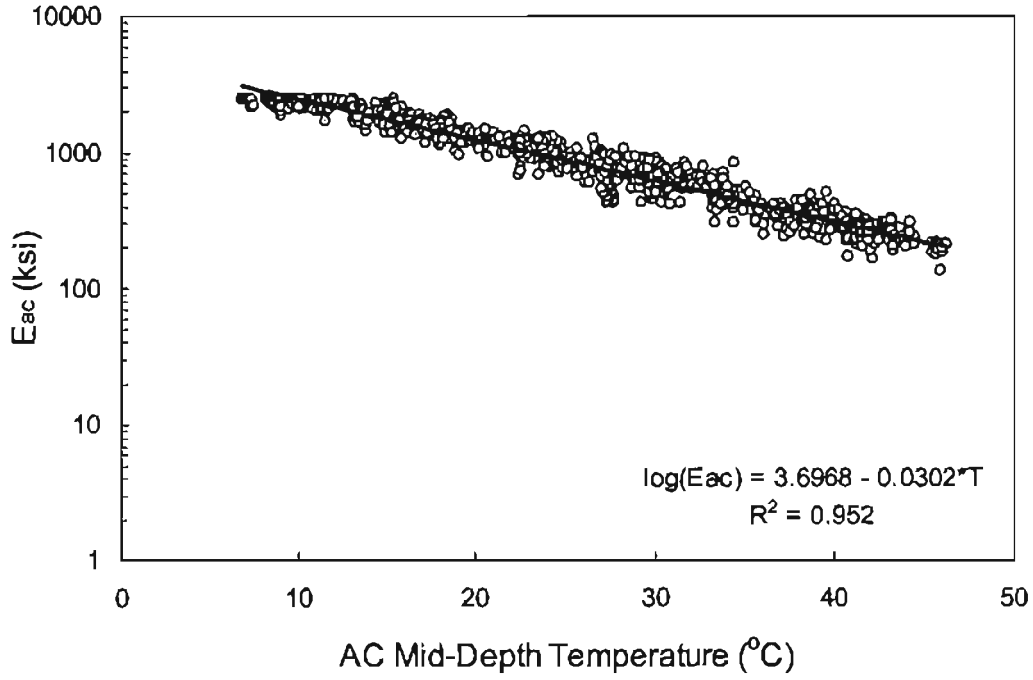

Figure 57. Predicted E_{ac} from ANN approach vs. temperature for WN pavement 1-0101

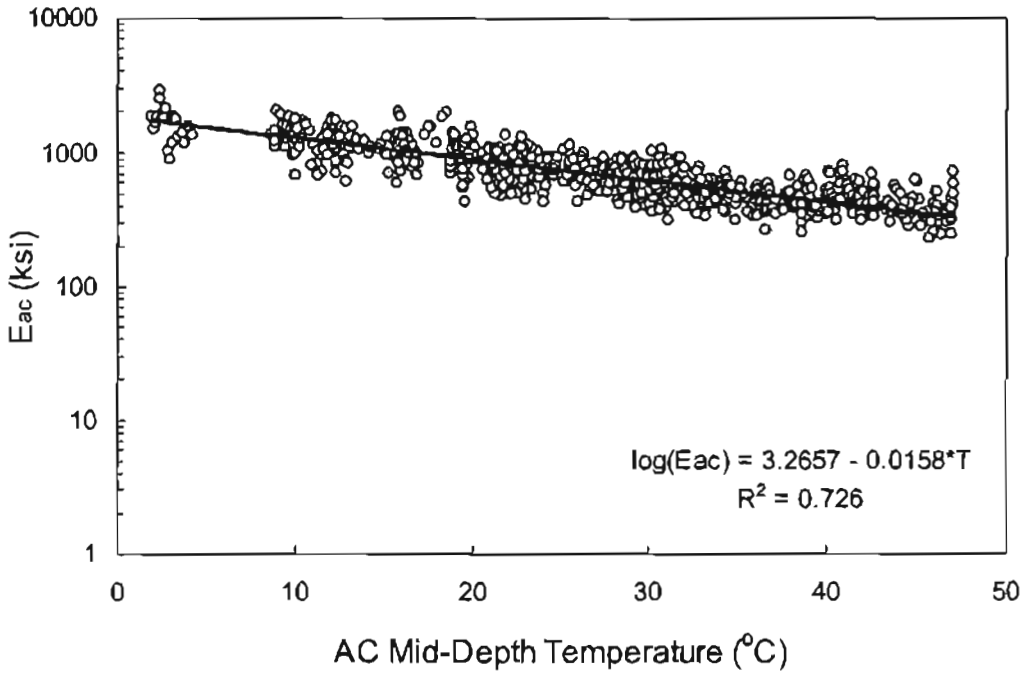

Figure 58. Predicted E_{ac} from the regression-based approach vs. temperature for WN pavement 1-0102

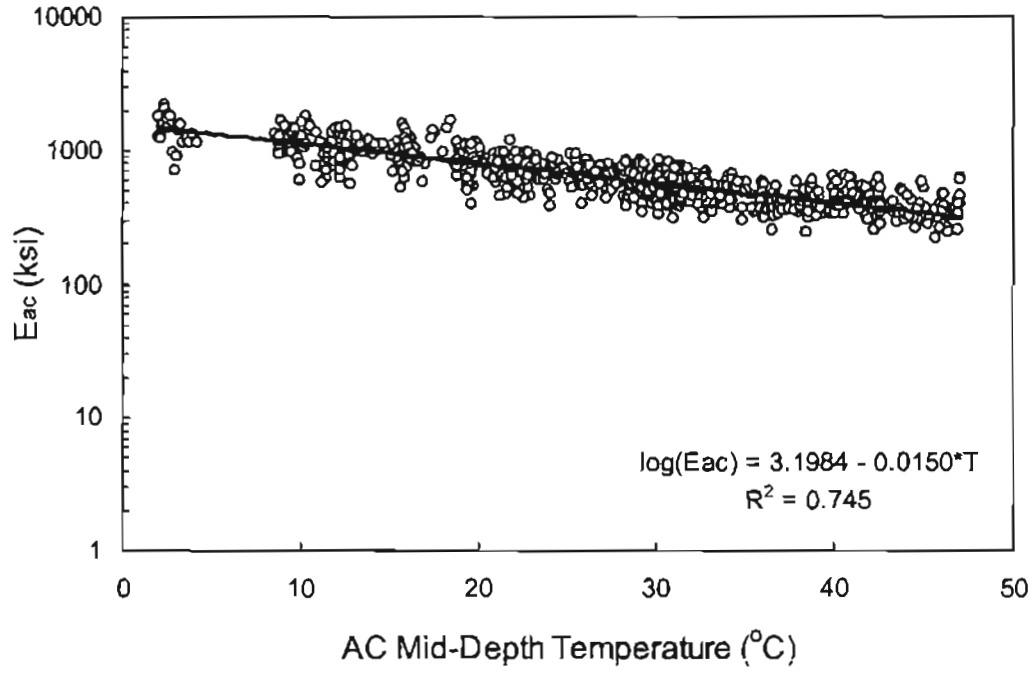

Figure 59. Predicted E_{ac} from Modulus 5.1 vs. temperature for WN pavement 1-0102

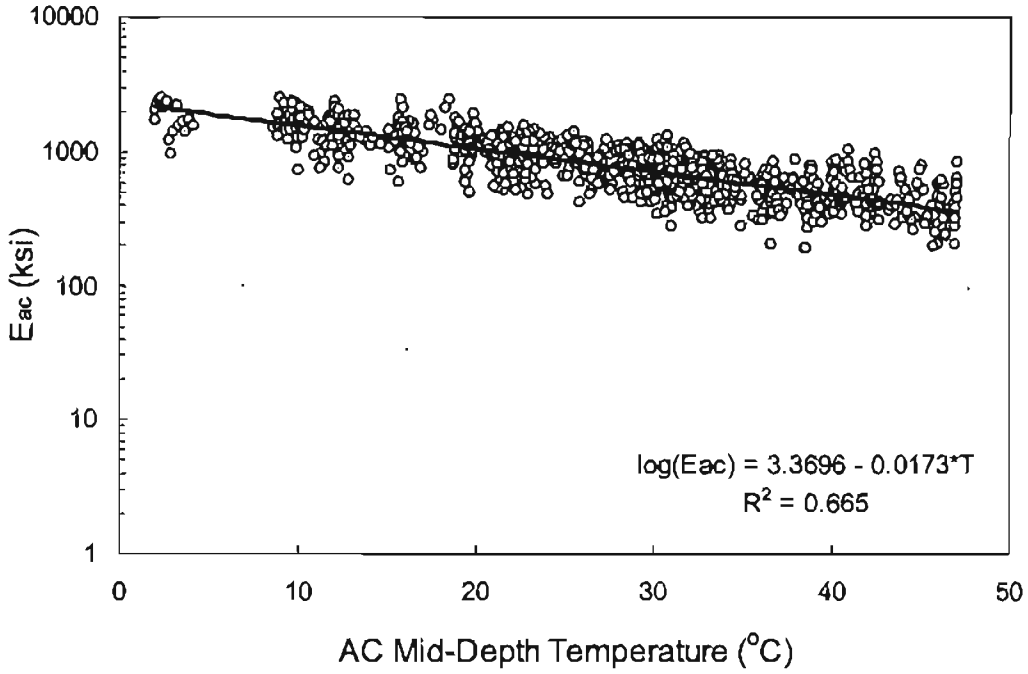

Figure 60. Predicted E_{ac} from ANN approach vs. temperature for WN pavement 1-0102

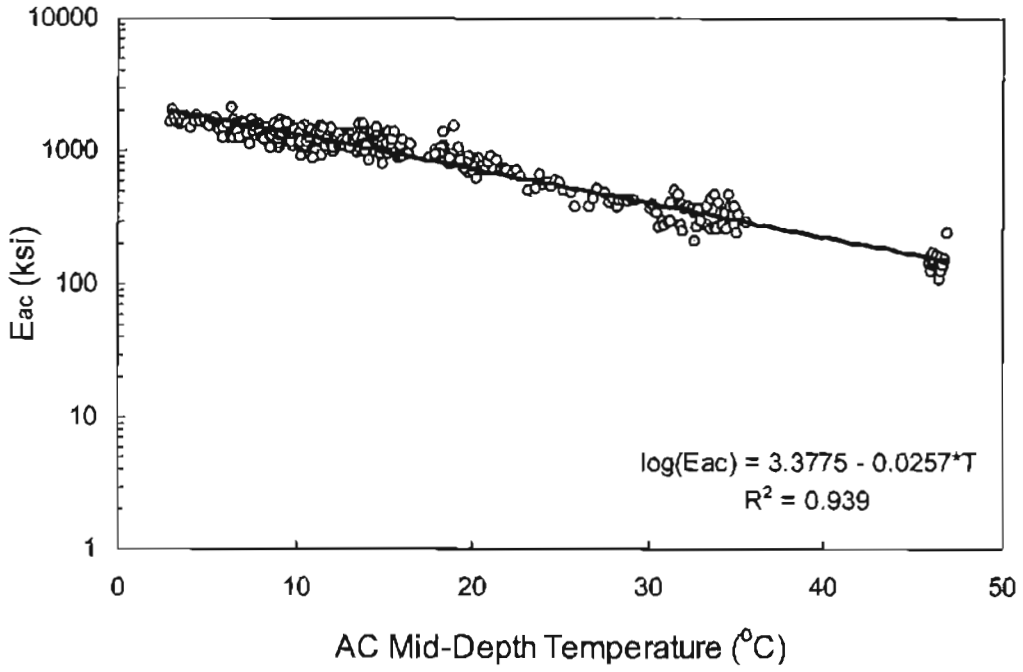

Figure 61. Predicted E_{ac} from the regression-based approach vs. temperature for WN pavement 51-0113

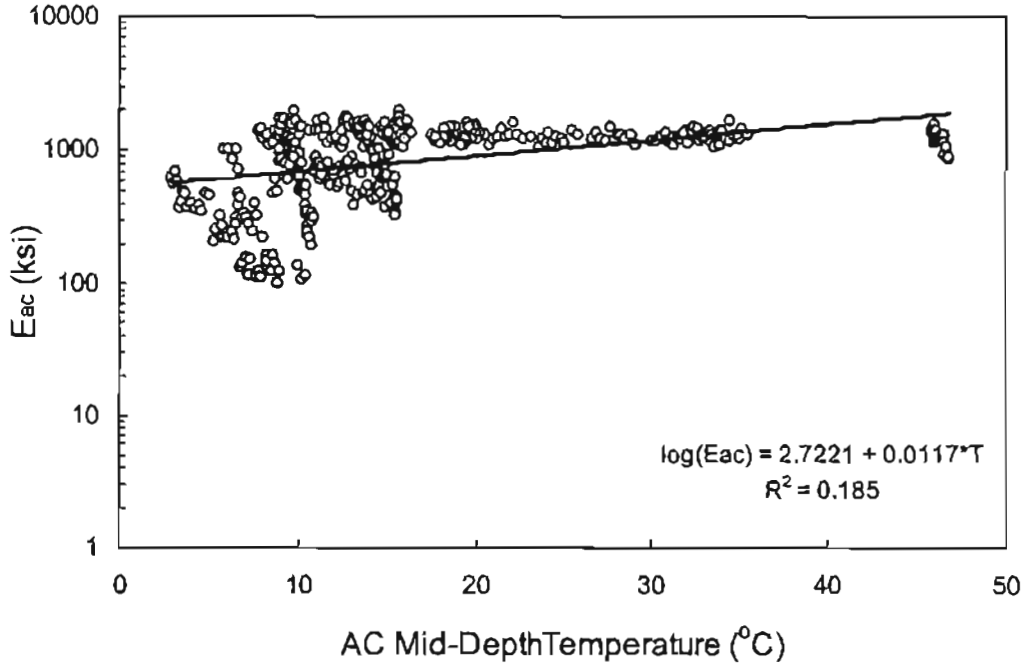

Figure 62. Predicted E_{ac} from Modulus 5.1 vs. temperature for WN pavement 51-0113

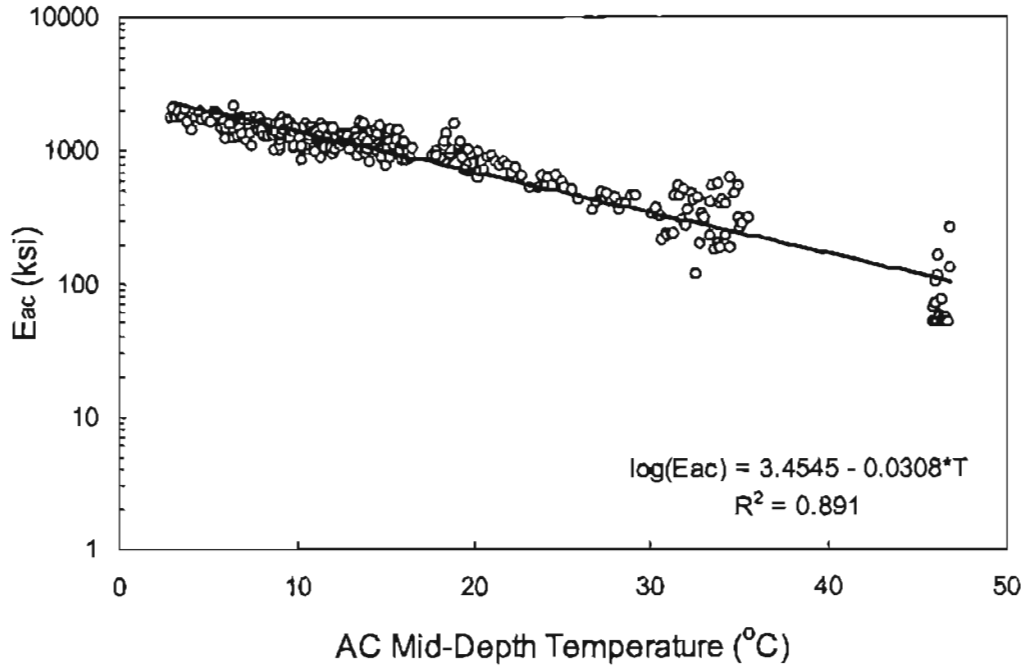

Figure 63. Predicted E_{ac} from ANN approach vs. temperature for WN pavement 51-0113

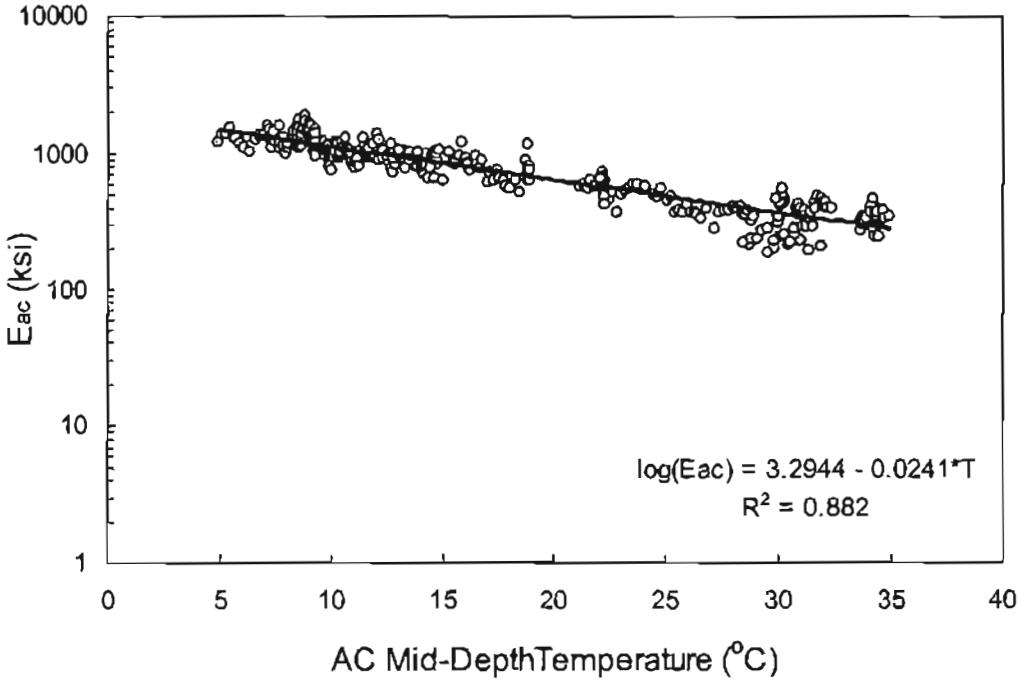

Figure 64. Predicted E_{ac} from the regression-based approach vs. temperature for WN pavement 51-0114

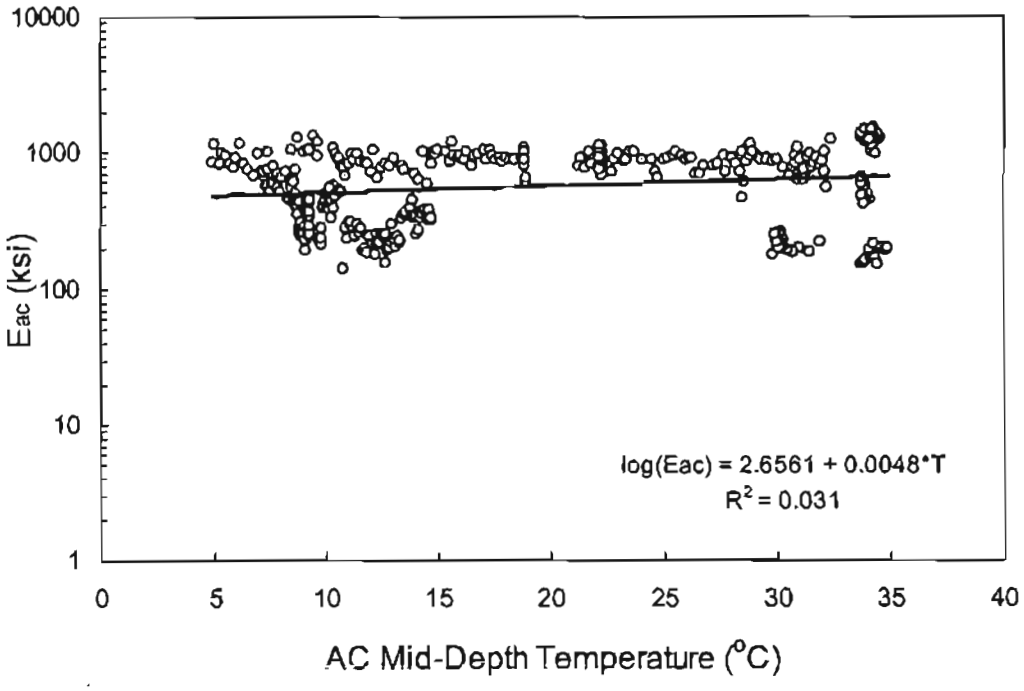

Figure 65. Predicted E_{ac} from Modulus 5.1 vs. temperature for WN pavement 51-0114

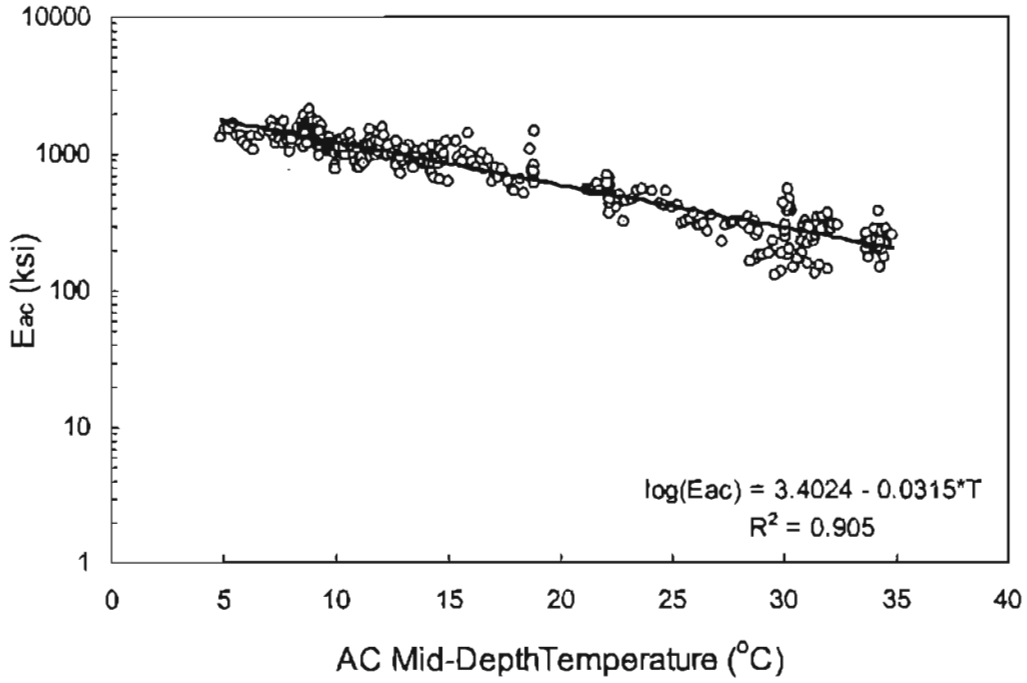

Figure 66. Predicted E_{ac} from ANN approach vs. temperature for WN pavement 51-0114

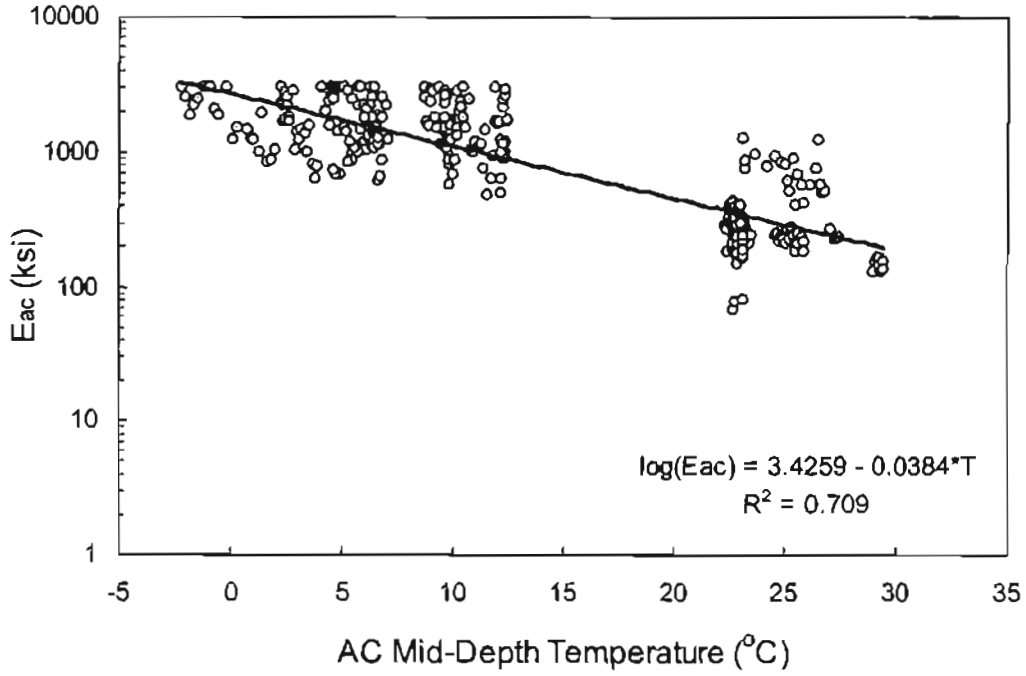

Figure 67. Predicted E_{ac} from the regression-based approach vs. temperature for WF pavement 10-0102

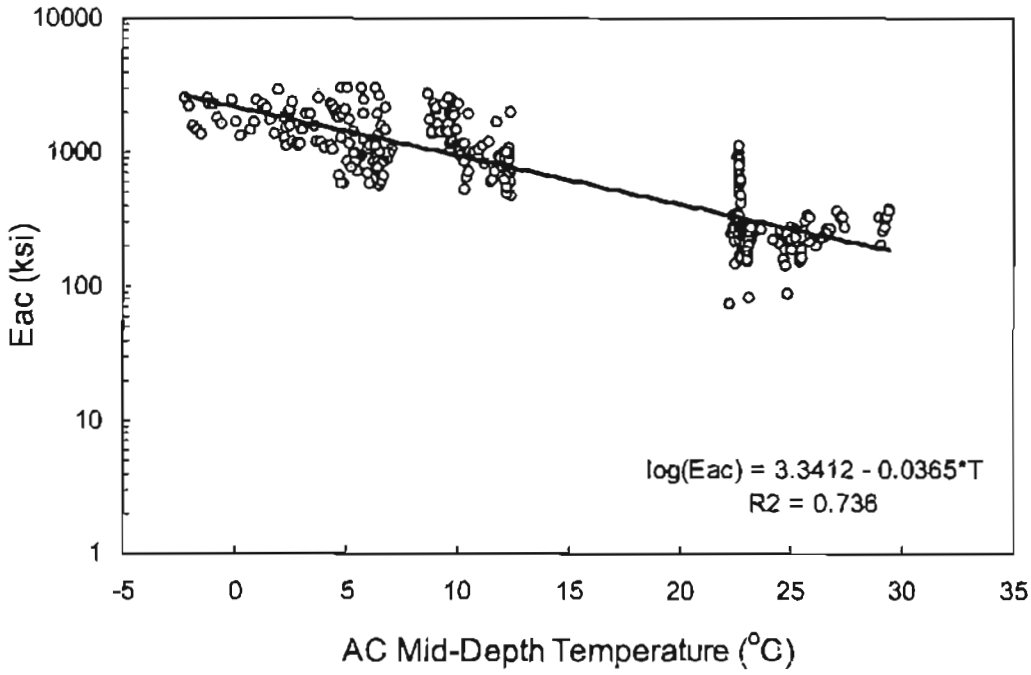

Figure 68. Predicted E_{ac} from Modulus 5.1 vs. temperature for WF pavement 10-0102

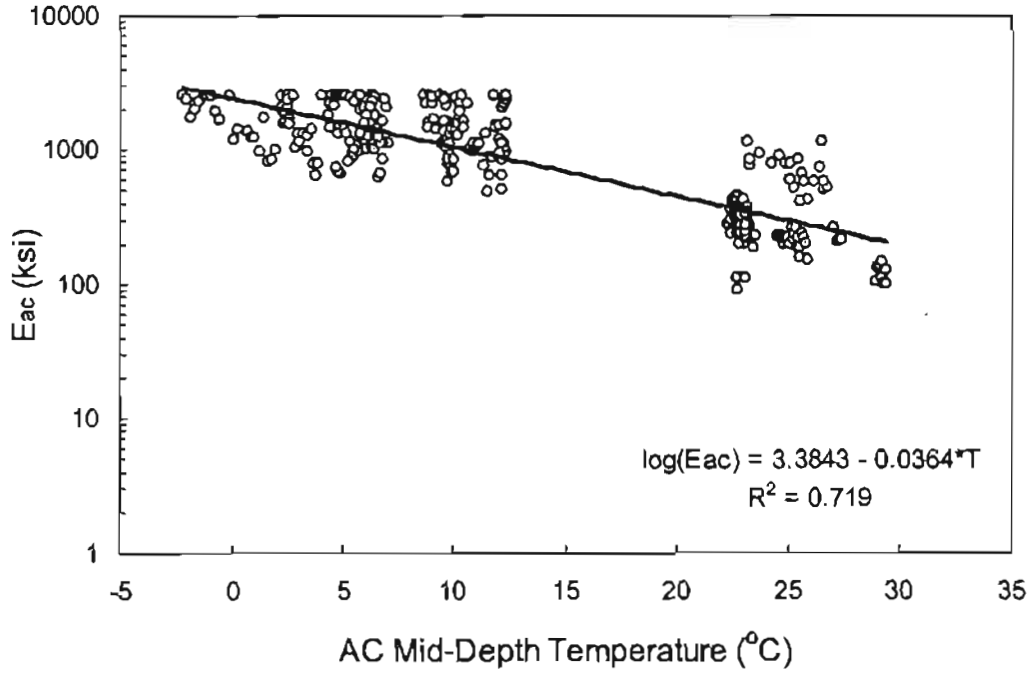

Figure 69. Predicted E_{ac} from ANN approach vs. temperature for WF pavement 10-0102

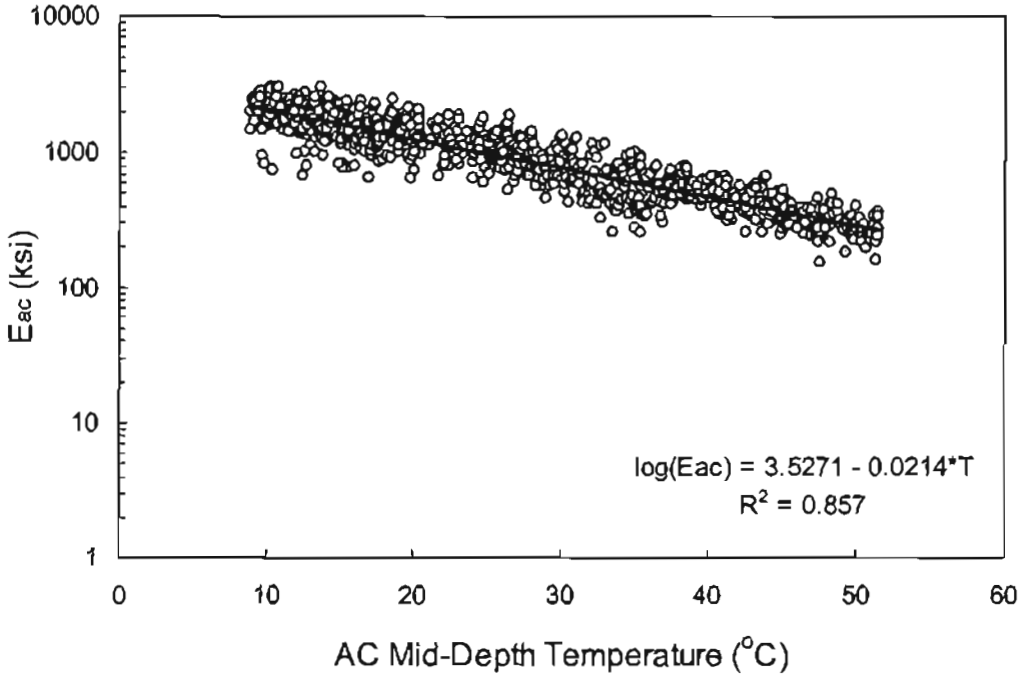

Figure 70. Predicted E_{ac} from the regression-based approach vs. temperature for DN pavement 40-0113

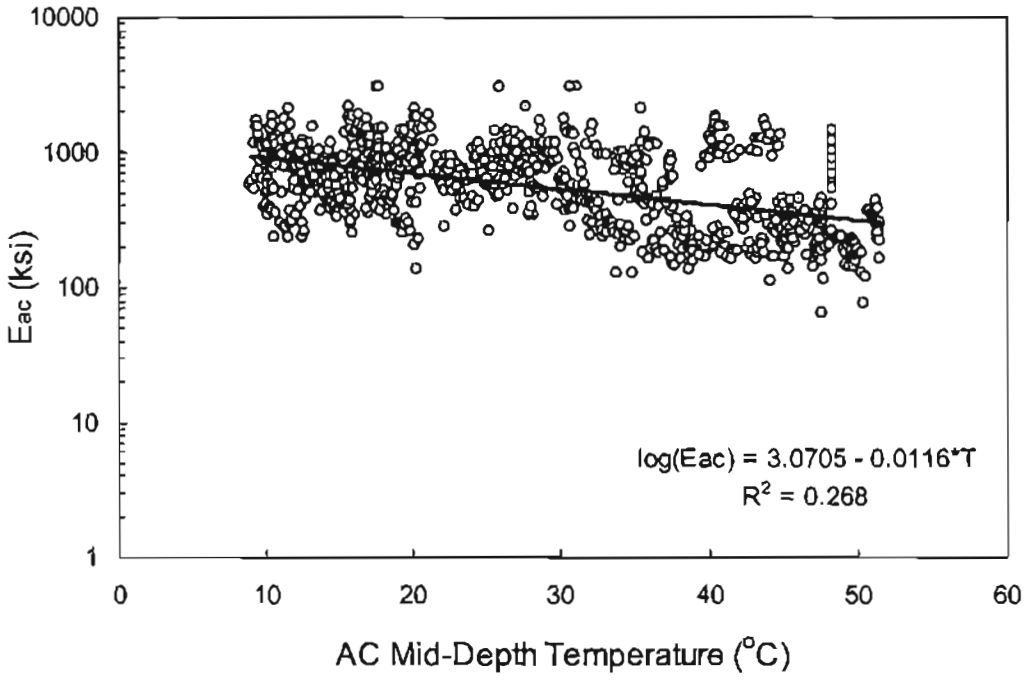

Figure 71. Predicted E_{ac} from Modulus 5.1 vs. temperature for DN pavement 40-0113

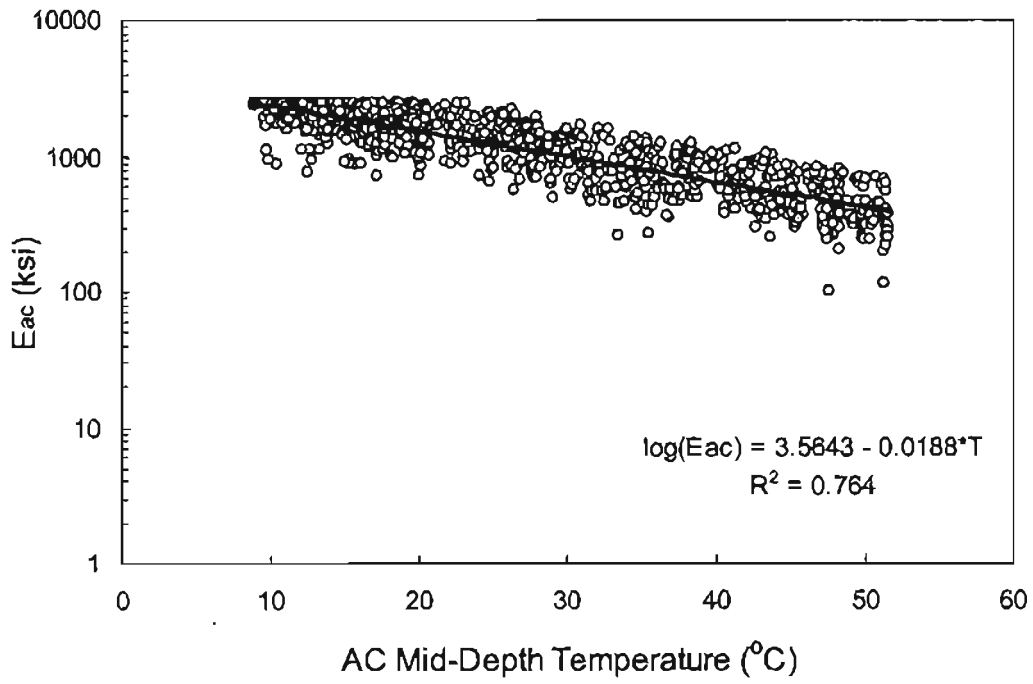

Figure 72. Predicted E_{ac} from ANN approach vs. temperature for DN pavement 40-0113

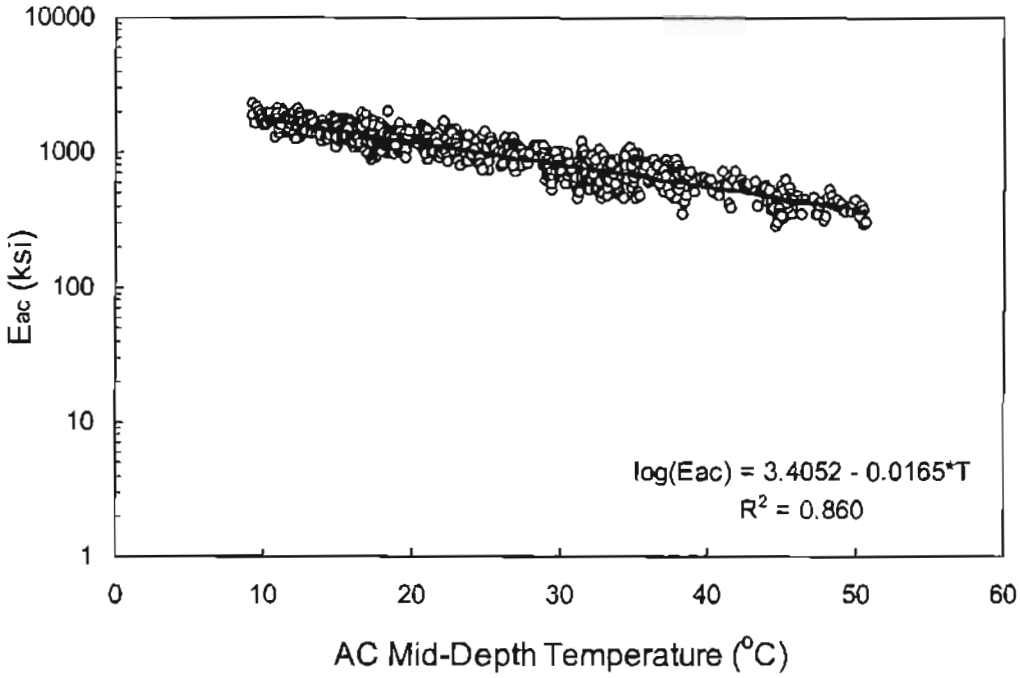

Figure 73. Predicted E_{ac} from the regression-based approach vs. temperature for DN pavement 40-0114

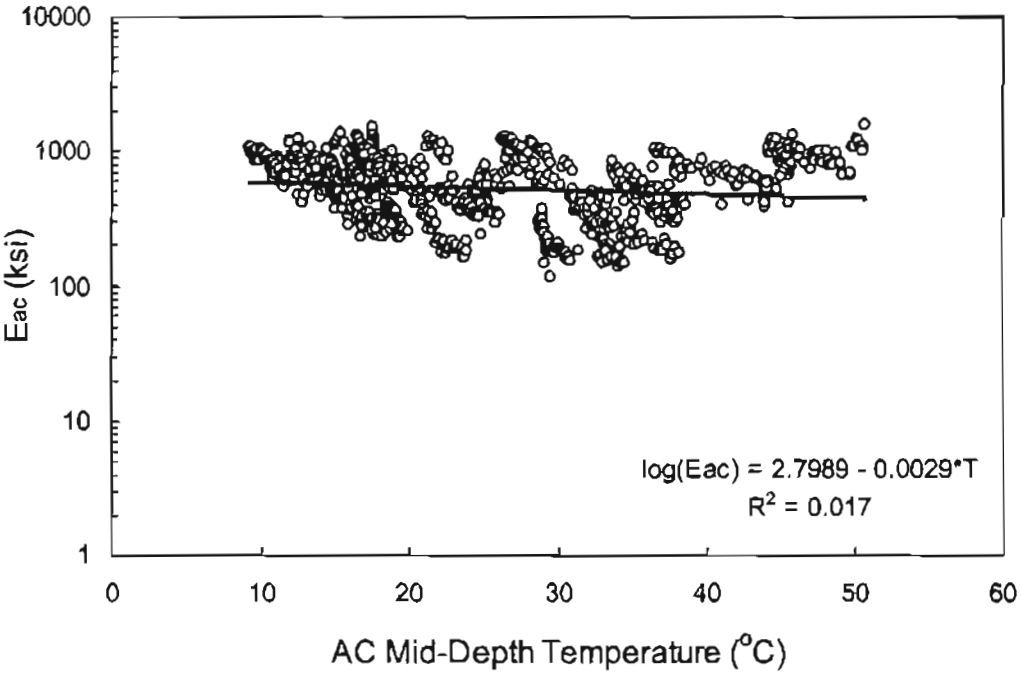

Figure 74. Predicted E_{ac} from Modulus 5.1 vs. temperature for DN pavement 40-0114

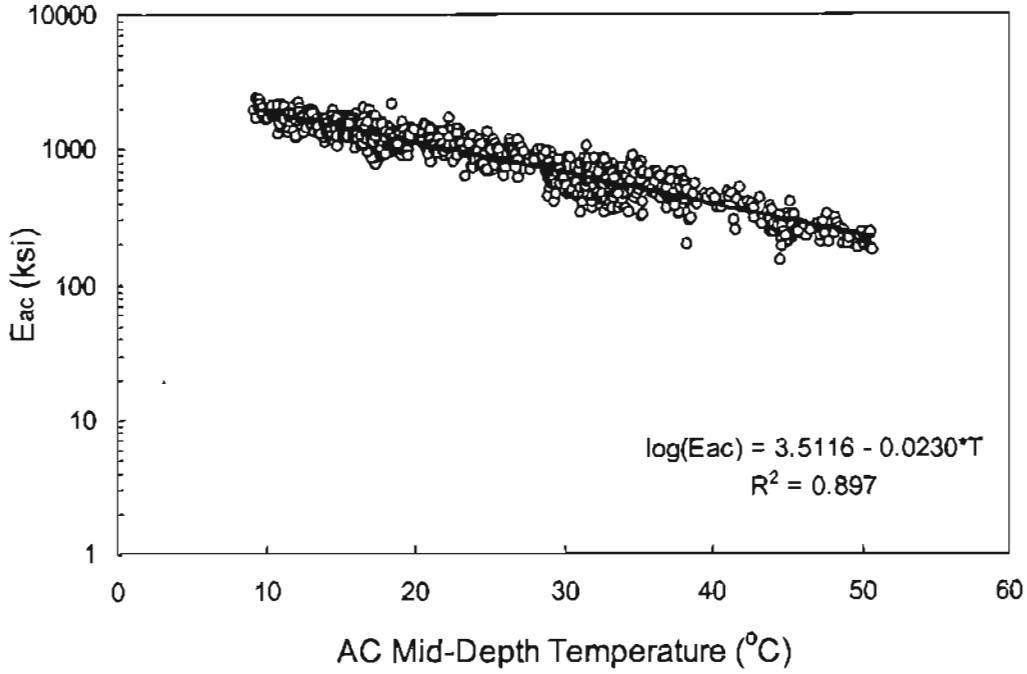

Figure 75. Predicted E_{ac} from ANN approach vs. temperature for DN pavement 40-0114

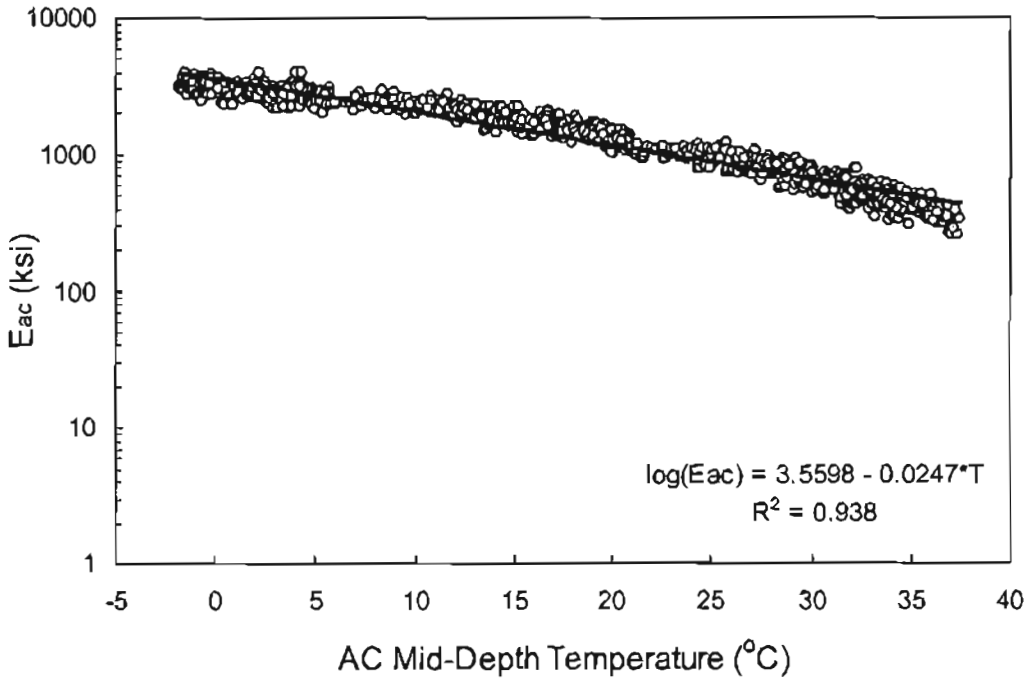

Figure 76. Predicted E_{ac} from the regression-based approach vs. temperature for DF pavement 32-0101

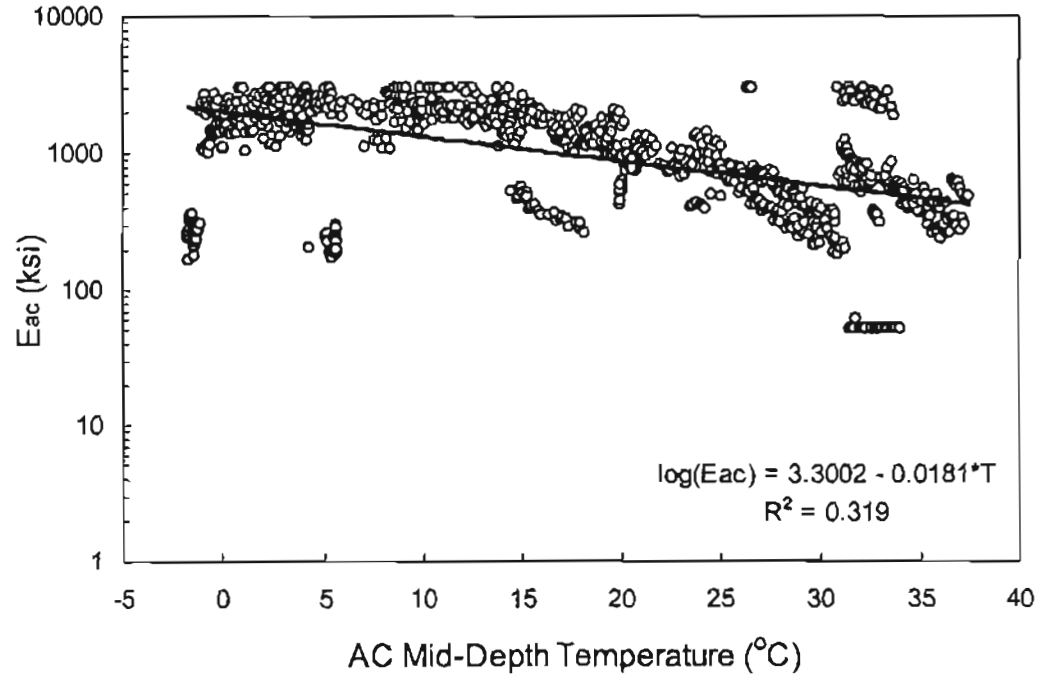

Figure 77. Predicted E_{ac} from Modulus 5.1 vs. temperature for DF pavement 32-0101

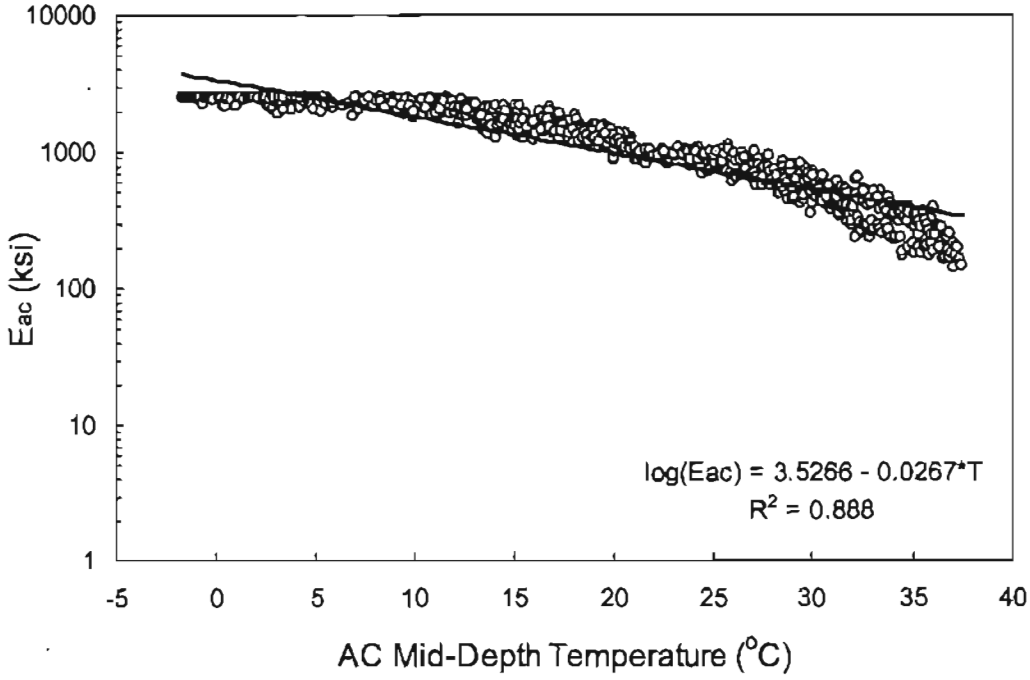

Figure 78. Predicted E_{ac} from ANN approach vs. temperature for DF pavement 32-0101

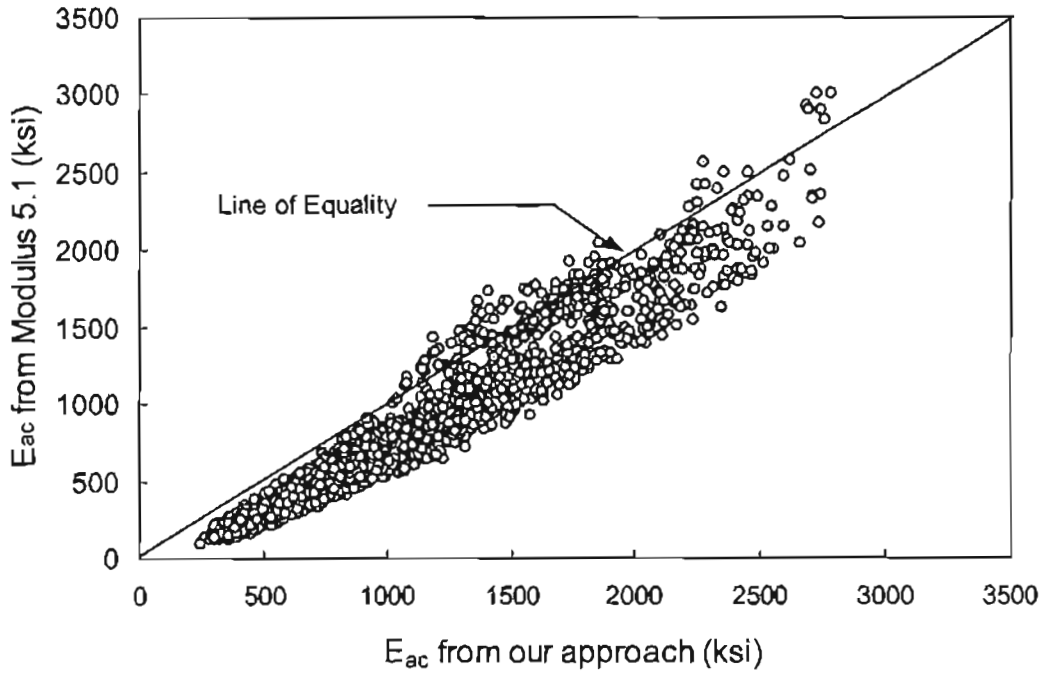

Figure 79. Comparison of E_{ac} predictions from the regression-based approach and Modulus 5.1 for intact WN pavement 1-0101

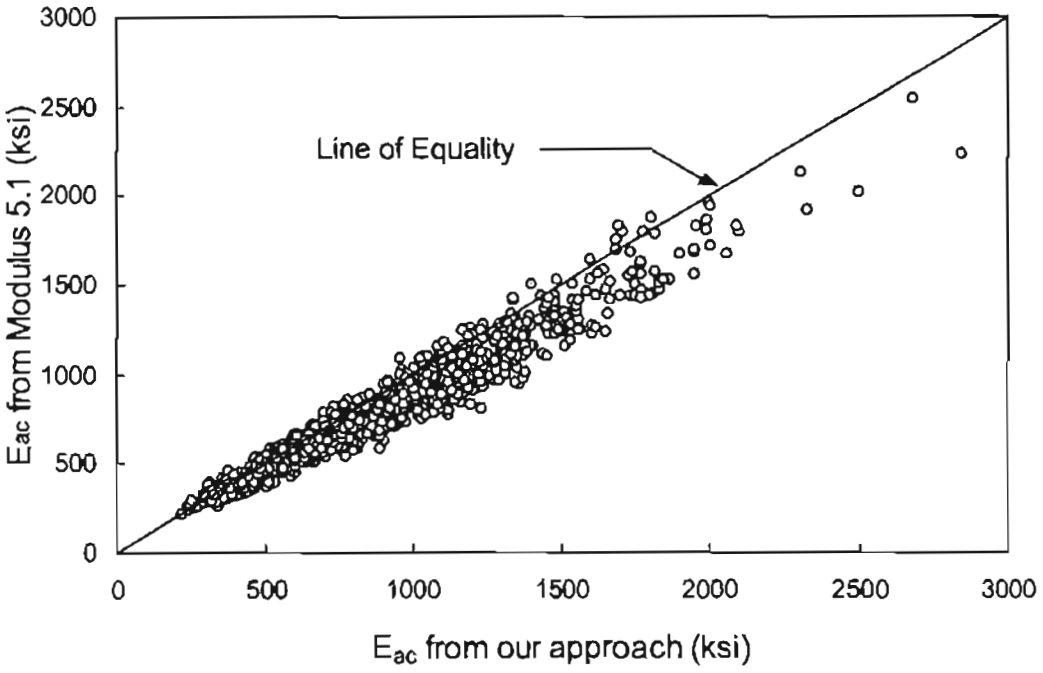

Figure 80. Comparison of E_{ac} predictions from the regression-based approach and Modulus 5.1 for intact WN pavement 1-0102

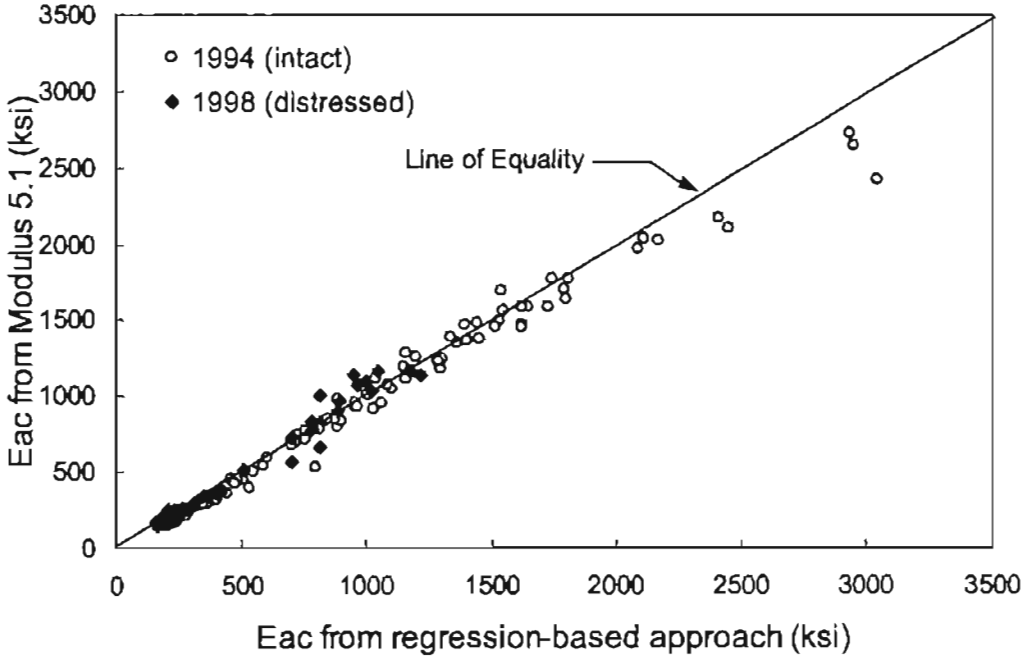

Figure 81. Comparison of Eac predictions from the regression based approach and Modulus 5.1 for intact and distressed Mn/ROAD pavements (1994 and 1998)

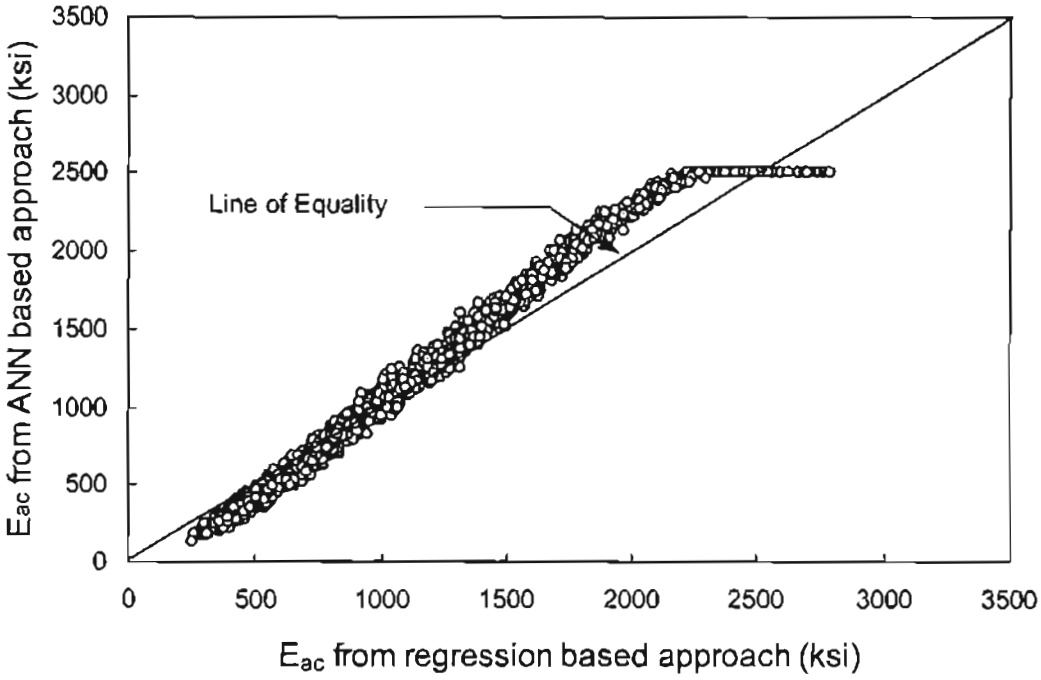

Figure 82. Comparison of E_{ac} prediction from the regression based approach and ANN approach for WN pavement 1-0101

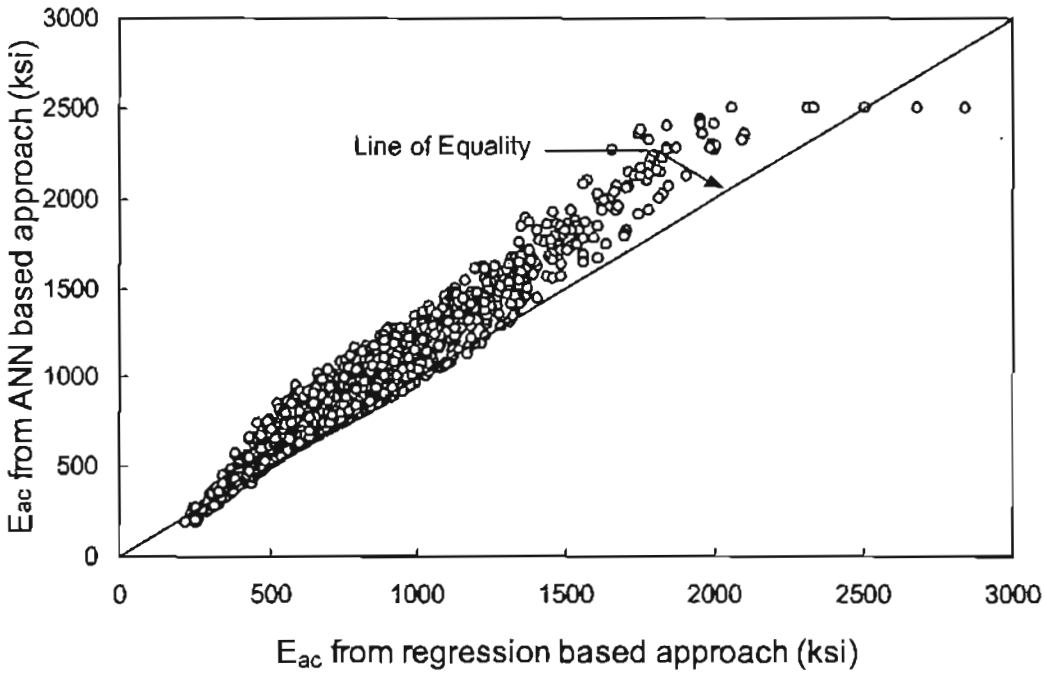

Figure 83. Comparison of E_{ac} prediction from the regression based approach and ANN approach for WN pavement 1-0102

than those from the regression based approach. The ANN approach, however, can not result in the E_{ac} value larger than 2500 ksi, which is the upper limit value used in training ANN.

Based on this study, the "*b*" values developed for the AC modulus-temperature relationships for each pavement were summarized in Table 20. The model from Mn/ROAD pavements was also included. The average "*b*" values of the pavements in the same climate regions were suggested as the regional "*b*" values.

It can be seen from Table 20 that "*b*" values in the AC modulus-temperature model vary with climate regions, which is probably due to the difference in physical properties of the asphalt mix used in these regions. Generally, larger "*b*" values were obtained in the freeze climate region than in the no-freeze region. Also the wet climate region resulted in larger "*b*" values than the dry climate region.

An accurate AC modulus-temperature model for the pavement in evaluation is very important in detecting distresses in AC layer. If state agencies do not have the models specific for their own asphalt mixes used, the regional models developed in this research could be applied as a substitute.

Another issue of note is that variations of actual AC thickness from their design values could cause variations in the development of the AC modulus vs. temperature relationship. AC thickness is needed as an input in most of the condition assessment procedures, and the design thickness is often used as the input value. However, from coring or Ground Penetration Radar testing of field pavements, it has been reported that the design thickness is usually not equal to the actual AC thickness. If the design thickness is smaller or larger than the actual thickness, the predicted AC modulus value will be higher or lower, respectively, than the actual value. This could cause variations in constructing the intact AC modulus-temperature relationship.

Table 20. Regional "b" values in AC modulus vs. temperature model

Pavement	"b" value	"a" value	region	Regional "b" value
1-0101	0.0240	3.566	WN	0.0235
1-0102	0.0158	3.266	WN	
51-0113	0.0257	3.378	WN	
51-0114	0.0241	3.294	WN	
10-0102	0.0389	3.438	WF	0.0327
Mn/ROAD	0.0265	3.335	WF	
4-0113	0.0214	3.527	DN	0.0189
4-0114	0.0165	3.405	DN	
32-0101	0.0247	3.560	DF	0.0247

The actual AC modulus of an aged asphalt layer may show higher values due to hardening. Thus, if this hardening effect on AC modulus outweighs the loss of the AC modulus due to distress, the predicted AC modulus value may not appropriately represent the condition.

The proposed procedure was applied to the 1994 and 1998 field data for Sections 2, 18, 22, and 28 from the Mn/ROAD test sites to demonstrate these issues. Based on the 1994 data of all four sections, the AC modulus vs. temperature relationship was obtained as follows:

$$\log(E_{ac}) = 3.2247 - 0.0265 * T \tag{73}$$

$$R^2 = 0.852$$

The AC modulus values corresponding to the 1994 and 1998 data were estimated using Eqs. 35 and 36. To examine the variations of the AC moduli by section and year of measurement, the temperature correction procedure was applied to get the AC moduli at a reference temperature of 25°C. Using Eq. 73, the following temperature adjustment factor is obtained:

$$\alpha = \frac{E_{ac,T_m}}{E_{ac,T_r}} = 10^{-b*(T_m - T_r)} \tag{74}$$

where b is 0.0265 for Mn/ROAD pavement.

This adjustment factor was then applied to the estimated AC modulus values to obtain the adjusted values at the reference temperature of 25°C. That is

$$Adjusted \quad E_{ac} = \frac{Estimated \quad E_{ac}}{\alpha} \tag{75}$$

Table 21 shows the adjusted AC modulus values at 25°C for each test section from both the 1994 and 1998 data.

The first observation from Table 21 is that the intact AC modulus values, E_{ac2}, varied from section to section. Section 22 had the lowest modulus of 291 ksi, while Section 18 had the highest at 445 ksi. Another observation is that the modulus values corresponding to distressed

Table 21. Comparison of AC modulus values for the Mn/ROAD test sections

Section	E_{ac1}[a], ksi	E_{ac2}[b], ksi	E_{ac3}[c], ksi	ERR1[d],%	ERR2[e],%
22	365	291	658	80.3	126.1
18	365	445	758	107.7	70.3
2	365	420	729	99.7	73.6
28	365	348	359	-1.6	3.2

[a]estimated E_{ac} at 25°C using Eq. 73 by neglecting the differences of intact AC moduli among sections;

[b]predicted E_{ac} at 25°C in 1994, which is first calculated using Eq. 35 or 36; and then applying temperature adjustment using Eq. 74;

[c]predicted E_{ac} at 25°C in 1998; which is first calculated using Eq. 35 or 36; and then applying temperature adjustment using Eq. 74;

[d]difference between E_{ac1} and E_{ac3} in percentage;

[e]difference between E_{ac2} and E_{ac3} in percentage.

conditions in 1998, E_{ac3}, are significantly higher than the intact values. This could be attributed to the aging effect of asphalt concrete. The differences in the modulus values ERR1 and ERR2 were calculated (last two columns in Table 21) to represent the significance of the aging effects and the distress condition in the AC layer. If the differences in intact AC modulus values are neglected, Section 18 and Section 2 will mistakenly be considered as the pavements with the least distress because their ERR1 values are the highest. On the other hand, if these differences are accounted for, Section 22 would be considered the pavement with least distress because it has the highest ERR2 value, which agrees well with the field observation. Based on both ERR1 and ERR2 values, Section 28 seems to have the most distress in the AC layer because its values are significantly lower than that of the other pavements.

To address this issue, one could conduct FWD tests at both the wheel path and the center of lanes. Usually, traffic induced distresses such as fatigue cracking are only localized to the area of wheel tracks. Therefore, the area in the center of each lane could be considered relatively intact. By comparing predicted E_{ac} values at both wheel path and the center of lanes, potential distresses in the AC layer under the wheel path could be detected. One benefit of this method is the elimination of the aging effect since both FWD tests were conducted at the same time.

Base Strength

Two criteria for estimating base layer condition described previously are the BDI and ε_{abc} adjusted for structural correction. It should be noted that these criteria were developed based only on a few field data points, representing a relatively narrow range of pavement structures.

When applying these criteria to pavements with structures significantly different from those used in their development, potential discrepancies in predictions should be expected.

In this research, the criteria for the condition indicators were set based on a critical CBR value of 100. If this basis were to be different in practice, the corresponding new criteria for these indicators could be determined using the same approach as described in "Findings." If pavements meet the criteria for any one of the indicators, the base layer should be considered to be in a poor condition. Doing so would help achieve a more robust condition assessment since measurement errors may affect the condition indicators differently.

The field data from the US 264 pavements were used to test this procedure. US 264 test sections are located at Hyde County, North Carolina. Among the 47 test positions, pavements were cored and DCP tests were carried out at two locations. It was reported that the calculated *CBR* values for those two locations were 60 and 80 respectively, indicating poor base condition. Figures 84 and 85 show the adjusted *BDI* values and adjusted ε_{abc} values, respectively, along all positions. It can be seen that the values of adjusted ε_{abc} at all positions are larger than 720 microstrain, which suggests poor base layer condition at all locations. Based on the adjusted BDI values, however, there are several points that fall outside the region corresponding to poor base condition. For this study, the adjusted ε_{abc} value as an indicator seems to perform better than the adjusted *BDI* value. This confirms that both indicators need to be checked to assess base layer condition.

Subgrade Strength

The criteria for proposed subgrade condition indicators (i.e., E_{sg} and structurally corrected BCI, ε_{sg}, and SSR values) were determined from the pavements with known subgrade

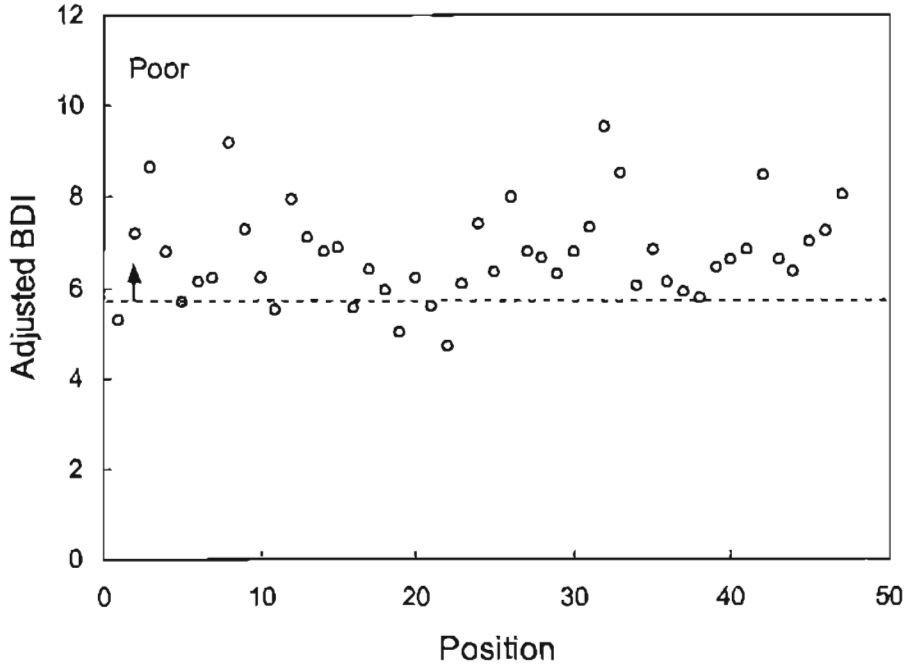

Figure 84. Adjusted BDI vs. position for aggregate base pavements from US 264

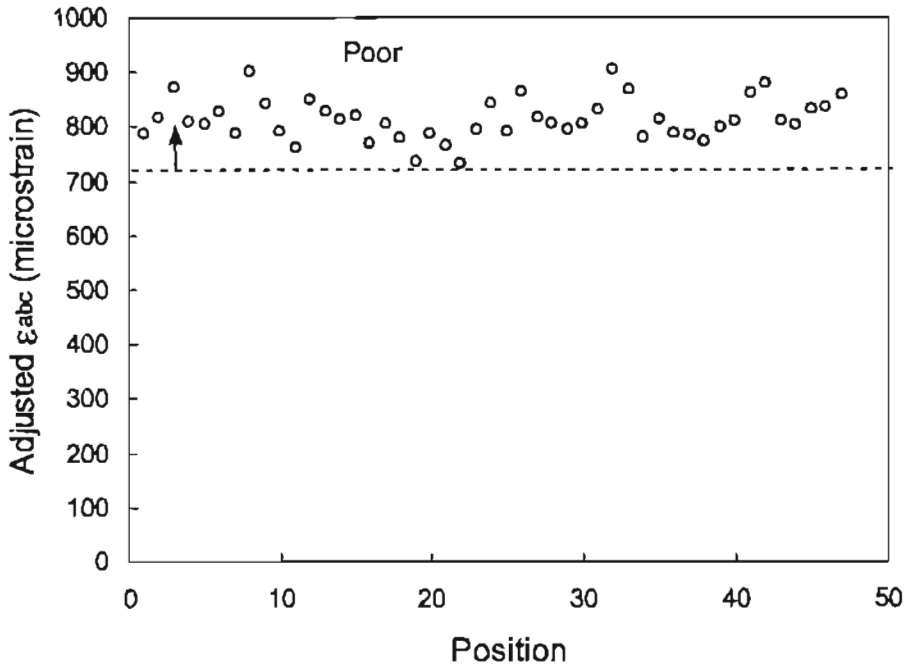

Figure 85. Adjusted ε_{abc} vs. position for aggregate base pavements from US 264

CBR values. A *CBR* value below 10 was considered to represent a poor subgrade condition. Again, if this basis were to be different in practice, the corresponding new criteria for these indicators could be determined using the same approach as described in "Findings." If an FWD measurement meets any one of the proposed criteria, the corresponding subgrade condition should be considered poor.

To test the performances of these different condition indicators, US 264 data were used. It has been reported that very weak subgrade exists in US 264 pavements. Figures 86 to 89 show the variation of adjusted *BCI*, adjusted ε_{sg}, adjusted *SSR*, and E_{sg}, respectively, along pavement positions. It can be seen that adjusted *BCI*, adjusted *SSR*, and E_{sg} values properly indicate poor subgrade condition, while adjusted ε_{sg} does not predict correctly at many positions.

As many state agencies use Modulus 5.1 program as a tool for subgrade modulus backcalculation, a comparison was made to demonstrate the difference in E_{sg} predictions from the proposed method in this research and the Modulus 5.1. Modulus 5.1 is a layered elastic theory based program where the static, linear elastic analysis was applied. The proposed method, on the other hand, is resulted from the dynamic, linear elastic analysis. Based on the study of the synthetic data, it was found that the deflections resulted from dynamic analysis are usually larger than from the static analysis. As pavements become very strong or subgrade is extremely weak, the static analysis, however, could result in larger deflections. These observations from the synthetic data indicate some trends between Modulus 5.1 and the proposed method in E_{sg} prediction. That is, generally the predicted E_{sg} value from Modulus 5.1 will be smaller than from the proposed method. As pavement becomes strong or subgrade becomes weak, this difference in E_{sg} prediction decreases. For the cases with extremely strong AC layer, the Modulus 5.1 prediction could be larger than the prediction of the proposed method.

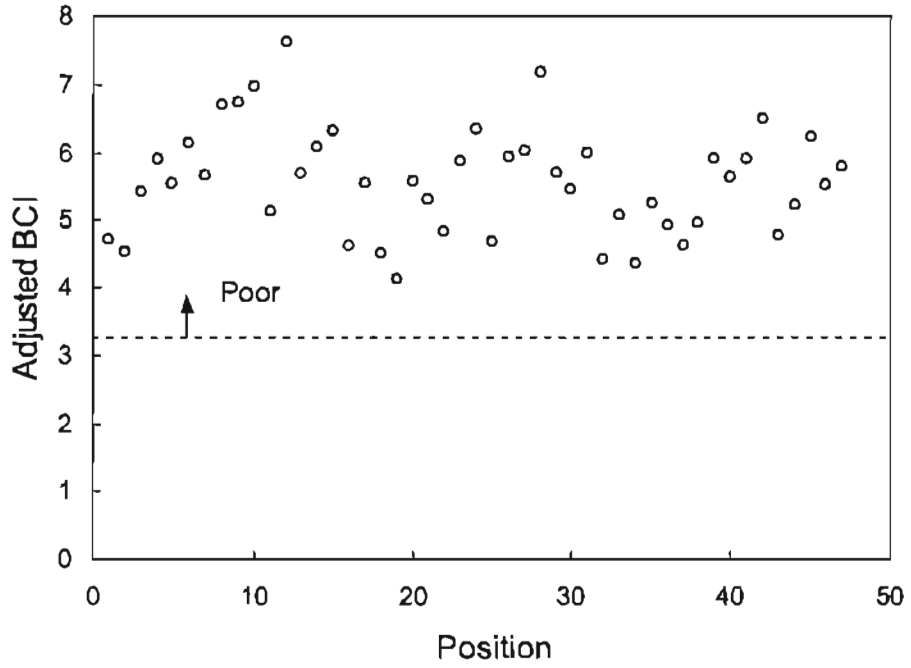

Figure 86. Adjusted BCI vs. position for aggregate base pavements from US 264

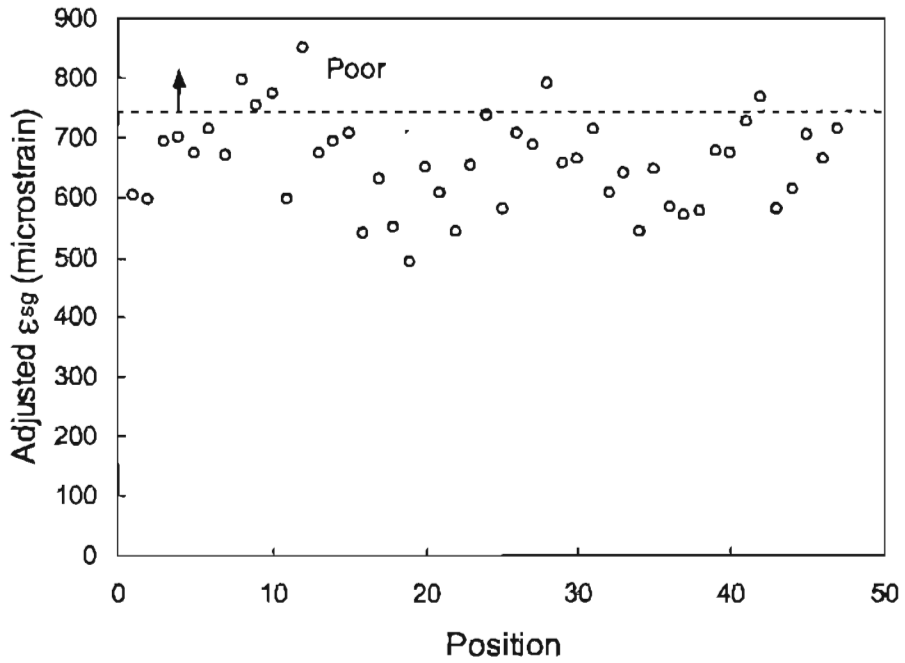

Figure 87. Adjusted ε_{sg} vs. position for aggregate base pavements from US 264

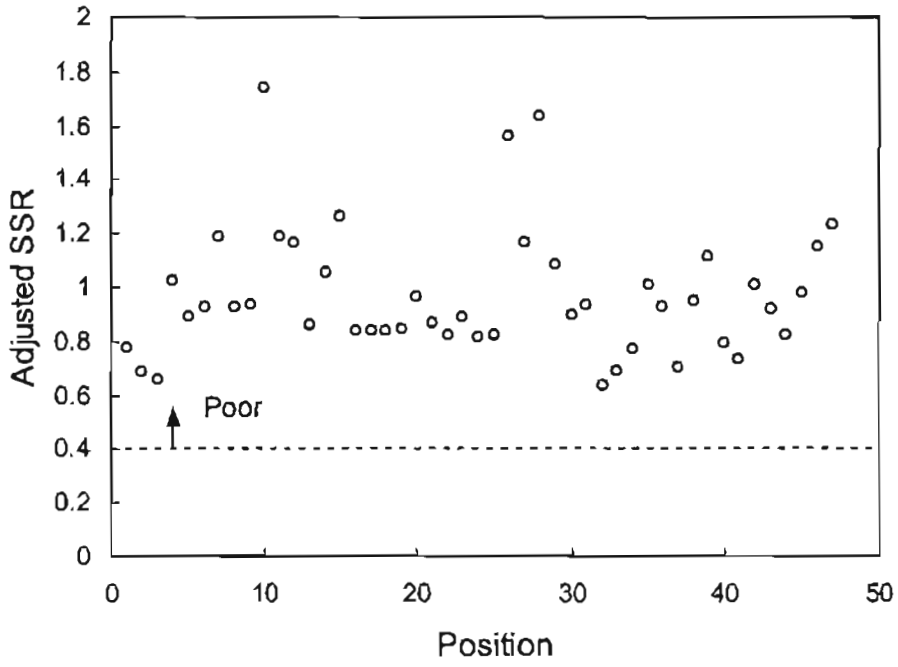

Figure 88. Adjusted SSR vs. position for aggregate base pavements from US 264

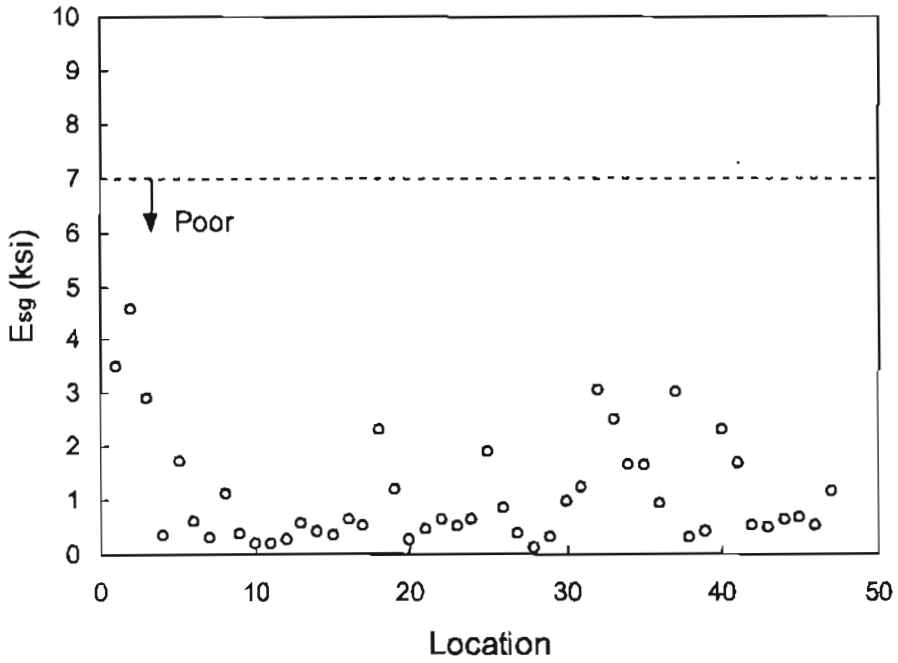

Figure 89. Predicted E_{sg} vs. position for aggregate base pavements from US 264

Figures 90 and 91 confirm these indications. From Figure 90, it can be seen that mostly E_{sg} predictions are slightly higher when using the proposed method. This is probably due to the thick AC layer thickness used. As subgrade modulus becomes stronger, the difference of E_{sg} prediction between both approaches increases. Figure 91 shows the predictions from both approaches for pavement 04-1036 at both winter and summer time. During the winter, because AC layer modulus become stronger, the prediction difference decreases significantly as expected. Comparing to Figure 91, the difference for pavement 04-1036 is more significant than for pavement 04-1001 due to the thin AC thickness used in pavement 04-1036.

CEMENT TREATED BASE PAVEMENTS

The challenge presented in this research was to determine a procedure for the determination of pavement layer condition based on FWD tests. As stated previously, the DBP BDI best represented upper layer condition, while D_{48} and F_3 were used as indicators for subgrade condition and stiff layer depth, respectively. Table 22 summarizes the indicators and their respective prediction methods. Important issues concerning the implementation of the proposed methods are described below. The limitations of the procedures are also included.

Debonding in the AC Layer

As discussed previously, practically no field data was available with debonding in the asphalt layer. Discontinuities under the load plate could not be modeled in the axisymmetric finite element formulation. Only six data points were available from the field database for the determination of a parameter capable of indicating asphalt layer debonding under FWD loads. BDI was found to be the best indicator for the data points available.

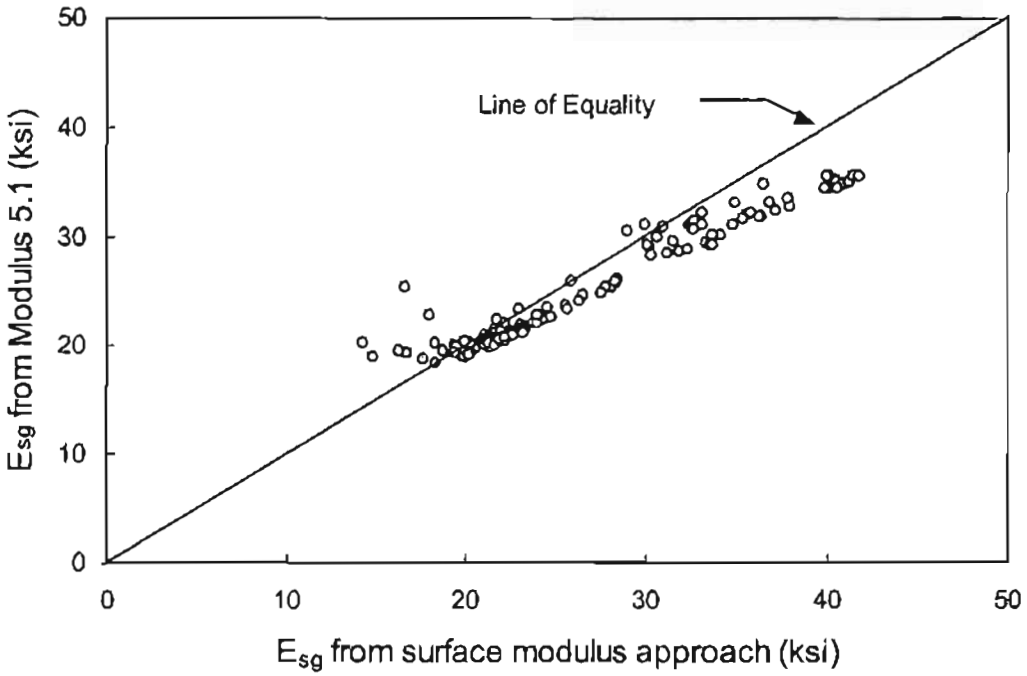

Figure 90. Comparison of predicted E_{sg} from surface modulus based approach and Modulus 5.1 for full-depth pavement 04-1001 (H_{ac} = 11 inches)

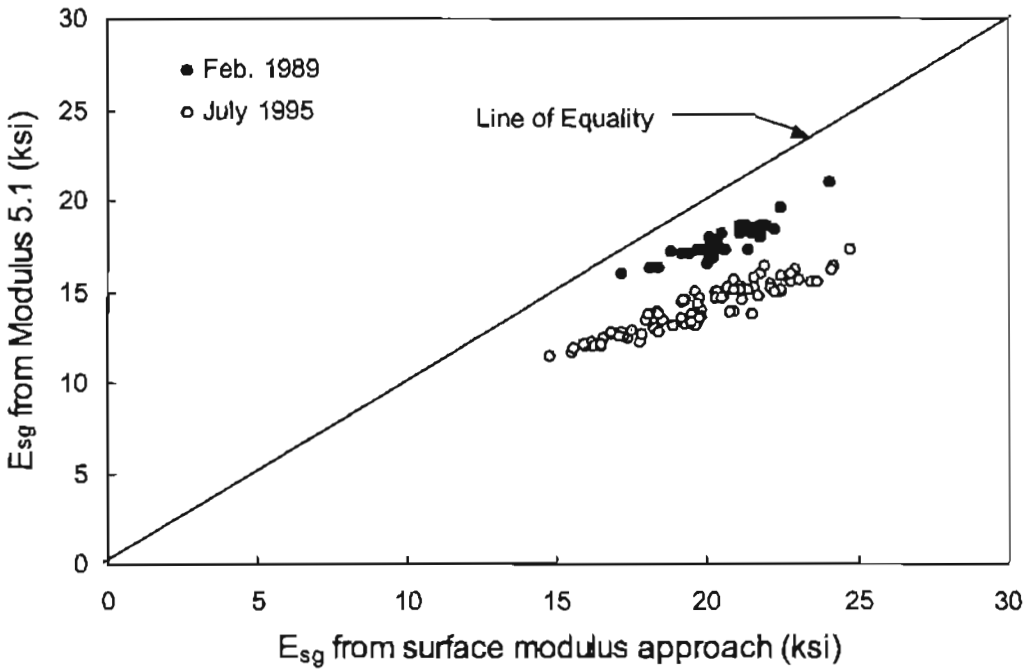

Figure 91. Comparison of predicted E_{sg} from surface modulus based approach and Modulus 5.1 for full-depth pavement 04-1036 (H_{ac} = 3.5 inches)

Table 22. Proposed methods for layer condition assessment using condition indicators for CTB pavements

Layer	Condition	Indicator	Proposed Method	Required Inputs	Criteria for Poor Condition
AC	Debonding	*BDI*	*BDI* Envelope	D_{12}-D_{24}	*BDI* $\geq$ 2.5 mils
CTB	Cracking	*BDI*	*BDI* Envelope	D_{12}-D_{24}	*BDI* $\geq$ 2.5 mils
Subgrade	Strength	D_{48}	Regression Method (Eq. 55)	D_{48}	*CBR* $\leq$ *10*
Stiff Layer	Depth	F_3	Regression Method (Eq. 56)	D_{24}, D_{36}, D_{48}	*N/A*

Cracking in CTB Layer

BDI was identified as the best indicator for cracking in the CTB layer, as described previously. Again, little field data was available for the development of a reliable condition indicator.

In this research, data from the NC 421 test sections were used to develop the prediction procedure. NC 421 field records contained test information from February of 1990 through August of 1993. Cores were taken at the same time as FWD testing in August '93, and the condition noted in field logs. These core logs were used to compile a list of test sites, both intact and cracked, that could be utilized in the design of a base layer condition algorithm. At location where the core log reported no damage, or an intact condition, FWD tests performed in that location earlier in the service life were considered intact. Special care was taken to note when overlay procedures took place. An overlay placed over a distressed section would, of course, make determining distress difficult. At locations where distress was noted in the field report, only the FWD test results from the most recent test could be included in the distressed database as condition prior to the coring procedure were unknown. Figure 92 shows a clear separation between intact and distressed field data cases at a BDI value of 2.5. The BDI envelope value of 2.5 was confirmed through tests of the synthetic database. A BDI value over 2.5 indicates some distress in the CTB layer, while a calculated BDI value of less than 2.5 indicates adequate condition in the base layer.

The BDI method is limited in that it does not clearly delineate the debonding distress condition from the CTB cracking distress condition. Figure 92 illustrates this limitation. The debonded asphalt layer cases appear above the BDI envelope, but the values are of the same order as the cracked cement treated base cases. For this reason, BDI can be used as a criterion to

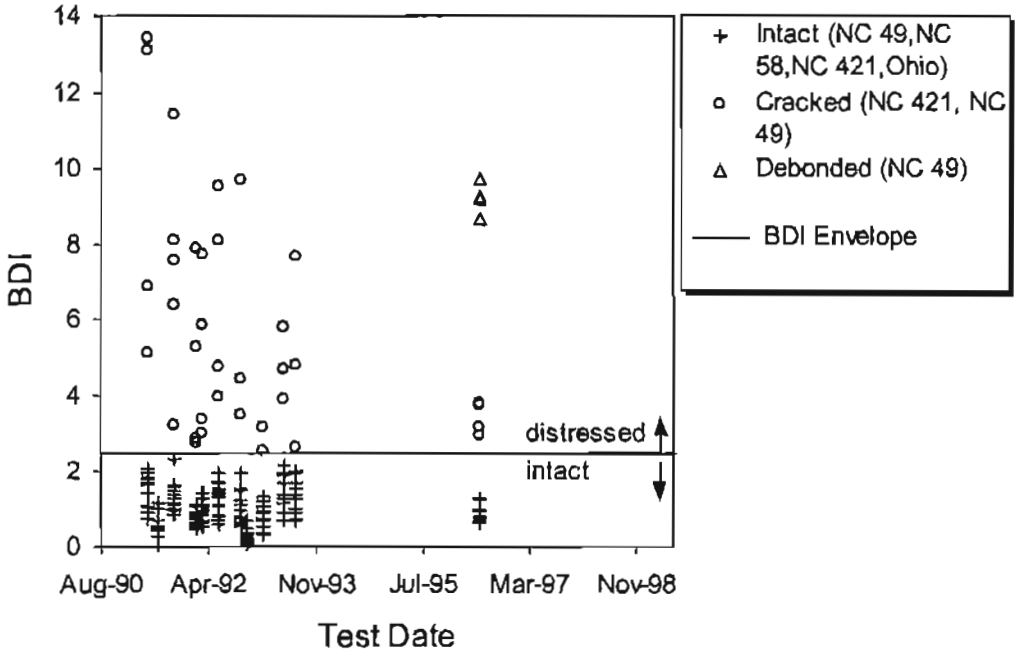

Figure 92. BDI as an indicator of CTB condition
(NC 49, NC 58, and NC 421)

determine if the upper layers of a CTB pavement are intact or distressed, but may not be useful in distinguishing which type of distress is present. Additional field data with a known debonding distress condition would be useful in developing a more unique procedure for distinguishing between debonding in the asphalt layer and cracking in the base layer. The determination of the BDI envelope and an explanation of how BDI was chosen as the DBP for distress identification are included in Appendix C.

Subgrade Strength

The deflection four feet from the load center (D_{48}) was identified as the best indicator of subgrade condition in CTB pavements. D_{48} performed the best in the parametric study of synthetic data, and was tested along with other parameters showing promise on NC 421 field data. CBR information was obtained from DCP testing of NC 421 test sections. The CBR criterion of 10 is a well accepted standard in the North Carolina Department of Transportation to separate poor subgrade condition from a stronger subgrade condition. CBR information was available for only a few test points on the August 1993 test day, therefore all available field data points were used in the development of the condition assessment procedure. Regression techniques were used to determine possible trends between DBP's and tested CBR values. For the field data available, D_{48} exhibited the best correlation with field CBR values.

A limitation of this method is the scarce amount of field data on which analysis based. The curve derived is the best scenario for the given field data, but could fluctuate with additional field cases. A prediction of subgrade condition will allow on-site personnel to determine, in a quick and simple way, whether the subgrade under the tested section is in need of replacement or other rehabilitation. The subgrade condition prediction results can be used with the upper layer

condition indicators to develop a rehabilitation strategy consistent with the conditions in the problematic pavement layers.

Depth to a Stiff Layer

The DBP F_3 was found to be the best indicator of stiff layer depth for CTB pavements. Field data with varying depth to a stiff layer were procured from DataPave 2.0. The five DBPs most likely to indicate stiff layer depth were tested using the field database information. Regression was performed to determine which parameter best fit the field data trend. F_3 was found to capture the field behavior closest.

The formulation of the regression equation, however, was based on a limited number of field data points. All the included field data were obtained from 50 feet outside the section tested, which raises the question of accuracy of the listed depths. Including test data recovered from sections with core data or other more accurate measures of stiff layer depth could be used to improve the model.

ASPHALT OVERLAIN PORTLAND CEMENT CONCRETE PAVEMENTS

The objective of this research was to determine a procedure for the determination of AC/PCC pavement layer condition based on FWD tests. As stated previously, the k-based approach best represented voids under the PCC slab, while ANNs and DBPs were used as indicators for subgrade condition and stiff layer depth. Table 23 summarizes the indicators and their respective prediction methods. Important issues concerning the implementation of the proposed methods are described below. The limitations of the procedures are also included.

Table 23. Proposed methods for layer condition assessment using condition indicators for AC/PCC pavements

Layer	Condition	Indicator	Proposed Method	Required Inputs	Criteria for Poor Condition
Subgrade	Strength	E_{sg}	ANN approach	D_{24}, D_{36}, D_{48}, H_{ac}, H_{pcc}	$E_{sg} \leq 10$ *ksi*
		D_{48}	Field Observations	D_{48}	$D_{48} \geq 0.43$ mils
Stiff Layer	Depth	*DSL*	By definition (Table 2)	D_{24}-D_{36}	$BCI \geq 3.2$ mils
		F_3	Field observations	F_3	$F_3 \geq 0.40$

Voids Under a PCC Slab

The unsupported area beneath the concrete slab, caused by excess moisture, pumping of fines and erosion, is defined as voids. Voids are normally created near transverse joints, working cracks, and edges. Where voids are present, overlaying slabs without properly restoring the voids prior to overlay placement will not enhance the pavement service life. Likewise, using void restoration techniques in areas where voids are not present could cause excessive lift in the slab. The ratio of estimated k-values of test points is used to predict the presence of voids under PCC slabs. The k-value is a modulus of subgrade reaction, which indicates the strength and support of the subgrade layer. Intuitively, this k-value could determine the support under the edge of a PCC slab. US 287 was used to evaluate the proposed analysis method for a field data scenario. Twelve joints in the US 287 section were tested, eight joints in good condition and eight joints in poor condition. The proposed method identified four of the six voided joints as poorly supported.

Subgrade Strength

As stated in "Findings," both ANN and DBP methods can be used to determine the condition of the subgrade layer in AC/PCC pavements. The subgrade ANN was trained initially with synthetic data exclusively. Although a consistent prediction was obtained from the synthetic ANN, field cases with laboratory resilient modulus information were added to the training set and seemed to make the ANN a more consistent predictor of subgrade condition. The ANN supplies subgrade effective modulus values based on a set of inputs that includes D_{24}, D_{36}, D_{48}, H_{ac}, and H_{pcc}.

The deflection basin parameter D_{48} is used as an indicator for subgrade condition. Synthetic data was used to develop a relationship between the deflection four feet from the load center and subgrade condition. As discussed previously, intuition suggests that the deflection measures farther from the load will represent behavior of the lower layers. In addition, the synthetic data correlate quite well to the field data deflection basins. Resilient modulus laboratory test data was available for a small number of cases in the Ohio state field database, and was used to test the envelope developed from the synthetic database.

Both the ANN and DBP procedures produce reasonable results for the condition of subgrade. The DBP method will give a more general idea of subgrade condition, while the ANN will report a discrete subgrade effective modulus value. Currently the most popular method available to predict the strength of subgrade is found in the AASHTO 1993 Guide. As discussed previously, the AASHTO prediction method produces effective moduli values that are not consistent and do not seem to represent the actual field conditions. A detailed explanation of the E_{sg} prediction network is contained in Appendix D. The DataPave database was tested using the prediction procedures and general seasonal trends were considered in validation of the proposed techinques.

Depth to a Stiff Layer

As stated in "Findings," both ANN and DBP methods can be used to determine the depth to a stiff layer in AC/PCC pavements. The DSL ANN was trained with synthetic data exclusively. The ANN supplies DSL values based on a set of inputs that includes D_{24}, D_{36}, D_{48}, H_{ac}, H_{pcc}, F_2, and F_3. An important inference here is that only three deflection measures, upper

layer thicknesses, and two shape factors are needed for prediction. No other layer information or ranges are required.

The deflection basin parameter F_3 is used as an indicator for stiff layer depth. Synthetic data was used to develop a relationship between the shape factor and DSL. As discussed previously, intuition suggests that the slope of the deflection basin measured farther from the load will represent behavior of the lower layers. In addition, the synthetic data correlate quite well to the field data deflection basins. Stiff layer depth information was known for only three test sections in Ohio.

Both the ANN and DBP procedures produce reasonable results for DSL. The DBP method will give a more general idea of shallow, moderate, or deep stiff layer, while the ANN will report a discrete DSL value. Again, the DSL prediction procedure is based on a small set of field data. The only cases available with known DSL were constructed in Ohio, over 100 feet above the stiff layer. DataPave information was used to test the prediction procedures in a general way. Seasonal trends were observed to have no effect on the DSL prediction, as would be expected.

PAVEMENT LAYER CONDITION EVALUATION PROCEDURES

The effort made here is to develop the applicable procedures for evaluating pavement layer conditions from the FWD raw data. Irregular deflection basins, i.e., nonmonotonic changes in the deflections, are sometimes observed from FWD testing. Two possible reasons for this are: incorrectly recorded sensor spacings and presence of discontinuities in pavement layers. Irregular deflections could cause problems in the evaluation of pavement layer conditions. Stubstad et al. (4) concluded that incorrectly recorded sensor locations could significantly change

the moduli values estimated using backcalculation programs. Thus, it is important to first check whether the deflection basin is irregular or not before performing deflection analysis. The two simple criteria described previously (Eqs. 4 and 5) as well as the SLIC method can be used to check irregular basins.

When irregularity due to incorrect sensor location input is detected in FWD deflection basins, correction can be made before processing the deflection information for condition evaluation. One example of the method to correct surface deflections is the SLIC method from Stubstad et al. (4). It needs to be noted that some of the condition assessment algorithms developed in this research could be applied even if the deflection basin is irregular. This is possible because these algorithms use a portion of deflection basin for condition evaluation of different layers. For example, cracking potential of AC layer in full-depth and aggregate base pavements requires *BDI* and H_{ac} as inputs, and therefore only deflections necessary for this evaluation are deflections at 12 and 24 inches from the load center. Similarly, base and subgrade conditions can be determined with a fewer sensor deflections instead of the full deflection basin.

After prescreening FWD raw data, the developed procedures are then applied. The following sections give the proposed procedures to predict pavement layer condition from the prescreened FWD deflections. These procedures are grouped by pavement type and presented in a flow chart with a stepwise description.

Aggregate Base Pavements

Figures 93 and 94 give the flow chart of the overall procedures in determining layer conditions of aggregate base pavements. The stepwise description of the procedure is presented below.

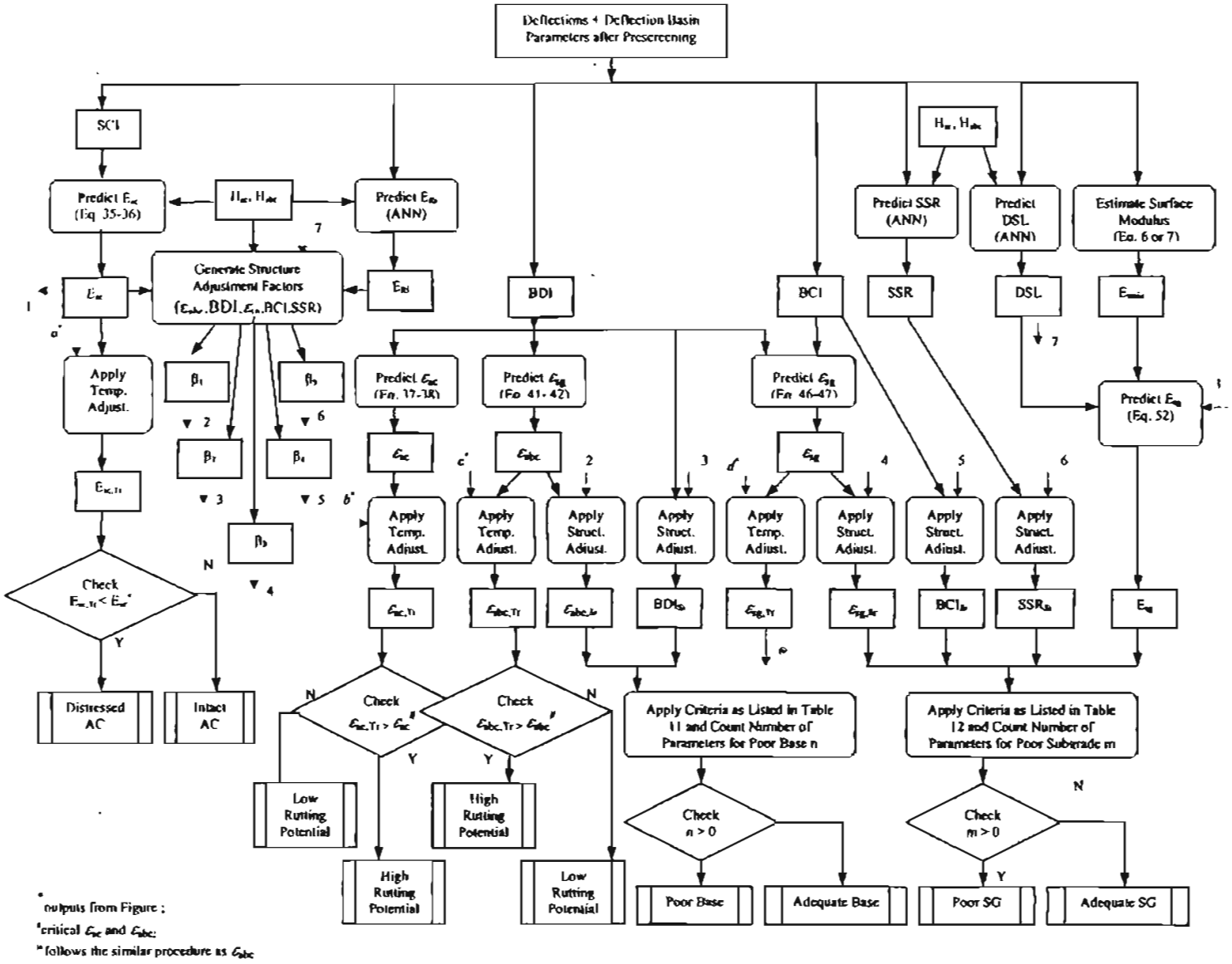

Figure 93. Layer condition assessment procedure for aggregate base pavement

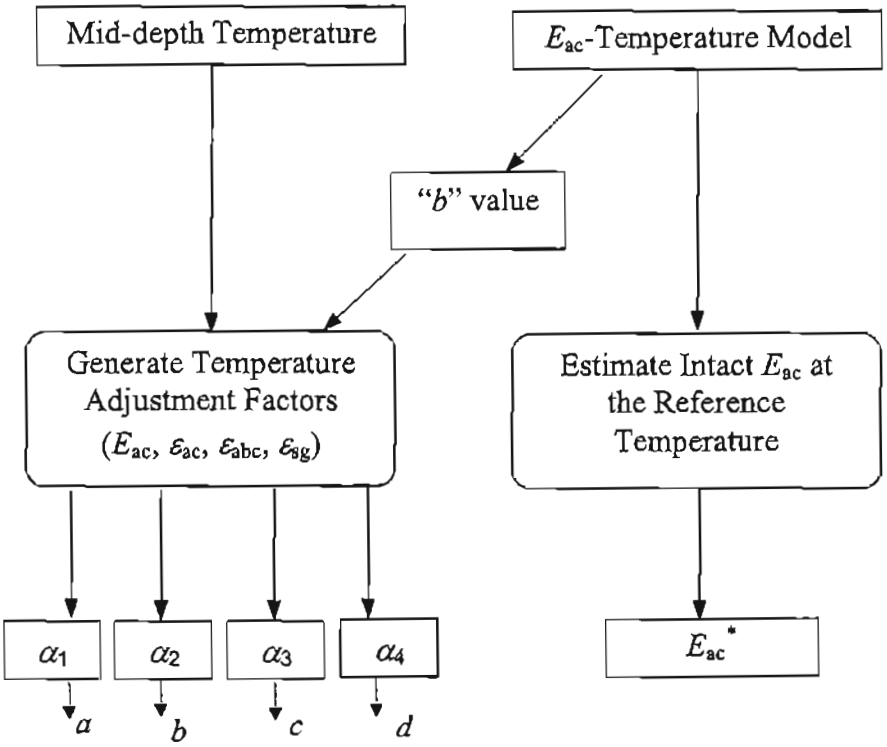

Figure 94. Procedure for generating temperature adjustment factors for aggregate base pavements

Step 1: *FWD data collection and prescreening*

a) Perform FWD test. If possible, the FWD test should be performed at both wheel path and center of lanes;

b) Collect surface deflections, thicknesses, and temperature information;

c) Input AC modulus-temperature model suitable for the pavement in question;

d) Calculate surface modulus profile using Eqs. 6 and 7;

e) Screen deflections using the SLIC method and the two proposed criteria (Eqs. 4 and 5);

f) Normalize deflections to 9000 lb;

g) Adjust deflections to the standard sensor spacings of 0, 8, 12, 18, 24, 36, 48 inches. As the other two sets of sensor spacings (0, 8, 12, 18, 24, 36, 60 inches and 0, 12, 24, 36, 48, 60, 72 inches) are also widely used by state agencies, the estimations of the deflection at 48 inch for the first set or the deflections at 8 and 18 inches for the second set are needed. To achieve this, the following equations were developed based on the synthetic database for aggregate base pavements:

$$\log(D_8) = 0.2576 * \log(D_0) + 0.8997 * \log(D_{12}) - 0.1503 * \log(D_{24}) - 0.0119 \quad (76)$$

$$R^2 = 0.999 \qquad SEE = 0.001$$

$$\log(D_{18}) = 0.3849 * \log(D_{12}) + 0.7336 * \log(D_{24}) - 0.1167 * \log(D_{36}) - 0.0025 \quad (77)$$

$$R^2 = 0.999 \qquad SEE = 0.001$$

$$\log(D_{48}) = -0.3520 * \log(D_{24}) + 1.0349 * \log(D_{36}) + 0.3228 * \log(D_{60}) + 0.0014 \quad (78)$$

$$R^2 = 0.999 \qquad SEE = 0.002$$

Step 2: *Assessing AC layer condition*

a) Calculate *SCI* and *BDI* values;

b) Predict mid-depth temperature using the *BELL3* method in Eq. 72;

c) Evaluate the "intact" AC modulus value at 25°C based on intact modulus vs. temperature model;

d) Predict the actual AC modulus, E_{ac}, using Eq. 35 or 36 or a trained ANN, and apply the temperature correction factor (Eq. 74) to estimate the actual AC modulus at the reference temperature of 25°C;

e) Compare the AC modulus values from Steps c) and d). If the actual AC modulus value is 30% less than the "intact" AC modulus value, the AC layer is considered distressed. Otherwise, the AC layer is considered intact;

f) If the AC layer is predicted to be intact from Step e), then predict ε_{ac} values (Eq. 37 or 38) from a trained ANN, and apply the temperature correction factor (Eq. 40) to determine the adjusted ε_{ac} value. If needed, pavement's remaining fatigue life can also be estimated using Eq. 18.

Step 3: *Assessing base layer condition*

a) Calculate *SCI* and *BDI* values from surface deflections;

b) Predict E_{ac} from either the regression-based approach (Eq. 35 or 36) or a trained ANN;

c) Predict E_{Ri} from the ANN-based approach;

d) Predict value of ε_{abc} from either *BDI* (Eq. 41) or *SCI* and *BDI* (Eq. 42), depending on AC thickness;

e) Apply "structural correction" to estimate adjusted values for *BDI* and ε_{abc};

f) Apply "temperature correction" to estimate adjusted ε_{abc} values, and N_d;

g) If either adjusted *BDI* value or ε_{abc} value is less than its pre-determined critical value, base layer is considered distressed;

h) Predict E_{abc} from the ANN-based approach.

Step 4: *Assessing subgrade condition*

a) Calculate values of *BDI*, *BCI*, F_3, F_2, and AI_4;

b) Predict E_{ac} value using the ANN-based procedure or regression approach (Eq. 35 or 36);

c) Predict E_{abc} value using the ANN-based procedure;

d) Predict *DSL* value using the ANN-based procedure;

e) Predict *SSR* and E_{Ri} values using the ANN-based procedures;

f) Calculate ε_{sg} value based on the *BDI* and *BCI* values (Eq. 46 or 47);

g) Apply "structural correction" to estimate adjusted *BCI*, ε_{sg}, and *SSR* values;

h) Apply "temperature correction" to estimate temperature adjusted ε_{sg} and N_d values;

i) Calculate E_{sg} from the surface modulus method:

   1) Determine E_{smin} from surface modulus profile;

   2) Calculate F_{ac} from H_{ac}, H_{abc}, and predicted E_{ac} (Eq. 53);

   3) Calculate E_{sg} using E_{smin}, F_{ac}, and *DSL* (Eq. 52);

j) Compare E_{sg} and adjusted *BCI*, ε_{sg}, and *SSR* values with their critical values. If any one of these values are in the critical range, subgrade condition is considered to be poor.

Full-depth pavements

The flow chart of the overall procedure of the determination of pavement layer conditions is shown in Figures 95 and 96. The stepwise description of the procedure is presented below.

Step1: *FWD data collection and prescreening*

a) Perform FWD test. If possible, FWD test should be performed at both wheel path and the center of lanes;

b) Measure surface deflections and collect thickness and temperature information;

c) Calculate surface modulus profile (Eqs. 6 and 7);

d) Screen deflections using the two proposed criteria (Eqs. 4 and 5) and the SLIC method;

e) Normalize deflection to 9000 lb;

f) Adjust deflections to the reference sensor spacings of 0, 8, 12, 18, 24, 36, 48 inches using the following equations:

$$\log(D_8) = 0.2313 * \log(D_0) + 0.9281 * \log(D_{12}) - 0.1555 * \log(D_{24}) - 0.0079 \quad (79)$$

$$R^2 = 0.999 \qquad SEE = 0.001$$

$$\log(D_{18}) = 0.4128 * \log(D_{12}) + 0.6848 * \log(D_{24}) - 0.0957 * \log(D_{36}) - 0.0022 \quad (80)$$

$$R^2 = 0.999 \qquad SEE = 0.001$$

$$\log(D_{48}) = -0.2814 * \log(D_{24}) + 0.8770 * \log(D_{36}) + 0.4005 * \log(D_{60}) + 0.0203 \quad (81)$$

$$R^2 = 0.999 \qquad SEE = 0.002$$

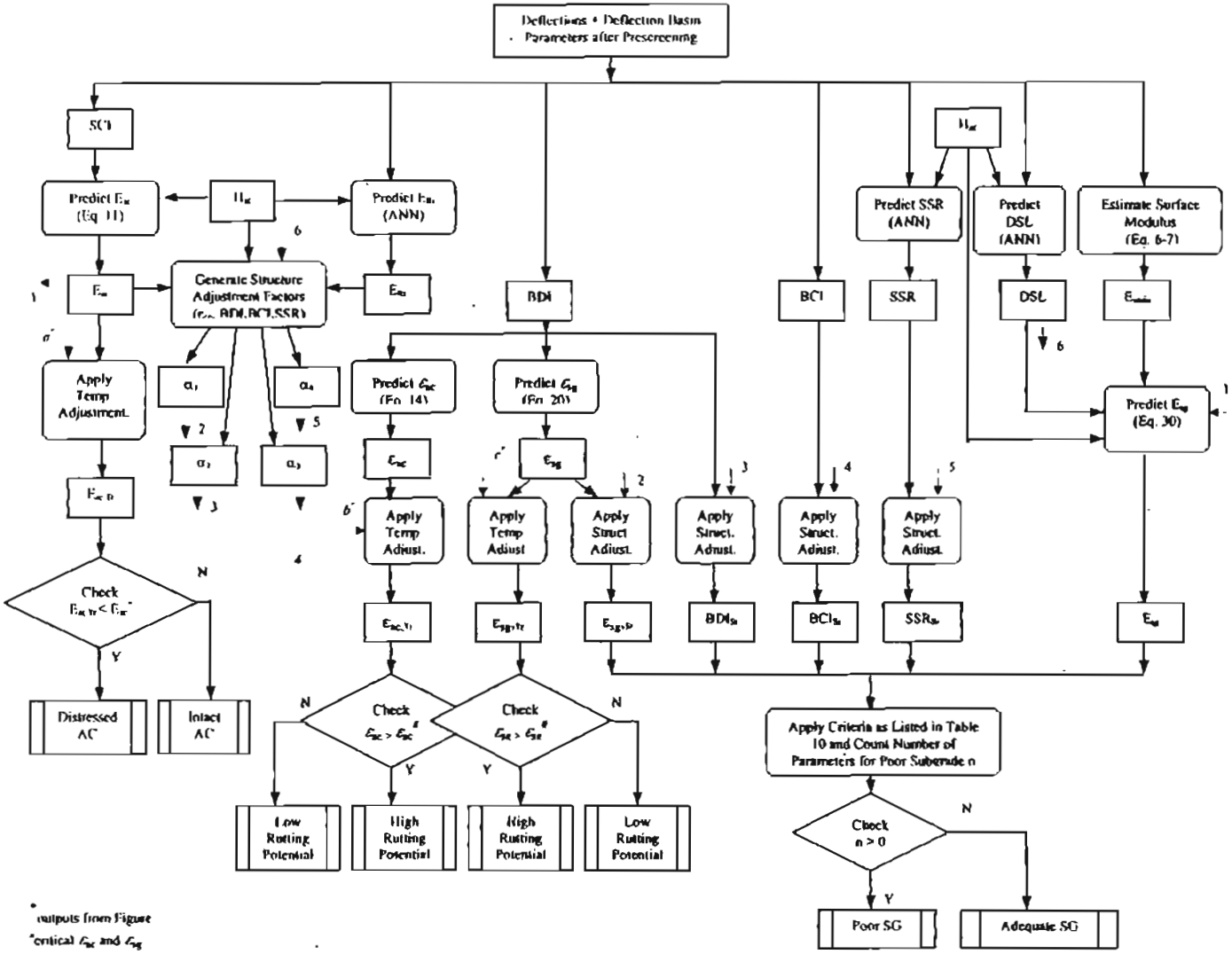

Figure 95. Layer condition assessment procedure for full-depth pavement

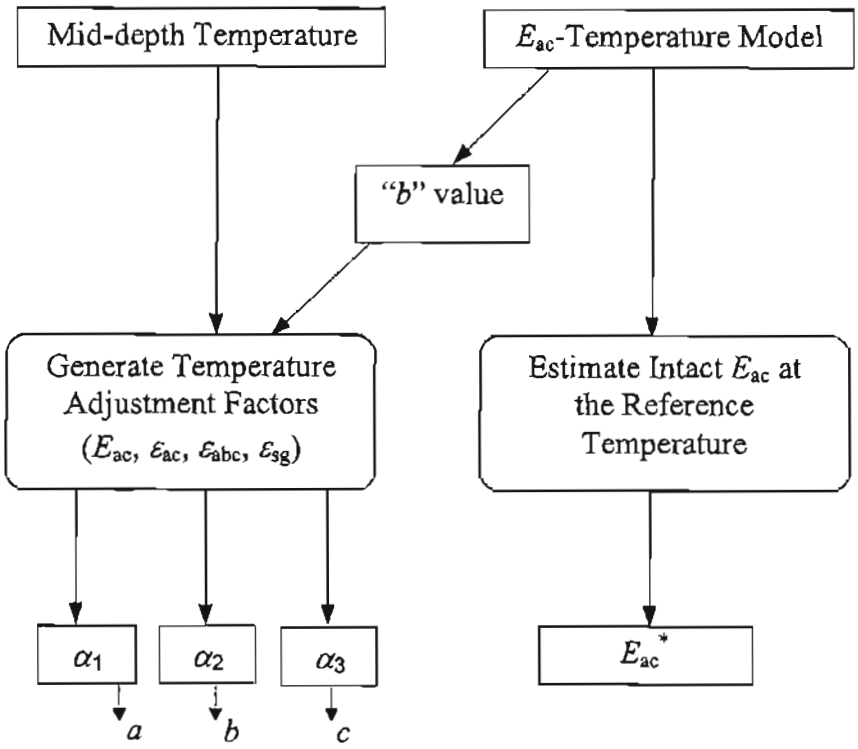

Figure 96. Procedure for generating temperature adjustment factors for full-depth pavements

Step 2: *Assessing AC layer condition*

a) Calculate SCI values, and predict mid-depth temperature using *BELL3* method (Eq. 72);

b) Calculate the "intact" AC modulus value at 25°C using pre-determined modulus vs. temperature equation;

c) Predict the actual AC modulus E_{ac} (Eq. 11), and apply "temperature correction" to estimate actual AC modulus at 25°C;

d) Compare the AC modulus values from Steps b) and c). If the actual AC modulus value is 30% less than the "intact" AC modulus value, the AC layer is considered distressed. Otherwise, the AC layer is considered intact;

e) If the AC layer is predicted to be intact from Step d), then predict ε_{ac} values (Eq. 14), and apply "temperature correction" to get the adjusted ε_{ac} value. Pavement's remaining fatigue life can also be estimated using Eq. 18.

Step 3: *Assessing subgrade condition*

a) Calculate values of *BDI*, *BCI*, F_3, F_2, and AI_4;

b) Predict E_{ac} value using the ANN-based procedure or regression approach (Eq. 11);

c) Predict *DSL* value using the ANN-based procedure;

d) Predict *SSR* and E_{Ri} values using the ANN-based procedures;

e) Calculate ε_{sg} value based on the *BDI* and *BCI* values (Eq. 20);

f) Apply "structural correction" to estimate adjusted *BCI*, ε_{sg}, and *SSR* values;

g) Apply "temperature correction" to estimate temperature adjusted ε_{sg} and N_d values;

h) Calculate E_{sg} from the surface modulus method:

1) Determine E_{smin} from surface modulus profile;

2) Calculate F_{ac} from H_{ac}, and predicted E_{ac};

3) Calculate E_{sg} using E_{smin}, F_{ac} and DSL (Eq. 30);

i) Compare E_{sg} and adjusted BDI, BCI, ε_{sg}, and SSR values with their critical values. If any of these values is in the critical range, subgrade condition is considered to be poor.

Cement Treated Base Pavements

The flow chart of the overall procedure of the determination of pavement layer conditions is shown in Figure 97. The stepwise description of the procedure is presented below.

Step 1: *Assessing upper layer condition*

a) Calculate BDI (Eq. 13) value;

b) Compare BDI to its critical value. If the calculated BDI is greater than 2.5, the pavement is considered distressed; and if the calculated BDI is less than 2.5, the pavement is considered intact.

Step 2: *Assessing subgrade condition*

a) Input the D_{48} value into the regression equation (Eq. 55) to estimate the corresponding CBR value;

b) Compare the estimated CBR value to its critical value. If the estimated CBR value is greater than 10, the subgrade is considered in good condition; and if the estimated CBR value is less than 10, the subgrade is considered in poor condition.

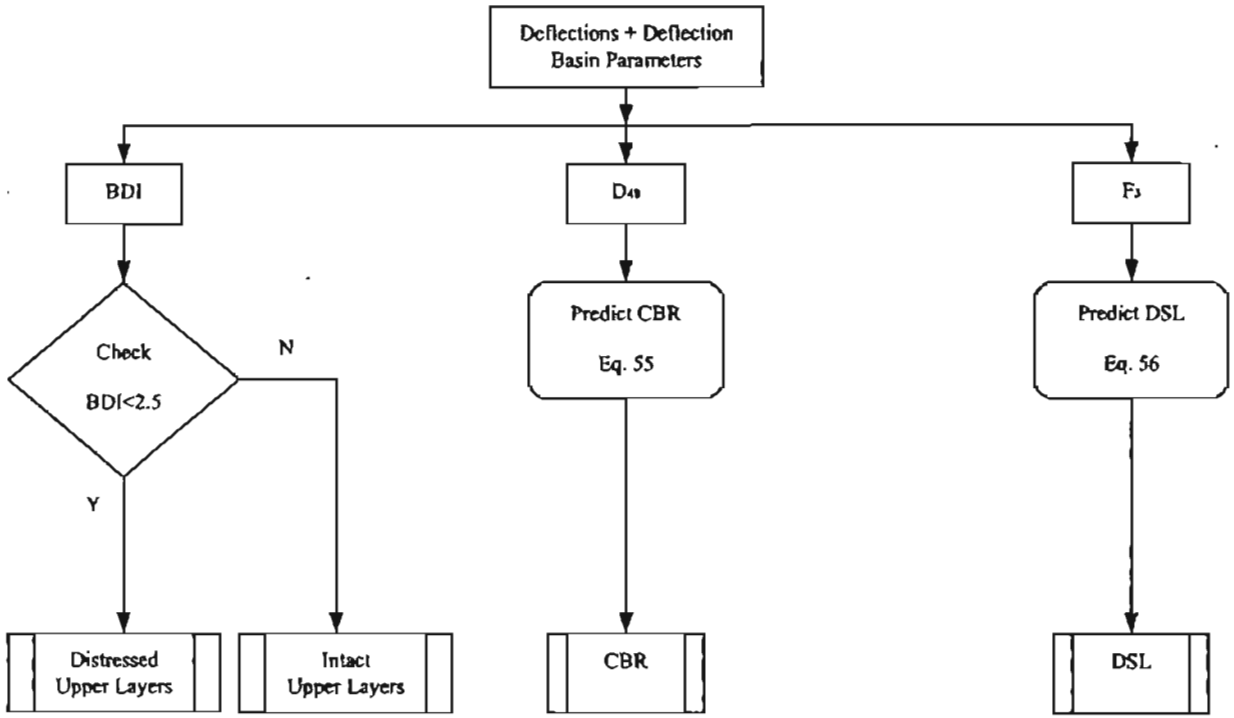

Figure 97. Layer condition assessment procedure for CTB pavements

Step 3: *Assessing stiff layer depth*

a) Calculate F_3 value;

b) Substitute the calculated F_3 value into Eq. 56;

c) Solve Eq. 56 for DSL predicted value.

Asphalt Overlain Portland Cement Concrete Pavement

The flow chart of the overall procedure of the determination of pavement layer conditions is shown in Figure 98. The stepwise description of the procedure is presented below:

Step 1: *Void Detection*

a) Perform FWD tests at the center and corner of slabs. To minimize curling effects, it is preferable to conduct the tests in the early morning;

b) Locate geophones at –12, 0, 12, 24, 48, 60, and 72 inches from the center of the loading plate;

c) For corner tests, locate loading plate on the down-stream corner as close as possible to the edge of the slab. If the loading offset from the slab edge is inevitable, measure the offset distance;

d) Calculate *AREA* (Eq. 65);

e) Estimate the radius of relative stiffness l (Eqs. 62 to 64) and the non-dimensional maximum deflection Δ_l (Eqs. 58 to 60);

f) Calculate modulus of subgrade reaction k (Eq. 57) and the concrete modulus of elasticity E_c (Eq. 66);

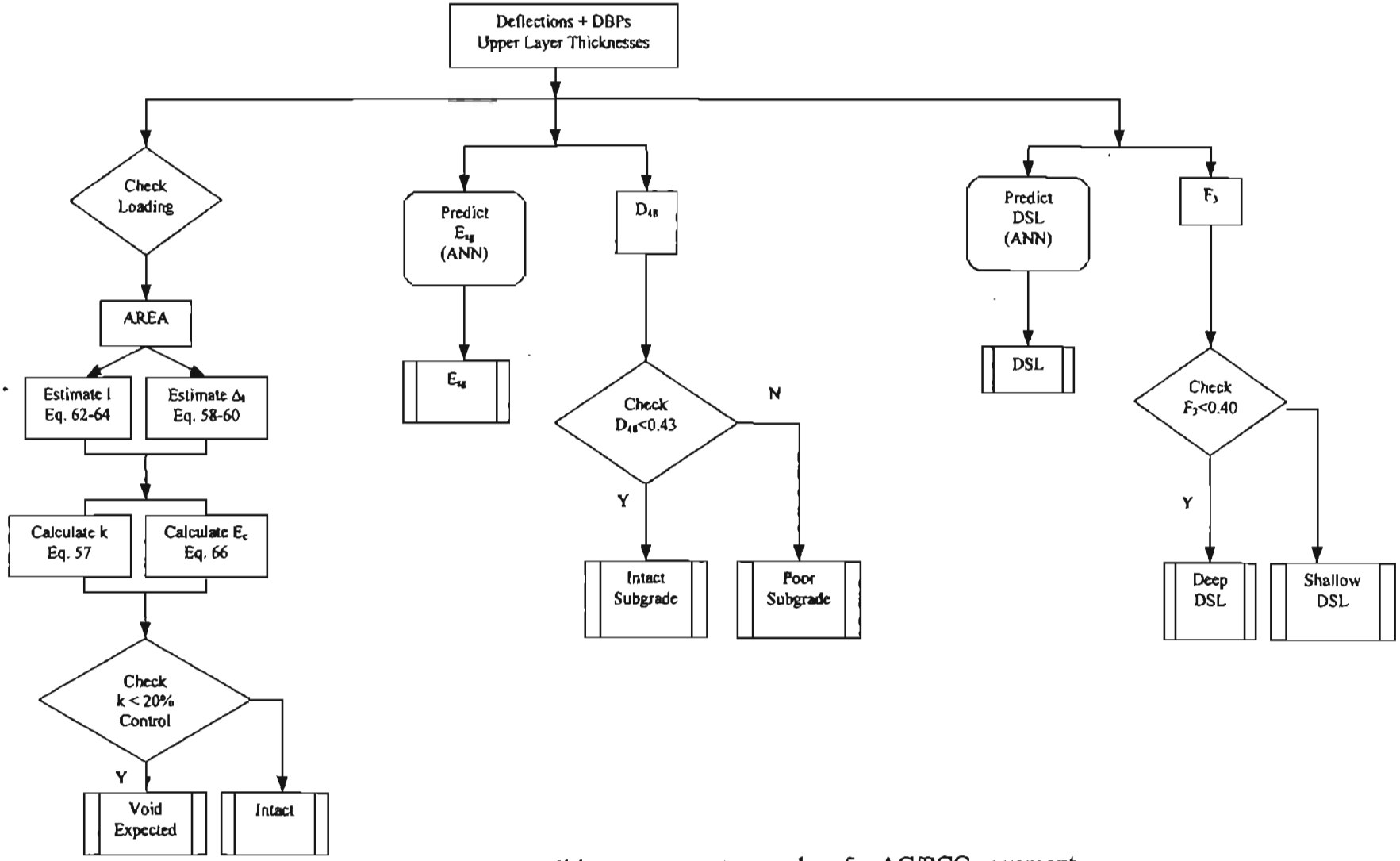

Figure 98. Layer condition assessment procedure for AC/PCC pavement

Calculate deflection parameter *AREA* (Eq. 65) and joint load transfer efficiency (Eq. 61). If the loading offset exists, correct the maximum deflection (Eq. 67) and the *AREA* value (Eq. 68);

g) Estimate the radius of relative stiffness l (Eqs. 62-64) and non-dimensional maximum deflection Δ_l (Eqs. 58-60);

h) Calculate the modulus of subgrade reaction k (Eq. 57) and the concrete modulus of elasticity E_c (Eq. 66);

i) Calculate the ratio of k-values at corner to center;

j) Plot the k-ratio values versus test position along the slab, then determine the control value of k-ratio, which is the lower bound of k-ratios expected for sound support condition, based on the k-ratio versus test position trend;

k) When the calculated k-ratio is less than 20% of the control value, locally weakened subgrade or a void is expected.

Step 2: *Assessing Subgrade Strength*

a) Deflection Value Based Approach Using ANN

1) Input normalized D_{24}, D_{36}, and D_{48} deflections (in mils), the asphalt layer thickness and the concrete layer thickness;

2) Retrieve discrete E_{sg} prediction;

b) Deflection Basin Parameter Approach

1) Compare the normalized D_{48} value with the D_{48} Poor/Good Envelope. If the recorded D_{48} value is less than 0.43, the subgrade is in good condition. If the recorded D_{48} value is greater than 0.43, the subgrade is in poor condition;

Step 3: *Assessing stiff layer depth*

a) Deflection Value Based Approach Using ANN

1) Compute F_2 and F_3 values;

2) Input the seven normalized deflections (in mils), the calculated F_2 and F_3 shape factors, the asphalt layer thickness (in inches) and the concrete layer thickness (in inches) into the ANN;

3) Retrieve discrete DSL prediction;

b) Deflection Basin Parameter Approach

1) Calculate F_3 values;

2) Compare the calculated F_3 values to its critical value. If the calculated F_3 value is less than 0.40, the stiff layer is deep. If the calculated F_3 value is greater than 0.40, the stiff layer may be shallow.

Asphalt Pavement Layer Condition Analysis Program --- APLCAP version 1.0

A user-friendly interactive computer program implementing the proposed condition evaluation procedures was developed using the Visual Basic language. A prototype version of APLCAP (Asphalt Pavement Layer Condition Analysis Program) includes the condition evaluation procedures for aggregate base pavements and full-depth pavements. The procedures for CTB pavements and AC/PCC pavements are not included in this version, since only limited field data were available to verify them. The detailed description about APLCAP is presented in Appendix F.

CHAPTER 4

CONCLUSIONS AND SUGGESTED RESEARCH

Condition assessment of pavement layers using deflection data has been investigated. Information obtained from the literature provided a background to begin construction and analysis of synthetic data generated from a FEM structural model. ANN feed-forward deflection value based analysis took place following the construction of structures indicative of standard neural network modeling procedures. The conclusions that follow are a digestion of the information presented in the findings from the research. When applied to field testing, using the FWD deflection measuring device, pavement layer condition can be estimated.

During research activities, several issues that were either beyond the scope of this research or could be used to enhance the findings of this research were discovered. Suggestions for the extension or improvement of this research are documented. This additional information is expected to improve the performance and precision of the outlined prediction techniques.

CONCLUSIONS

The investigation of techniques to predict the condition of pavement layers using FWD deflection data produced several results pertinent to layer condition prediction. These results are enumerated as follows:

- Synthetic data generated by dynamic FEM forward models reasonably estimates actual field conditions for the ranges of pavements under consideration.
- The dynamic effect is important in simulating pavement responses under FWD loading. The nonlinearity of unbound aggregate base and subgrade is important to estimate responses of

aggregate base and full depth pavements, but not so for cement treated and AC/PCC pavements.

- For full depth and aggregate base pavements, a reasonable AC modulus-temperature relationship was observed when applying the dynamic, nonlinear analysis in the forward modeling. Also, the results from the proposed procedures, based on the dynamic, nonlinear analysis, in detecting base and subgrade condition agreed well with the DCP test results.
- For full depth and aggregate base pavements, E_{ac} can be used as an indicator to detect cracking and stripping in AC layer. *BDI* and ε_{abc} were found to be good indicators for base layer condition, while *BCI*, ε_{sg}, *SSR*, and E_{sg} appeared to be good condition indicators for subgrade. For intact pavements, the pavement overall fatigue cracking and rutting potentials are mainly controlled by ε_{ac}, ε_{abc}, and ε_{sg}.
- Temperature adjustment is an important procedure in assessing condition of asphalt-surfaced pavements. Based on the synthetic database developed from nonlinear finite element analysis, temperature correction factors were developed for various condition indicators. These adjusted indicators were found to be able to predict fatigue cracking and rutting potentials of full depth and aggregate base pavements fairly well.
- The predicted E_{ac} values from the dynamic analysis based procedure were found to be larger that those from the static analysis based procedure. This trend could be more significant in the E_{sg} predictions.
- The minimum surface modulus, E_{smin}, was found highly related to subgarde modulus in full depth and aggregate base pavements. Based on the dynamic, linear elastic analysis, the relationship between E_{smin} and E_{sg} was established. The E_{sg} predictions from this relationship agreed well with the DCP test results.

- For full depth and aggregate base pavements, the analyses from both synthetic data and field data showed that *SCI* can be used to predict the AC modulus. Also, high correlation was found between *BDI* and ε_{ac}.
- The DBP BDI can be used to assess upper layer condition in CTB pavements.
- Deflection values from the sensor four feet from the FWD load center (D_{48}), can be used to estimate subgrade condition in CTB pavements.
- Stiff layer depth in CTB pavements can be determined using the F_3 shape factor.
- A k-based approach can be used to detect voids under PCC slabs in AC/PCC pavements. This approach takes into consideration variations in void detection due to testing location (center, edge, or corner loading).
- Subgrade condition in AC/PCC pavements can be estimated using either an ANN with inputs D_{24}, D_{36}, D_{48}, H_{ac}, and H_{pcc}, or a regression approach based on the D_{48} deflection value.
- DSL in AC/PCC pavements can be estimated using either an ANN with inputs D_{24}, D_{36}, D_{48}, H_{ac}, H_{pcc}, F_2, and F_3, or a regression approach based on the F_3 shape factor.
- ANN is a powerful tool in engineering practice. The ANNs with optimized structures were found to be able to predict pavement critical stresses, strains, layer modulus, and depth to a stiff layer.
- ANNs can be much improved with the inclusion of field data into the training set.
- The pavement layer condition assessment procedures developed from this research are different from traditional deflection analysis programs in that the relationships used in estimating the condition of different layers in these procedures are independent of each other. That is, subgrade condition can be estimated without needing to know the upper layer conditions, if one chooses to do so.

- The pavement layer condition assessment procedures developed from this research are different from traditional deflection analysis programs in that some of the relationships constituting these procedures do not require all seven deflections, but only a portion of deflection basin. This feature allows the analysis of irregular deflection basins that are observed frequently in distressed pavements for layer condition assessment.

SUGGESTED RESEARCH

While the condition of pavement layers has been a topic of great interest and debate for years, much is yet to be learned. Though many techniques have been developed and utilized for some time, current procedures can be enhanced. The following are several topics still in need of investigation:

- High quality field data is crucial to the prediction of pavement layer condition. More effort should be spent in the construction and data collection phase of all projects. Well documented information through the life of the project can then be used to learn about the behavior of a specific pavement type.
- The proposed ANNs and DBP based methods can be extended to multi-load deflection analysis. This additional dimension should yield more accurate and reliable estimation of pavement layer condition. The dynamic, nonlinear finite element forward model and artificial neural networks adopted in this research can be readily extended to the multi-load deflection analysis.
- Full data sets in the DataPave field database could be used to improve the effectiveness of prediction models. The current database is void of much of the

condition and layer thickness information expected. The addition of this data could further improve layer condition estimation.

REFERENCES

(1) Navneet Garg and Marshall R. Thompson, "Triaxial Characterization of Minnesota Road Research Project Granular Materials," In Transportation Research Record 1577, TRB, National Research Council, Washington, D. C.,1998, pp. 27-36.

(2) B. Lanka Santha, "Resilient Modulus of Subgrade Soils: Comparison of Two Constitutive Equations," In Transportation Research Record 1462, TRB, National Research Council, Washington, D. C.,1994, pp. 79-90.

(3) A. M. Johnson and R. L. Baus, "Simplified Direct Calculation of Subgrade Modulus from Nondestructive Pavement Deflection Testing," In Transportation Research Record 1406, TRB, National Research Council, Washington, D. C., 1993, pp. 133-141.

(4) Stubstaad, R. N., Irwin, L. H., Lukanen, E. O., and Clevenson, M. L., "It's 10 o'clock – Do You Know Where Your Sensors Are?," Transportation Research Board, 79th Annual Meeting, Washington, D. C., Jan, 2000.

(5) D. A. Van Deusen and D. E. Newcomb., "Strains due to Load in Frozen and Thawed Flexible Pavements." The 4thInt. Conf. on the Bearing Capacity of Roads and Airfields, Minneapolis, Minnesota, Proc. Vol. 1 (1994) pp. 683-704.

(6) Lukanen, E. C., Stubstaad, R., and Briggs, R., *Temperature Predictions and Adjustment Factors for Asphalt Pavement*, final Report submitted to Federal Highway Administration.

(7) Garg, N., and Thompson, M.R., "Mechanistic-Empirical Evaluation of the Mn/ROAD Low Volume Road Test Sections," Illinois Cooperative Highway and Transportation Research Program Report FHWA-IL-UI-262, Urbana, IL, 1998.

(8) Gabr, M. A. Lambe, P. C., Coonse, J. W., and Hopkins, K. P., Dynamic Cone Penetrometer Criteria for Transportation Research Studies, Raleigh, NC, 1999.